THE UNIVERSITY OF CALGARY

Modelling of Solid Particle Thermals

by

Mark Yeomans

A THESIS

SUBMITTED TO THE FACULTY OF GRADUATE STUDIES

IN PARTIAL FULFILLMENT OF THE REQUIREMENTS FOR THE

DEGREE OF MASTER OF SCIENCE

DEPARTMENT OF MECHANICAL ENGINEERING

CALGARY, ALBERTA

May, 1997

Abstract

A theoretical two phase flow model is proposed to describe the behaviour of glass particle thermals released into a non-stratified water environment. The model assumes a background fluid flow field consisting of a Hill's spherical vortex to describe flow within the thermal and potential flow theory to describe flow outside. Theoretical results are given for uniform and nonuniform thermal speeds using Stokes and non-Stokes drag relationships. The uniform thermal results using a Stokes drag relationship display almost identical thermal behaviour to polystyrene thermal results from Topham et al's research (1994).

Laboratory thermal experiments were performed using four different glass particle grain sizes. The experiments were videotaped and later analyzed with the use of a computer, which enabled a comparison to be carried out with the theoretical results. Laboratory and theoretical results compared very well for both uniform and nonuniform thermal speeds using a non-Stokes drag relationship.

Acknowledgements

I would like to thank the following people and organizations for their help and support with this thesis project.

My supervisor, Dr. R.D. Rowe, for his guidance, technical support, scholarly attitude and patience. Working with him was a very enjoyable educational experience.

Brandon Ferguson, from the machine shop, for fabricating portions of the laboratory apparatus, helping assemble the argon ion laser used to illuminate the particle thermals and for his assistance in performing experiments.

Dr. David Topham for help with the laboratory apparatus and for his technical advice throughout this project.

Doug Phillips, from Academic Computing Services, for his expertise in analyzing the laboratory thermals.

Nova Gas Transmission Ltd., my present employer, for their financial assistance and support.

The University of Calgary and The Department of Mechanical Engineering for their financial assistance and support.

Dedication

To Laura

and

my parents

Table of Contents

Page

Chapter 2 continued

Chapter 3 - Experimental Equipment and Procedure

Chapter 4 - Experimental Observations

Page

Chapter 5 - Theoretical Results

Chapter 6 - Analyses of Theoretical and Laboratory Results

Chapter 7 - Conclusions and Recommendations

Page

Appendices

List of Tables

Page

List of Figures

Page

Page

Page

List of Symbols

Symbol	Description
a	Maximum radius of the vortex or thermal, cm
a_p	Maximum radius of the particle crescent, cm
b	The vertical distance from the maximum radius of a thermal measured to its bottom, cm
b_p	The vertical distance from the top of the particle crescent to its bottom (depth), cm
c	Coefficient
C_D	Coefficient of drag
C_L	Lift coefficient (equal to 0.5 for a spherical particle)
d	Particle diameter, cm
e	Exponential coefficient
g	Gravitational acceleration, cm/s^2
j	Coefficient
K	Constant determined from laboratory experiments for use with the nonuniform thermal speed relationship, $cm/s^{1/2}$
k_p	Added mass coefficient for particles (equal to 0.5 for spherical particles)
L	Length scale, cm
m	Exponential coefficient
m_f	Mass of a fluid element, g

Symbol	Description
m_p	Mass of a particle, g
n	Exponential coefficient
N_R	Reynolds number (Figure 2.5)
Q	A constant equal to $a^3 g \frac{(\rho_1 - \rho)}{\rho_1}$, cm^4/s^2
r	Radial dimension, cm
r_p	Radius of a particle, cm
s	Exponential coefficient
t	Corresponds to the theoretical time in the particle and fluid equations. It is measured from the point source release of a thermal, s
t_e	Experimental time measured from the initial release of a thermal having a radius of 2 cm, s
U	Vertical velocity of a thermal, cm/s
u_r	Local velocity of fluid element in radial direction, cm/s
u_z	Local velocity of fluid element in vertical direction, cm/s
u(t)	Vector quantity of the velocity of fluid flow field, cm/s
v(t)	Vector quantity of the velocity of a particle, cm/s
V_T	Terminal velocity of a particle, cm/s
w	Equal to **u** - **v** (Difference between fluid and particle velocities), cm/s
Y(t)	The location of a particle at time t, cm

Symbol	Description
z	Vertical distance measured to the maximum radius of a thermal. Frame of reference relative to point of release, cm
z_p	Vertical distance measured to the maximum radius of the particle crescent. Frame of reference relative to point of release, cm
z_T	Vertical dimension with a frame of reference relative to the center of the thermal, cm
z_c	Depth at which particles permanently separate from the thermal cloud, cm
α	Entrainment coefficient for the growth of an expanding thermal (equal to 0.25)
ω	Vorticity, 1/s
Γ	Circulation around a vortex, cm^2/s
Ψ	Stream function, cm^3/s
μ	Dynamic viscosity of fluid, g/cm·s
ρ	Fluid density inside of a thermal, g/cm^3
ρ_0	Fluid density outside of a thermal, g/cm^3
ρ_1	Reference density of the system; equal to ρ_0 at $t = 0$ (point of release), g/cm^3
ρ_L	Density of water (1.0 g/cm^3 at 5° C)
ρ_s	particle density, g/cm^3
Δt	Difference between theoretical and experimental values of time ($\Delta t = t - t_e$), s
υ	Kinematic viscosity of the fluid, cm^2/s

Chapter 1

Introduction

1.1 Background

"Cutting CO_2 emissions painful", "Bid to cut greenhouse gas emissions failing", "Oil cleanup far from complete" and "Correcting leak to cost a bundle - Swan Hills" were four Canadian environment stories in the December 12, 1996, edition of the Calgary Herald. Environmental concerns are growing and stories such as these are becoming more prominent in national and local news. Engineering solutions are required to resolve many of these environmental problems. Fluid modelling is one tool engineers can use to predict accurately the spread of pollutants into the atmosphere, oceans and freshwater environments, which will in turn help provide solutions.

Fluid flow modelling predicts fluid motions in many types of situations, which engineers use to design structures and facilities. With an appropriate model it is possible to predict the behaviour of solid particles in two phase applications. Many pollutants consist of two or three phases. Some examples of two phase flow include waste disposal in the ocean and waste effluent releases into lakes and rivers.

Pollutants and contaminants come from many different sources. Some sources of water and air pollution are natural (volcanoes and forest fires), domestic (sewage and furnace emissions), commercial (effluents and emissions), agricultural (manure, fertilizer, operation of machinery, dust, etc.), industrial (gas plants, refineries, manufacturing and processing plants, leaks and spills) and transportation (emissions) related sources. Control of air and water pollution is not always easy, for it is impractical to eliminate all emissions of a specific pollutant. However, it is reasonable to expect control of emissions to the lowest possible level consistent with available technology at a reasonable cost. Therefore, in practice, emission control limits are established in order to enforce and protect air and water quality standards.

Water pollution occurs when the discharge of wastes impairs water quality or disturbs the natural ecological balance. Contaminants that cause problems include disease-causing organisms, organic matter, solids, nutrients, toxic substances, color, foam, heat and radioactive materials. Many of the same contaminants are also released into the atmosphere. Pollution sources involving combustion processes emit nitrogen oxides (NO_x), sulfur oxides (SO_x), carbon dioxide (CO_2), carbon monoxide (CO),

hydrocarbons (e.g., CH_4) and ozone (O_3) into the atmosphere. Other gaseous pollutants commonly released are chlorofluorocarbons (CFC's) and hydrogen sulfide (H_2S). Carbon dioxide, nitrogen oxides and methane are thought to be the gases responsible for the greenhouse effect and nitrogen oxides and sulfur oxides are responsible for acid rain.

In Alberta, primary sources of pollution entering the environment are from domestic (sewage), industrial (gas and processing plants, refineries) and commercial effluents (e.g., thermal pollution from power plants and pulp and paper effluents). Currently, there is extensive work being done to predict accurately the spread of gaseous plumes in the province. Gaseous H_2S plumes can result from oil well and pipeline blowouts. Due to the acute toxicity of H_2S, it is necessary to predict accurately plume dispersion and gas concentrations at distances from the point of release.

In Calgary, there is a site along the Bow River contaminated with creosote. A wood treating facility was located there in the 1950's. Creosote, used to treat wood at the facility, was spilled extensively. Through the years, the creosote has migrated through the soil to the groundwater aquifer and into the river. Presently, the province is studying feasible ways to clean it up. Models have been developed to predict how far the creosote contamination has moved and how much further it will move with time.

Environmental flow modelling in air and water is similar. In both instances, models take into account fluid entrainment, buoyancy forces, drag forces and momentum to predict, for example, plume or thermal growth and dispersion. With ever growing environmental concerns, it is becoming necessary to improve previously developed

models and to develop new ones. Through this work, engineers can better design facilities to limit negative effects of pollutants on the environment.

1.2 Purpose

The **purpose** of this thesis is to examine in detail the behaviour of solid particle thermals using an existing particle and fluid flow model. In the last few years, there have been many theoretical particle models developed. Many of these are based on the same theories and ideas, but differ in their complexity. However, there has been very little laboratory work done to verify them.

The laboratory portion of this thesis emulates the laboratory experiments performed by B.G. Krishnappan (1977) and Y.G. Lee (1992), with a few modifications. They include a different size water tank, release mechanism and lighting source. Krishnappan studied the motion of two phase thermals in hopes of understanding the motion of dredged material when dumped near the surface of deep water. The glass particle sizes used by Krishnappan are the same as those used here. Experimental work done by Lee, was performed using various sizes of polystyrene particles. A theoretical one-dimensional two phase thermal model was also developed by Lee. Cathy Laureschen (1992) also performed similar experiments, but with bubbles.

1.3 Literature Review

A tremendous amount of theoretical and experimental research has been devoted to analyzing the behaviour of thermals. The classic definition of a thermal by Scorer (1978) is "a body of buoyant fluid in another fluid environment in which it can mix". The origins of this definition comes, in part, from glider pilots who encountered warm buoyant masses of air while flying. The definition of a thermal has also been extended to include negatively buoyant masses, which move downwards under the influence of gravity. A detailed review of solid particle thermals was recently provided in Lee's (1992) thesis.

In 1990, 20 Gigatonnes of debris and garbage were dumped into the ocean (Luketina and Wilkinson, 1994). Luketina and Wilkinson have performed research in the area of negatively buoyant thermals. Their work focussed on determining the maximum depth at which particulate matter would reach when dumped in water. Debris dumped in water behaves as a two phase thermal, consisting of an internal vortical flow field with negative buoyancy. The particle thermal reaches a maximum depth when its downward motion is slowed by its loss of buoyancy due to entrainment of surrounding fluid and from the particles separating from the thermal.

Noh and Fernando (1993) have recently performed research studying the sedimentation of two-dimensional particle clouds (thermals). They performed experiments, which released glass particles and dye into a water tank. Their experimental apparatus and methods are very similar to the experimental portion of this thesis project.

From their research they determined the critical depth (z_c) when particle clouds pass from the *thermal regime* to the *particle-settling regime*. They defined the *thermal regime* as the phase when the particle clouds move in the convectional fluid motions characteristic of thermals and the *particle-settling regime* as the phase when the particles descend as individual particles with little disturbance to the background fluid. They concluded that z_c did not correspond to the point when the thermal fluid velocity equalled the terminal velocity of the glass particles, but at a thermal speed greater. They also found no distinct changes in the horizontal growth of the thermal cloud at the transition point between regimes and that turbulence generated in the *thermal regime* continues for a period time after the transition point.

The particle model used in this research is based on the work by Auton et al ("The force exerted on a body in inviscid unsteady nonuniform rotational flow", 1988). In their research they examined several particle motion equations from other researchers in order to resolve some inconsistencies with them. From their review they proposed their own particle equation, which considers forces on a small rigid sphere in nonuniform rotational flow. It was developed by first considering the forces on an undisturbed flow field and secondly, by considering the forces on the disturbed flow field. The disturbed flow field considers the presence of the small rigid sphere. Several conditions must be satisfied by the equation, including Navier-Stokes, continuity, no-slip and incompressibility. The no-slip condition implies the local fluid velocity matches the particle velocity at any location.

Many researchers have simplified the particle equation because of its complexity. Ruetsch and Meiburg (1993) introduced a simplified equation which includes, the forces due to buoyancy and drag (Stokes), the force a fluid sphere of the same size would experience in the absence of the particle, the added mass effect and the Basset history term. These various forces and factors are discussed in Chapter 2. Their paper investigated the motion of bubbles in two-dimensional vortical flows by performing numerical simulations. Tio et al (1993) introduced another equation which included a lift force term. For the analysis in this thesis, the Basset and lift force terms will be neglected.

One paper, in particular, spawned the work of this thesis. In "The Dynamics of Solid Particle and Bubble Groups" Topham et al (1994) studied the dynamics of a two phase thermal, and a particle motion equation similar to Auton et al (1988) is introduced. Forces due to gravity and buoyancy, acceleration of the local fluid element, added mass and drag are incorporated in their equation. Their particle model requires an assumed thermal flow field. Topham et al chose a background flow field consisting of a Hill's spherical vortex with potential flow theory outside of the vortex. J.S. Turner (1964) found these two flow fields together describe the fluid motion of a buoyant single phase fluid thermal very well. Turner assumed at any instantaneous moment, a Hill's spherical vortex of constant size and strength described the interior motion of a thermal. Other assumptions included a constant translational thermal velocity and linear thermal growth due to entrainment.

Topham et al performed four theoretical simulations, using the model described above, using 0.054 cm diameter polystyrene particles with a specific gravity of 1.04. For this size of particles, the terminal velocity is 0.635 cm/s in water. The four simulations were performed at uniform translational speeds of 1.0, 0.635, 0.50, and 0.45 cm/s. For the two higher speeds, some particles partially separated from the thermal, while others remained within it. The ones entrained, followed the internal circulation of the thermal. However, at longer times, all particles migrated towards the vortex center, on the outer edge of the thermal (symmetrical). For the two lower speeds, the particles separated more quickly from the thermal. Permanent particle separation from the thermal was observed for speeds lower than the terminal velocity of the polystyrene particles.

Originally, a goal of this thesis was to validate Topham et al's particle and fluid flow model using another type of particle. Glass particles were chosen because they can be obtained easily commercially in very accurate sizes. Laboratory experiments were performed using 0.0548, 0.046, 0.0358 and 0.0274 cm diameter glass particles, which all have a specific gravity of 2.50, and fluorescein dye. After performing a few experiments, it became apparent that the particle thermals, especially ones with 0.0274 cm diameter glass particles, do not travel at uniform velocities. The particle thermals visibly decelerated in the water tank. Therefore, at this point, a relationship for a nonuniform translational velocity was also added to the scope of this work.

It is well documented that single phase thermals have a velocity that varies inversely with the square root of time. In Chapter 8 of Scorer (1978) this relationship is

discussed. From the glass particle experiments performed in this work, the square of the distance travelled by the thermal and time were plotted. The same relationship as Scorer was found true for two phase thermals even with phase separation. It is believed that this relationship results from the separated particle's wakes being entrained into the thermal. As a result, a simple relationship was developed to incorporate a nonuniform velocity into the fluid flow model. The relationship was developed from the derivations for point source releases by Morton, Taylor, and Turner (1956). Since their relationship only describes the thermal velocity after the initial acceleration, it is necessary to determine the approximate time when the acceleration ends, and its respective maximum velocity. Lee (1992) developed a theoretical relationship to determine both of these parameters, which is used to determine the maximum velocity and time for glass particles. Lee's relationship is dependent on the specific gravity of the particles and the mass used.

For polystyrene particles Topham et al used a Stokes drag relationship in their particle model. However, the four glass particles sizes have terminal velocities in water in the non-Stokes flow regime. Therefore, it is necessary to modify the drag force term in their particle model. Two papers, one by Sene et al (1993) and the other by Tio et al (1993), both incorporated a non-Stokes drag term into an almost identical particle model. Sene et al used a very simple linear drag law and this is used here.

1.4 Organization of Thesis

This thesis consists of seven chapters in the main body and five appendices. The first half of Chapter 2 discusses the background fluid flow field used in the particle model. As mentioned previously, the background flow field consists of a Hill's spherical vortex within the thermal and potential flow theory outside. A nonuniform thermal velocity is also introduced in this section. The second half of the chapter discusses the particle motion equations. Several examples are presented in the later half of the chapter to demonstrate their use in the particle thermal model.

Chapter 3 contains a description of the experimental equipment used in the laboratory along with the procedure for performing experiments. The argon ion laser, used as a light source for the experiments, is discussed in detail. Other key components of the experimental apparatus include the water tank and the release mechanism. The various data parameters extracted from the videotapes of the experiments are explained in this section.

The laboratory observations are contained in Chapter 4, which includes raw data from several of the laboratory experiments and some digitized frames from the experimental videotapes. The raw data and frames are for the largest and smallest glass particles used in the experiments. The digitized frames show the sequential development of a particle thermal.

Chapter 5 consists of theoretical simulations performed for 0.0548 cm diameter glass particles for various flow conditions. The first half of the chapter considers a

thermal travelling at a uniform speed and the second half is for a nonuniform speed in the model. Both Stokes and non-Stokes drag relationships are used in the uniform and nonuniform thermal speed models. Results with a Stokes drag relationship in the thermal models are included for comparison purposes. The same simulations for 0.0274 cm diameter particles can be found in Appendix C. At the end of Chapter 5 a comparison is carried out with the theoretical polystyrene results from Topham et al and the 0.0274 cm diameter glass particle results, for similar flow conditions.

Chapter 6 compares the theoretical simulations with the laboratory experiments for the 0.0548 and 0.0274 cm diameter glass particles. For a uniform translational velocity, both Stokes and non-Stokes drag are examined while only non-Stokes drag is studied in the nonuniform case. Lastly, Chapter 7 contains all the findings and conclusions from this research and recommendations for future related research.

The first appendix contains the raw data for all the laboratory experiments performed. Only a couple of experiments exhibiting ideal thermal behaviour were examined in detail in the main body for 0.0548 and 0.0274 cm diameter particles. The second appendix contains more in depth derivations of equations included in Chapter 2. The third appendix contains theoretical results for 0.0274 cm diameter particles similar to those presented for 0.0548 cm diameter particles in Chapter 5. Appendix four includes examples of the computer code used to perform the theoretical simulations. Lastly, Appendix five contains a copy of Topham et al's paper entitled "The Dynamics of Solid Particle and Bubble Groups" (1994). It is beneficial to read this paper before reading the

remainder of this thesis, because it provides a good overview of research specific to the modelling of solid particle thermals. The pictures enclosed on the last page of their paper are of poor quality. Please refer to the pictures in Chapter 4 (pages 60, 61, 64 and 65), which show similar solid particle thermal behaviour to the ones enclosed in Topham et al's paper.

Chapter 2

Theory

2.1 Fluid Motion

2.1.1 Background

Turner (1964) suggested the use of an expanding Hill's spherical vortex and potential flow theory to model the fluid flow field of a thermal. He integrated the equations describing these two types of flows and solved for the flow field. His results compared closely with experimental results for turbulent buoyant single phase thermals. Figure 2.1 is a copy of a plot from his paper which shows the flow field for a rising buoyant thermal. The location of the fluid elements were made dimensionless by dividing their location at each time interval by the expanding radius of the thermal. At all

values of time the thermal, assuming a spherical shape, will have a dimensionless radius of unity. The plot shows the fluid streamlines around a buoyant single phase thermal. As the thermal moves upwards the external fluid, depending on its initial radial distance, can become entrained within the vortex. External fluid can be entrained at all points along the thermal boundary. The center of the vortex is located on the outer edge of the thermal. Not shown, is the right side of the thermal. Symmetry exists and it is a mirror image of the left, with circulation in the opposite direction. For a downward moving thermal, the fluid streamlines are in the opposite direction. Turner's flow field for a buoyant single phase thermal is the one used to model the background fluid motions of a negatively buoyant two phase thermal. Turner used spherical coordinates, whereas cylindrical coordinates will be used. Thermals with both uniform and nonuniform translational velocities will also be considered.

2.1.2 Internal Flow - Expanding Hill's Spherical Vortex

A Hill's spherical vortex is a constant axisymmetric vortex, where the vorticity distribution within the vortex is given by $\omega = \frac{15U}{2a^2} r$, and outside the vorticity is zero. The circulation around the vortex is $\Gamma = 5Ua$. Due to entrainment, a buoyant thermal spreads and grows in size. To use a Hill's spherical vortex it is necessary to have a thermal radius increasing in size, i.e., an **expanding** Hill's spherical vortex.

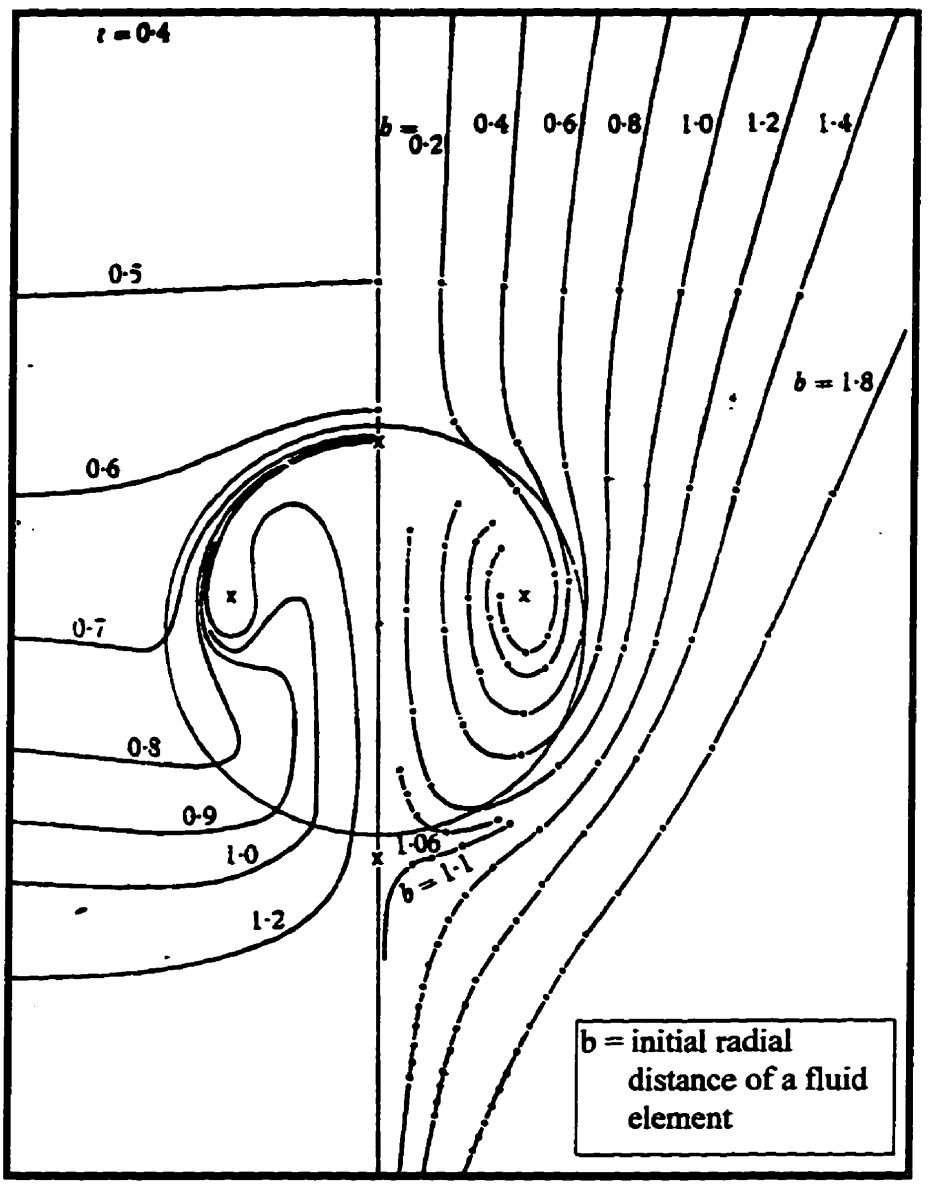

Figure 2.1 The motion of particles into an expanding spherical vortex, plotted using a coordinate system in which the spherical boundary is fixed in size. The tangent of the half-angle of spread is $\alpha = 0.25$. The right side of the diagram shows the paths of particles which started on a plane at right angles to the direction of motion. The points marked are separated by equal time intervals if the vortex has a constant forward velocity. The left side of the diagram shows the successive shapes into which a plane of fluid is distorted by the passage of the vortex. (Turner, 1964)

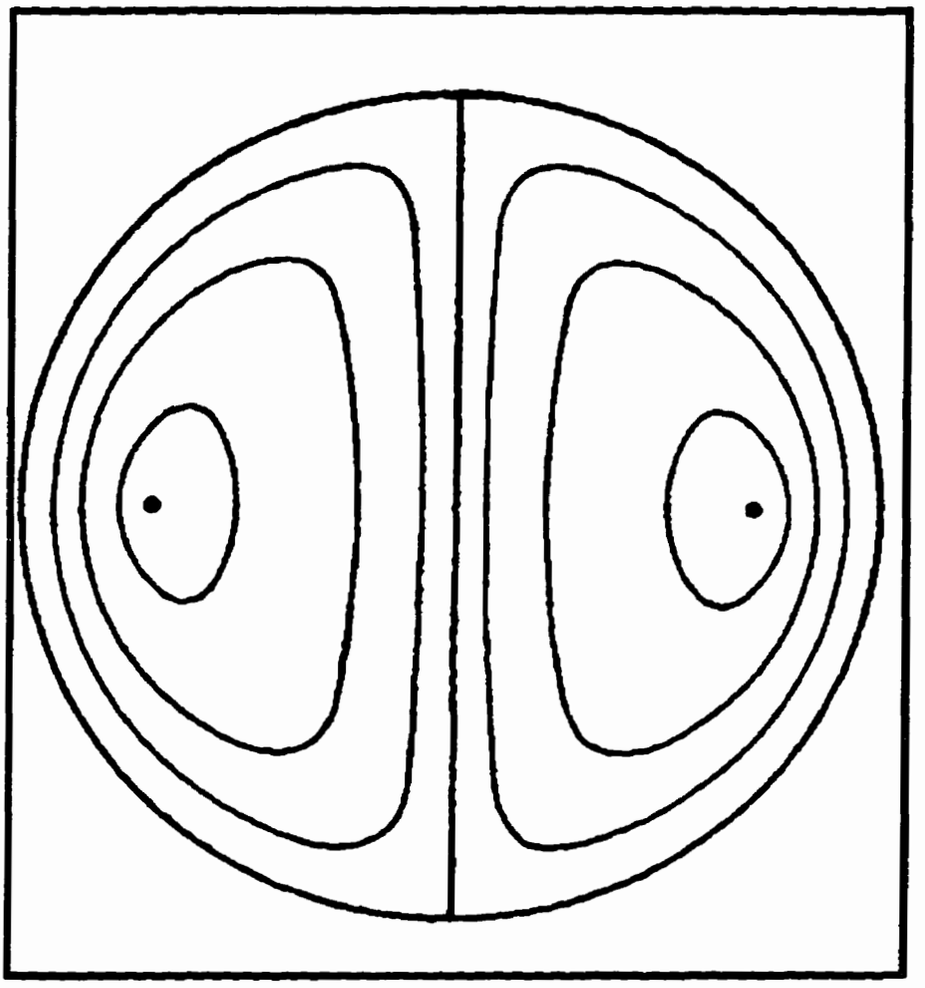

Figure 2.2 Streamlines of a Hill's spherical vortex. If a velocity U is impressed on the whole system from top to bottom there is a spherical vortex of radius a moving with velocity U in a fluid at rest. The motion of the fluid external to the vortex is irrotational. (Milne and Thomson, 1967)

Turner was the first to consider a Hill's spherical vortex this way. Considering the sequential development of a thermal, with constant velocity U, the vortex increases in strength, but is constant at any moment in time. To simplify the fluid flow model, Turner only considered a thermal travelling at a constant velocity U.

Starting with the stream function for a Hill's spherical vortex, in cylindrical coordinates, the axisymmetric velocity components can be determined. The stream function for a coordinate system fixed at the center of the vortex is:

$$\Psi = \frac{3Ur^2}{4a^2}\left(a^2 - r^2 - z_T^2\right) \qquad (2.1)$$

In the equation, r and z_T are the radial and vertical coordinates, U is the translational thermal velocity and a is the radius of the vortex or thermal. U and z_T are positive in the downwards direction. By partially differentiating equation (2.1) with respect to r and z_T the internal velocity flow field is:

$$u_z = \frac{3U}{2a^2}(2r^2 + z_T^2 - a^2) \qquad (2.2)$$

and

$$u_r = \frac{-3Urz_T}{2a^2} \tag{2.3}$$

A full derivation of the fluid flow field can be found in Appendix B. The linear radial growth of the vortex (thermal), defined by Turner is:

$$a = \alpha Ut \tag{2.4}$$

In equation (2.4) α is the entrainment coefficient, which is equal to the tangent of the half angle of spread in radians. The half angle of spread is approximately 15° making the entrainment coefficient equal to 0.25. By inserting equation (2.4) for the expanding radial growth of a thermal into equations (2.2) and (2.3) they now represent the velocity components of an expanding Hill's spherical vortex. This is the velocity flow field within a thermal.

At this point, Turner introduced dimensionless quantities to non-dimensionalize his fluid equations. This enabled him to solve for dimensionless quantities to create Figure 2.1. In this work equations (2.2) and (2.3) are numerically integrated as a system of equations in real time. Subsequent dimensionless plots are created by dividing the fluid locations in the radial r and vertical z directions by the expanding vortex radius a.

2.1.3 Potential Flow Theory

Potential flow theory can be used to model irrotational flow around spherical objects. By using potential flow theory to model the external flow field the thermal is considered as a stationary spherical object with flow approaching at velocity U. Starting with the stream function for potential flow theory, in cylindrical coordinates, the axisymmetric velocity components can also be determined. The stream function for flow approaching a stationary spherical object is:

$$\Psi = \frac{-Ur^2}{2} + \frac{Ua^3r^2}{2}\left(z_T^2 + r^2\right)^{-3/2} \tag{2.5}$$

The coordinate system is one fixed at the center of the spherical object and z_T and U are positive in the downwards direction. By partially differentiating equation (2.5) with respect to r and z_T the fluid flow field around the sphere is found. A full derivation is contained in Appendix B.

$$u_z = U\left[1 + \frac{a^3\left(r^2 - 2z_T^2\right)}{2\left(z_T^2 + r^2\right)^{5/2}}\right] \tag{2.6}$$

and

$$u_r = \frac{-3Ua^3 r z_T}{2\left(z_T^2 + r^2\right)^{5/2}} \tag{2.7}$$

Equations (2.6) and (2.7) represent the fluid flow field outside the boundary of a thermal.

2.1.4 Nonuniform Thermal Velocity

Turner (1964) assumed a constant thermal velocity to simplify his fluid model. In other research (e.g., Scorer (1978)) it has been shown that single phase thermals travel at nonuniform translational velocities. Figure 2.3 shows a linear relationship when the square of the vertical distance travelled by a single phase thermal is plotted versus time, which suggests a nonuniform velocity. In this work, identical plots were made with the experimental data for glass particle thermals (refer to Chapter 4). The same linear relationship was found. As a result, a nonuniform thermal velocity was added to the scope of this work.

Morton, Taylor, and Turner (1955) investigated the behaviour of plumes and instantaneous point sources (thermals). By manipulating their conservation equations for volume, momentum, and density deficiency relationships can be found for a nonuniform translational thermal velocity and the thermal radius. The three conservation equations

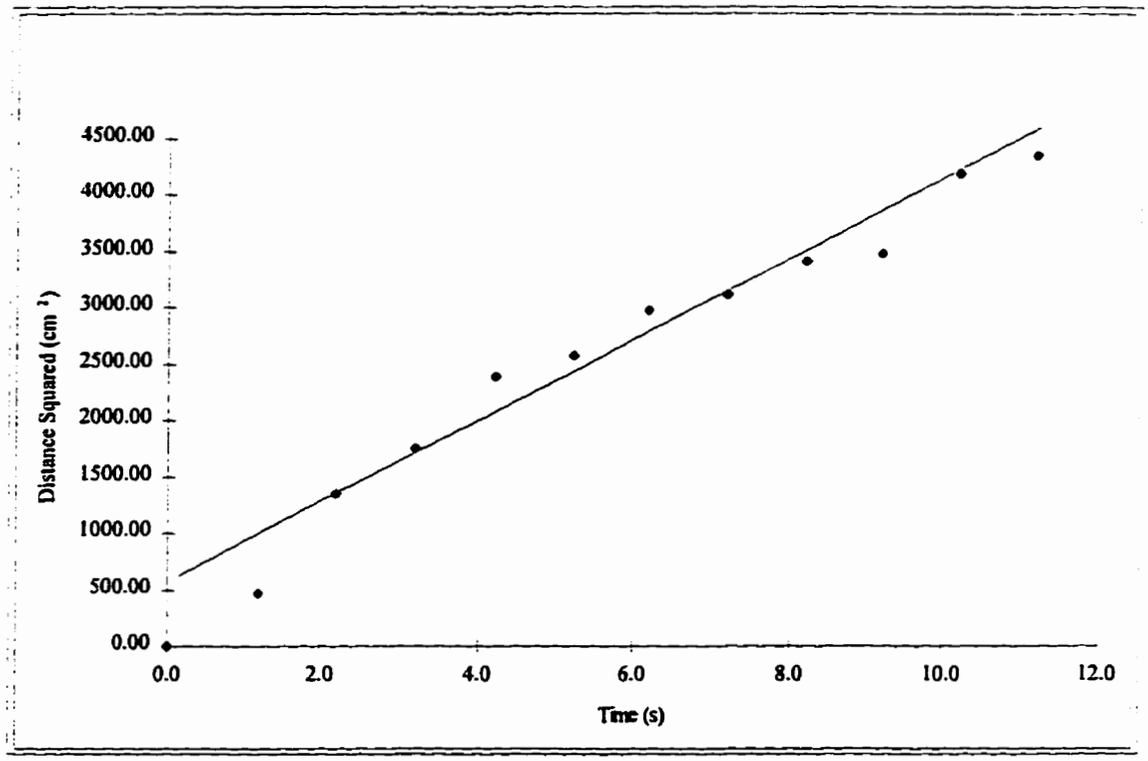

Figure 2.3 Square of Vertical Distance Travelled by a Thermal versus Time

for volume, momentum and density deficiency are:

$$\frac{d}{dt}\left(\frac{4}{3}\pi a^3\right) = 4\pi a^2 \alpha U \tag{2.8}$$

$$\frac{d}{dt}\left(\frac{4}{3}\pi a^3 \rho U\right) = \frac{4}{3}\pi a^3 g(\rho_0 - \rho) \tag{2.9}$$

$$\frac{d}{dt}\left(\int(\rho_1-\rho)\cdot d(\text{volume})\right)=4\pi a^2\alpha U(\rho_1-\rho_0) \qquad (2.10)$$

where:

a = mean radius of a thermal cloud
U(t) = the mean thermal velocity
αU = the rate of entrainment at the cloud surface
ρ = fluid density inside of a thermal
ρ_0 = fluid density outside of a thermal
ρ_1 = reference density of the system = $\rho_0(0)$ = density outside of a thermal at the point of release

From the above equations the following two relationships for the thermal radius a and velocity U are derived.

$$a=(2\alpha Q)^{\frac{1}{4}}t^{\frac{1}{2}} \qquad (2.11)$$

$$U=\frac{Q^{\frac{1}{4}}}{(2\alpha)^{\frac{3}{4}}t^{\frac{1}{2}}} \qquad (2.12)$$

where: $Q=a^3g\frac{(\rho_1-\rho)}{\rho_1}$, cm^4/s^2

t = theoretical time, s

Thus, from expression (2.12) the thermal velocity varies inversely with the square root of time, which is the behaviour Figure 2.3 suggests. Equation (2.11) shows a relationship

for the radial growth of the vortex for a nonuniform thermal velocity. A lengthy derivation of these equations is contained in Appendix B.

Introducing $K = \frac{Q^{\frac{1}{4}}}{(2\alpha)^{\frac{3}{4}}}$ as a constant reduces equations (2.11) and (2.12) to:

$$a = 2\alpha K t^{\frac{1}{2}} \tag{2.13}$$

$$U = \frac{K}{t^{\frac{1}{2}}} \tag{2.14}$$

2.1.5 Initial Theoretical Time

To use a nonuniform thermal velocity relationship in the particle and fluid models an appropriate initial theoretical time is required. Upon release, a thermal initially accelerates until its maximum velocity is reached. Equation (2.14) does not incorporate into it this initial acceleration phase, only the deceleration phase afterwards. Therefore, to perform theoretical simulations an initial time is selected when the maximum velocity occurs or at a time thereafter. The initial acceleration phase will be ignored.

Lee (1992) formulated equations for single phase thermals. From his equations, the maximum velocity and the thermal's corresponding size can be found. It is assumed that these equations are valid for two phase thermals because single phase behaviour is

observed for a period of time after release. This is due to the rapid turbulent mixing of the glass particles and dye.

The maximum velocity is dependent on the volume and mass of particles used. Table 2.1 gives the maximum thermal velocities for the various glass particles studied along with the theoretical times when they are achieved. Two velocities are given for 0.0359 cm diameter particles because two different masses were used in the laboratory experiments.

For the theoretical simulations performed in Chapters 5 and 6, an initial time is found by inserting a velocity equal to a value less than the maximum velocity into equation (2.14). The constant K is determined from the laboratory experiments, by taking the slopes of best fit lines on plots similar to Figure 2.3. Note, K is equal to the square root of the slope divided by a factor of two.

Table 2.1 Maximum Thermal Velocity

Particle Diameter (cm)	Mass Used (g)	Maximum Velocity (cm/s)	Time of Maximum Velocity (s)	Vortex Radius at Maximum Velocity (cm)
0.0274	14.60	-23.16	0.123	1.80
0.0359	15.20	-23.32	0.123	1.83
0.0359	22.80	-24.95	0.132	2.09
0.0460	22.20	-24.84	0.131	2.07
0.0548	22.80	-24.95	0.132	2.09

2.1.6 Frame of Reference

The current frame of reference is one centered on the vortex and moving with the same velocity as the thermal. This frame of reference is sufficient for a thermal moving at a constant velocity, but introduces problems for one moving at a nonuniform speed because of the accelerating frame of reference. Therefore, the frame of reference is transformed to one fixed at the point of release. By making a fixed frame of reference, the radial coordinate r remains unchanged, but the vertical coordinate changes. The new fixed vertical coordinate is designated as z and is shown in Figure 2.4. The theoretical time t = 0 s is for a point source release from the origin. Since the experiments are performed with a starting thermal radius a = 2 cm, and not from a point source, experimental and theoretical times do not correspond with each other. To avoid confusion experimental times are designated as t_e.

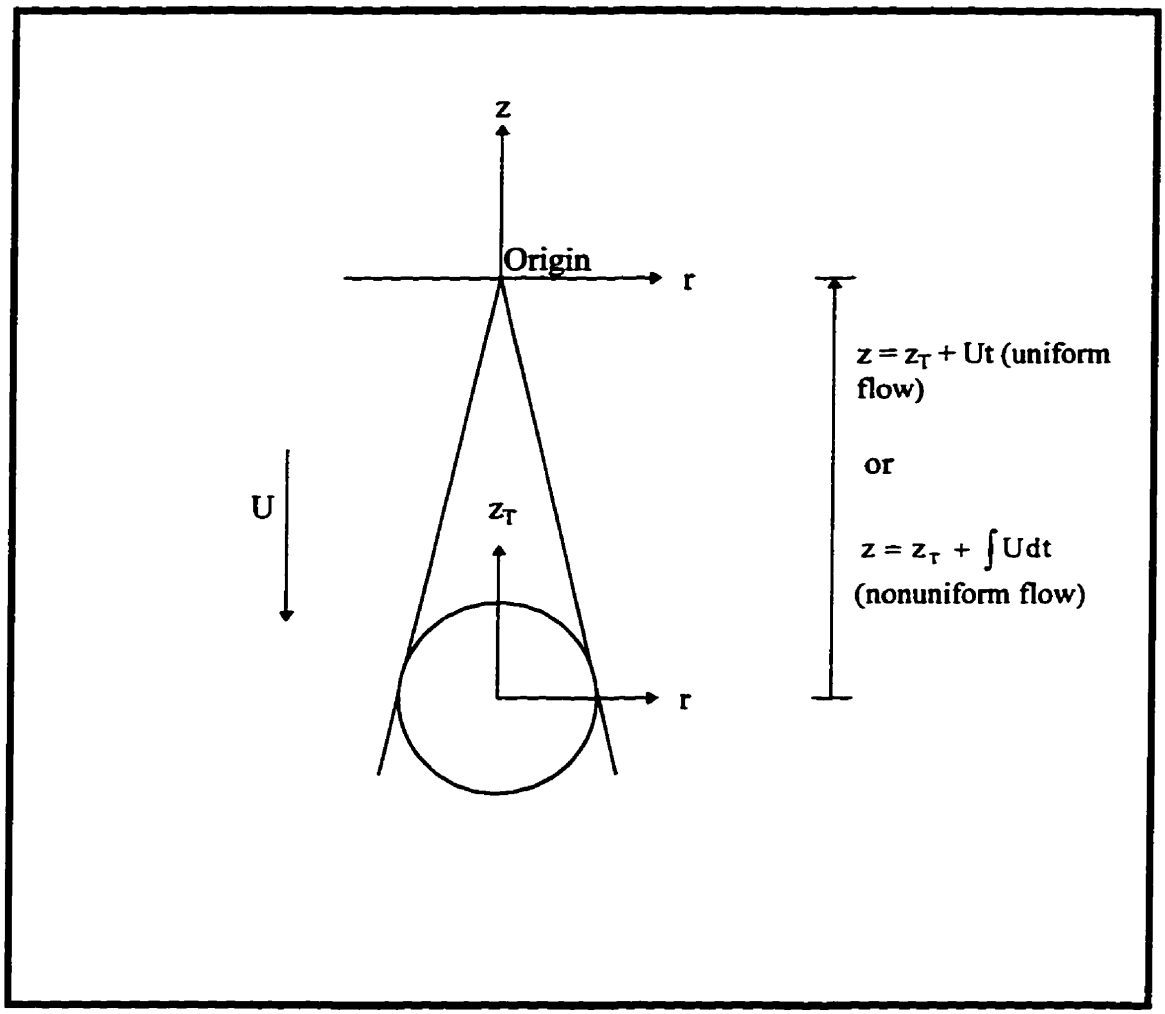

Figure 2.4 Frame of Reference

With a fixed frame of reference, with U and z positive upwards, the fluid flow equations for a nonuniform speed thermal are:

i.) Hill's Spherical Vortex

$$u_z = \frac{-3U}{2a^2}\left[2r^2 + \left(z - \int U dt\right)^2 - a^2\right] + U \tag{2.15}$$

$$u_r = \frac{3r\left(z - \int U dt\right)U}{2a^2} \tag{2.16}$$

ii.) Potential Flow Theory

$$u_z = -U\left[1 + \frac{a^3\left(r^2 - 2\left(z - \int U dt\right)^2\right)}{2\left(\left(z - \int U dt\right)^2 + r^2\right)^{5/2}}\right] + U \tag{2.17}$$

$$u_r = \frac{3a^3 Ur\left(z - \int U dt\right)}{2\left(\left(z - \int U dt\right)^2 + r^2\right)^{5/2}} \tag{2.18}$$

2.1.7 Assumptions

A summary of the assumptions in using a Hill's spherical vortex and potential flow theory to model the background fluid motions of a two phase thermal include:

- Assumed Flow Field — The flow inside and outside of a thermal is described using an expanding Hill's spherical vortex and potential flow theory.

- Spherical Thermal Shape — Actual thermals have a slightly flattened shape. The thermal is treated as a perfect sphere.

- Initial Theoretical Time — When a uniform thermal velocity is assumed in the models, the initial theoretical time is not an issue because the velocity relationship is valid for all values of time. For the nonuniform thermal velocity relationship, a theoretical time is selected when the thermal reaches its theoretical maximum velocity or at a time thereafter. It is also assumed that the theoretical maximum velocity relationship

given by Lee (1992) for single phase thermals can be applied for two phase thermals.

- Finite Thermal Boundary — There is a sharp boundary between irrotational fluid outside the thermal and rotational fluid inside. Entrained fluid quickly shares the vorticity of the inner fluid.

- Constant Vorticity — By using an expanding Hill's spherical vortex, it is assumed there are only small instantaneous differences in vorticity due to expansion and mixing.

- Inviscid Fluid — Viscous effects of the fluid are neglected.

2.2 Particle Motion

2.2.1 Background

There has been extensive theoretical work done modelling the behaviour of small particles in various types of flow situations. Maxey and Riley (1982) derived an equation of motion for small spherical particles in an unsteady nonuniform flow field. The intention of their work was to resolve problems in previously derived equations. More recently, Auton (1988) has also developed a similar equation of motion for a small particle moving through an inviscid fluid in which there is an unsteady nonuniform rotational velocity flow field. This type of flow field is used to describe the fluid motions of a two phase thermal.

Auton's equation of motion considers a small rigid sphere, of radius r_p, located at $\mathbf{Y}(t)$ in a flow field the velocity of which in the absence of the particle is $\mathbf{u}(t)$. The presence of the particle is assumed to have no influence on the flow field and the velocity of the particle $\mathbf{v}(t)$ is as follows:

$$m_p \frac{d\mathbf{v}}{dt} = \mathbf{g}(m_p - m_f) + (1 + k_p) m_f \frac{D\mathbf{u}}{Dt} - k_p m_f \frac{d\mathbf{v}}{dt}$$

$$+6\pi r_p \mu[\mathbf{u} - \mathbf{v}] + 6\pi r_p^2 \mu \int_0^t \frac{d(\mathbf{u} - \mathbf{v})/d\tau}{\sqrt{\pi\upsilon(t-\tau)}} d\tau - m_f C_L (\mathbf{u} - \mathbf{v}) \times (\nabla \times \mathbf{u}) \qquad (2.19)$$

In equation (2.19) m_p is the mass of the particle, m_f is the equivalent mass of fluid that the particle occupies, **v** is the velocity of the particle, **g** is acceleration due to gravity, k_p is the virtual mass coefficient that is equal to 0.5 for a spherical particle, μ is the dynamic viscosity of the fluid, υ is the kinematic viscosity of the fluid, t corresponds to time, τ is the time domain for the Basset history term, C_L is the lift coefficient which is equal 0.5 for a spherical particle and ω is the vorticity. The first term on the right side is the body force due to gravity and buoyancy, the second results from the acceleration of the local fluid element, the third is the force due to the added mass, the fourth is Stokes drag, the fifth term is the Basset history force and the last term is the force due to lift on the particle. The acceleration of the local fluid element considers the force a fluid sphere, of the same size, would experience in the absence of the particle. It should also be noted, that equation (2.19) employs two different derivatives. The first derivative,

$$\frac{D}{Dt} = \frac{\partial}{\partial t} + \mathbf{u} \cdot \nabla$$

corresponds to the (substantive) derivative following a fluid element. The second derivative,

$$\frac{d}{dt} = \frac{\partial}{\partial t} + \mathbf{v} \cdot \nabla$$

corresponds to the (total) derivative along the particle path.

The derivation of equation (2.19) is based on finding the forces associated with the undisturbed flow, without the particle, and with the disturbance flow created by the presence of the particle. One assumption necessary in order to obtain the force on a fluid sphere in an undisturbed flow is that the fluid sphere radius, r_p, must be small compared to variations in the flow length scale, L (i.e., $\frac{r_p}{L} << 1$). In summary, the equation of motion can be applied to small spherical particles with a wide range of densities and which obey Stokes drag law.

The Basset history force represents the memory effect of a highly viscous slow moving Newtonian fluid on the particle motion. In a paper by Reeks and McKee (1984), they investigated the influence of the Basset force on particle dispersion. They found the initial velocity difference between the fluid and the particle, when the particle is first introduced into the flow, characterizes the tendency of the particle to disperse later on. Reeks and McKee concluded that the Basset history had negligible effect when flow was turbulent. To simplify the model the Basset history is neglected in this work because it is believed to have small affect on particle motion in turbulent flow fields. The lift force term is also neglected in order to simplify the particle equation further. Equation (2.19) is reduced to:

$$m_p \frac{dv}{dt} = (m - m_f)g + (1 + k_p) m_f \frac{Du}{Dt} - k_p m_f \frac{dv}{dt} + 6\pi r_p \mu (u - v) \qquad (2.20)$$

which is the equation for particle motion studied here. With the use of a cylindrical coordinate system equation (2.20) becomes:

$$(m_p + k_p m_f)\frac{dv_z}{dt} = (m - m_f)g + 6\pi\mu r_p (u_z - v_z) + (1 + k_p) m_f \left[\frac{\partial u_z}{\partial t} + u_z \frac{\partial u_z}{\partial z}\right] \qquad (2.21)$$

and

$$(m_p + k_p m_f)\frac{dv_r}{dt} = 6\pi\mu r_p (u_r - v_r) + (1 + k_p) m_f \left[\frac{\partial u_r}{\partial t} + u_r \frac{\partial u_r}{\partial r}\right] \qquad (2.22)$$

Equations (2.21) and (2.22) are the equations of particle motion in the vertical and radial directions. Except for the buoyancy and gravity force term in the vertical direction, the equations are identical. The equations in this form are numerically integrated to solve for particle trajectories. It is necessary to assume an initial particle velocity at the moment of release in the theoretical model. Assuming no-slip between particles and fluid it is assumed that the particle velocity is equal to the local fluid velocity at the time of release.

2.2.2 Non-Stokes Drag

The glass particles studied vary in grain size from 0.0274 to 0.0548 cm and have a specific gravity of 2.50. The Stokes and non-Stokes Reynolds numbers are tabulated on page 35 for the various glass particles. The Reynolds number for Stokes drag is at the particles terminal velocity and the non-Stokes Reynolds numbers are at maximum and terminal velocities of the particles.

The terminal velocity of the particles is calculated from the force balance on a settling particle assuming a spherical shape. From the balance of drag and buoyancy forces, a general equation for the terminal velocity is:

$$V_T = \left[\frac{4}{3}\left(\frac{g}{C_D}\right)\frac{\rho_s - \rho_L}{\rho_L} d\right]^{1/2}$$

where: d = diameter of particle, cm
C_D = coefficient of drag
ρ_s = particle density, g/cm^3
ρ_L = liquid density, 1.0 g/cm^3 is the density of water at 5° C
V_T = terminal velocity of particle, cm/s

The expression for the terminal velocity varies depending on the Reynolds number of the settling particle. The coefficient of drag is a function of the Reynolds number, which is depicted in Figure 2.5 for the different flow regimes. Even though many particles are

involved, it is assumed that the terminal velocity for a single isolated particle can be used rather than the somewhat slower hindered settling velocity of closely spaced particles.

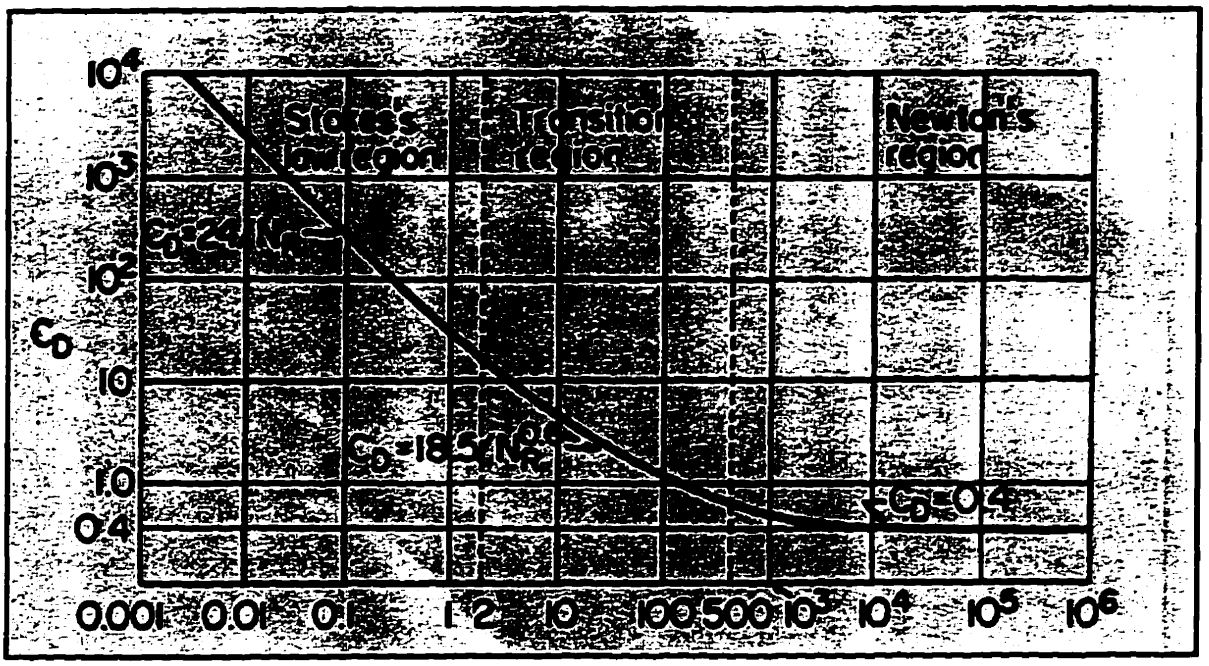

Figure 2.5 Correlation for drag coefficient for spherical particles (Ramalho, 1983) (N_R is equal to the Reynolds Number, Re)

Table 2.2 Stokes and Non-Stokes Reynolds Numbers and Terminal Velocities for Various Glass Particle Sizes

Diameter (cm)	Stokes Terminal Velocity (cm/s)	Stokes Re	Non-Stokes Terminal Velocity (cm/s)	Maximum Thermal Velocity (cm/s)	Non-Stokes Re (Terminal Velocity)	Non-Stokes Re (Maximum Velocity)
0.0548	-16.23	58.84	-6.10	-24.95	22.12	90.46
0.0460	-11.46	34.90	-5.00	-24.84	15.23	75.67
0.0359	-6.96	16.52	-3.76	-24.95	8.93	59.24
0.0274	-4.05	7.34	-2.76	-23.16	5.00	41.95

* Temperature = 5 °C (Dynamic Viscosity of Water = 0.0151 g/cm's)
Specific Gravity of water = 1.0

For spherical particles the Reynolds number is calculated by:

$$Re = \frac{\rho_L d v_z}{\mu_L}.$$

where: v_z is the vertical particle speed in cm/s
$\mu_L = 0.0151$ g/cm·s, is the dynamic viscosity of water at 5°C

Stokes drag lies in Re < 2, the transition region lies in 2 < Re < 500 and Newton's region lies in Re > 500. As can be seen all of the Reynolds numbers lie outside of the regime for Stokes drag. The Reynolds numbers are still small and the case of Stokes drag will still be studied for comparison purposes. Sene, Hunt and Thomas (1993) modified Auton's particle equation by inserting a non-Stokes drag relationship into it. For simplicity they proposed a linear drag law which they found sufficient for bubbles having a diameter less than 2 mm. In an earlier paper Sene (1985) found that the particular choice of drag law did not matter provided that an appropriate terminal velocity V_T is used. By replacing the Stokes drag term $6\pi\mu r_p(u_{r,z} - v_{r,z})$ in equations (2.21) and (2.22) with $g\left(\frac{m_p - m_f}{V_T}\right) \cdot w_{r,z}$ the equations are rewritten as:

$$\left(m_p + k_p m_f\right)\frac{dv_z}{dt} = (m - m_f)g - g\left(\frac{m_p - m_f}{V_T}\right) \cdot w_z + \left(1 + k_p\right)m_f\left[\frac{\partial u_z}{\partial t} + u_z \frac{\partial u_z}{\partial z}\right] \quad (2.23)$$

and

$$\left(m_p + k_p m_f\right)\frac{dv_r}{dt} = -g\left(\frac{m_p - m_f}{V_T}\right) \cdot w_r + \left(1 + k_p\right)m_f\left[\frac{\partial u_r}{\partial t} + u_r \frac{\partial u_r}{\partial r}\right] \quad (2.24)$$

where: $\boldsymbol{w} = \mathbf{u} - \mathbf{v}$, is the difference between fluid and particle velocities
V_T is the terminal velocity of the particle (non-Stokes terminal velocity in equations (2.23) and (2.24))

2.2.3 Assumptions

There are several assumptions used in the derivation of the particle motion equations. A summary of these are:

- Type of Flow — Even though the glass particles fall in the region of non-Stokes drag (Re>2), the case of Stokes drag (Re<2) will also be examined.

- Initial Particle Velocity — To solve for the particle trajectories, it is assumed the initial particle velocity upon release is equal to the fluid velocity at that location (i.e., no-slip).

- Assumed Flow Field — The background flow field consists of an expanding Hill's spherical vortex and potential flow theory. This type of flow field models the particle motions of a two phase thermal. For other flow applications, another flow field can be used to predict the particle motion as well.

- Multiple Particles — The particle motion equations follow the path of one particle. However, to model the trajectories of

multiple particles it is assumed that the different particle trajectories do not affect each other.

- Spherical Particles — Glass particles have an irregular grain shape, but the mean diameter is used to approximate a spherical particle.

2.2.4 Examples

To demonstrate how the particle model works, the following examples are performed with glass particles having a specific gravity of 2.50. The first set of examples show the trajectory of a single glass particle relative to the motion and expansion of the thermal. Each plotted point is obtained by dividing the radial r and vertical z_T components of the particle's trajectory by the thermal radius a for each time increment. At all values of time the thermal has a dimensionless radius of unity. This kind of plot helps to visualize the interaction between the particles and the flow field of a thermal.

Figure 2.6 shows the trajectory of a single glass particle, having a diameter of 0.0274 cm (Stokes drag assumed), travelling relative to a thermal with a uniform translational velocity of U = -4.05 cm/s. The uniform translational velocity is at the terminal velocity of the particle. Initially the glass particle travels outside of the thermal, but after time it starts to move upwards where it eventually becomes drawn into the vortex again. In this situation, the particle model uses an expanding Hill's spherical

vortex for the flow field within the thermal and switches to potential flow theory for fluid motions outside.

Figure 2.7 shows the same glass particle as in figure 2.6, but now non-Stokes drag and a nonuniform thermal speed are assumed. For this situation there is permanent particle separation from the thermal for longer values of time. An expanding Hill's spherical vortex is used to describe the flow field for the short period of time that the particle remains within the thermal and potential flow theory is used once the particle travels outside. In the nonuniform case, the thermal starts at a speed faster than the terminal velocity of the glass particle. As the thermal moves downwards the thermal slows down inversely with the square root of time. When the thermal starts to travel slower than the particle's terminal velocity, it not possible for the particle to become re-entrained within the thermal. To display this the largest glass particle size studied (diameter = 0.0548 cm) is used because it has the highest non-Stokes terminal velocity (-6.10 cm/s). The thermal has a speed of -2.0 cm/s at the end of the 25 second simulation.

To compare the theoretical and experimental data, it is necessary to model multiple particle trajectories. As stated before, one assumption in doing this is that each particle trajectory has negligible effects on each other. To track the behaviour of multiple particles, 14 glass particles are evenly distributed, within the initial 2 cm thermal, in the particle thermal model. Due to symmetry, only one half of a thermal is considered in the theoretical simulations.

Figure 2.8 is a plot of a thermal moving at a uniform speed with glass particles having a diameter of 0.0274 cm (Stokes drag assumed). However, the theoretical simulation is only 25 seconds in duration, which is the approximate length of the corresponding laboratory experiments. Some particles become entrained within the thermal while others do not. Referring back to Figure 2.6, if the simulation would have been performed for a longer time period, all of the particles would become entrained in the vortex again. Figure 2.9 is a plot of the same thermal as in Figure 2.8, but now conventional radial r and vertical z coordinates are plotted. This is useful to track particle growth and dispersion. Figures similar to these can be found in Chapters 5 and 6.

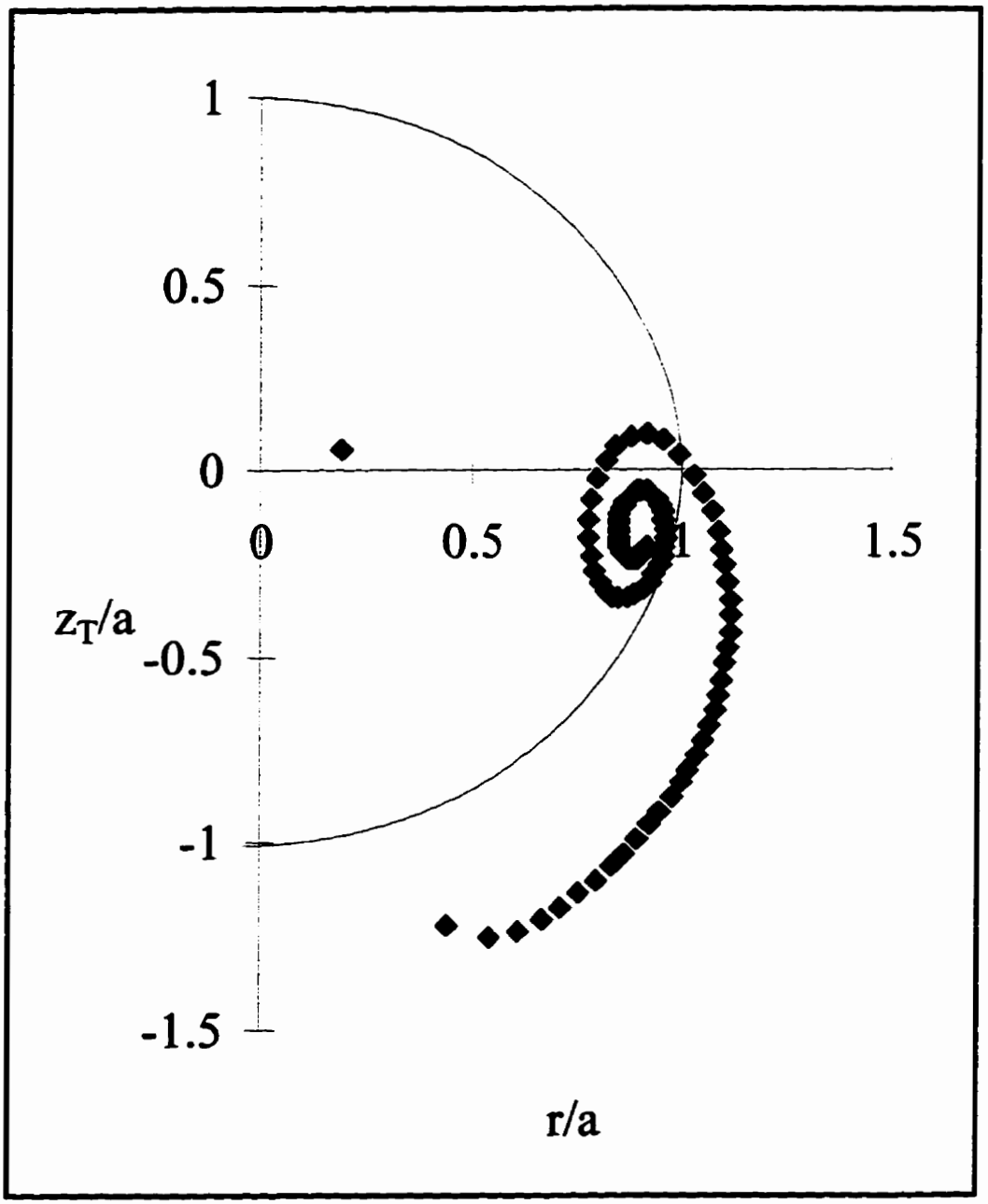

Figure 2.6 A single glass particle (diameter = 0.0274 cm) trajectory starting within a thermal having a uniform translational velocity (U = -4.05 cm/s). The experimental duration is 100 seconds and the particle started at the coordinates 0.38 cm (radial) and 0.12 cm within the initial 2 cm radius thermal.

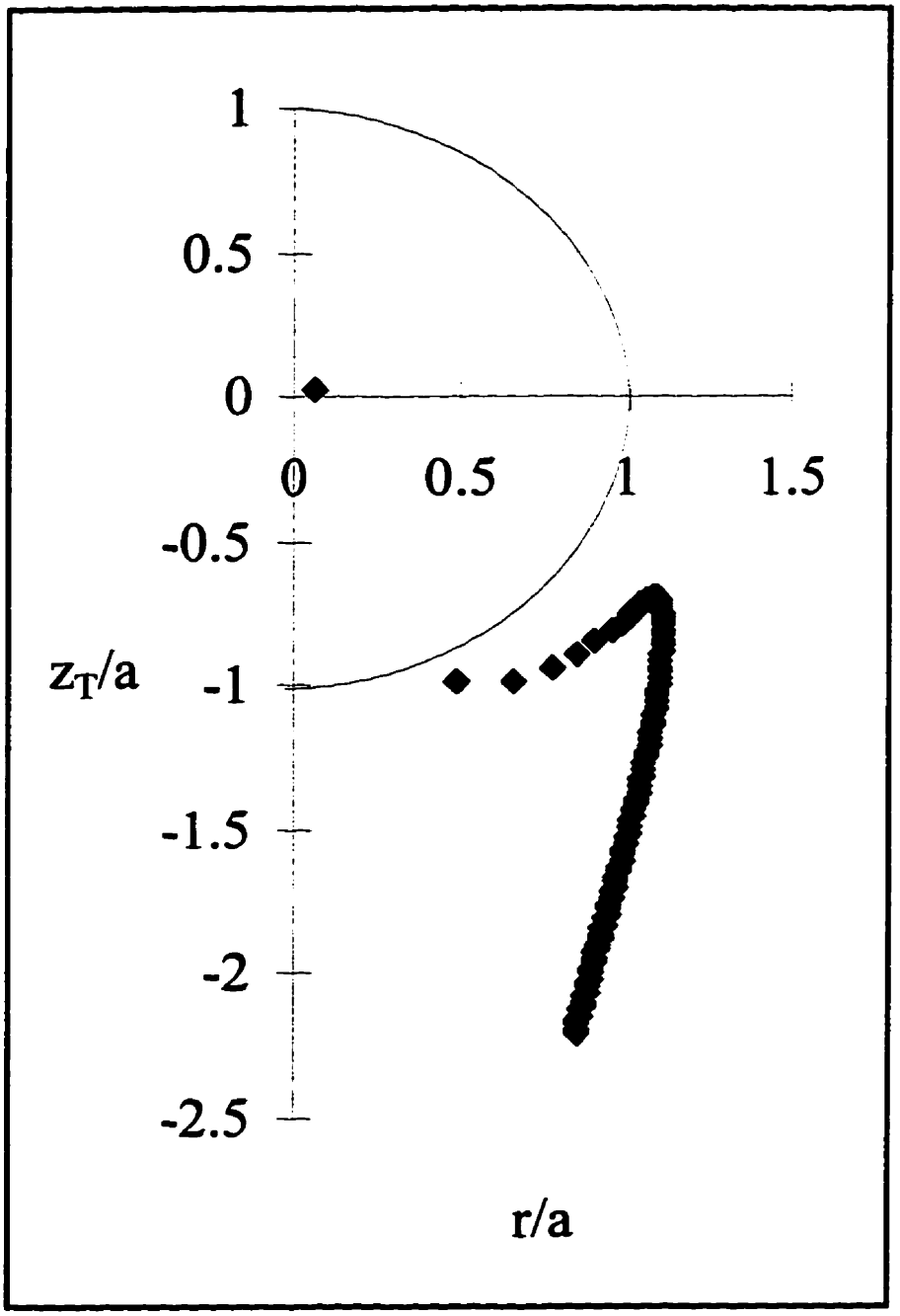

Figure 2.7 A single glass particle (diameter = 0.0548 cm) trajectory starting within a thermal having a nonuniform translational velocity (U = -25.0 cm/s to start; maximum thermal velocity). The experimental duration is 25 seconds and the particle started at the coordinates 0.38 cm (radial) and 0.12 cm (z direction) within the 2 cm initial thermal.

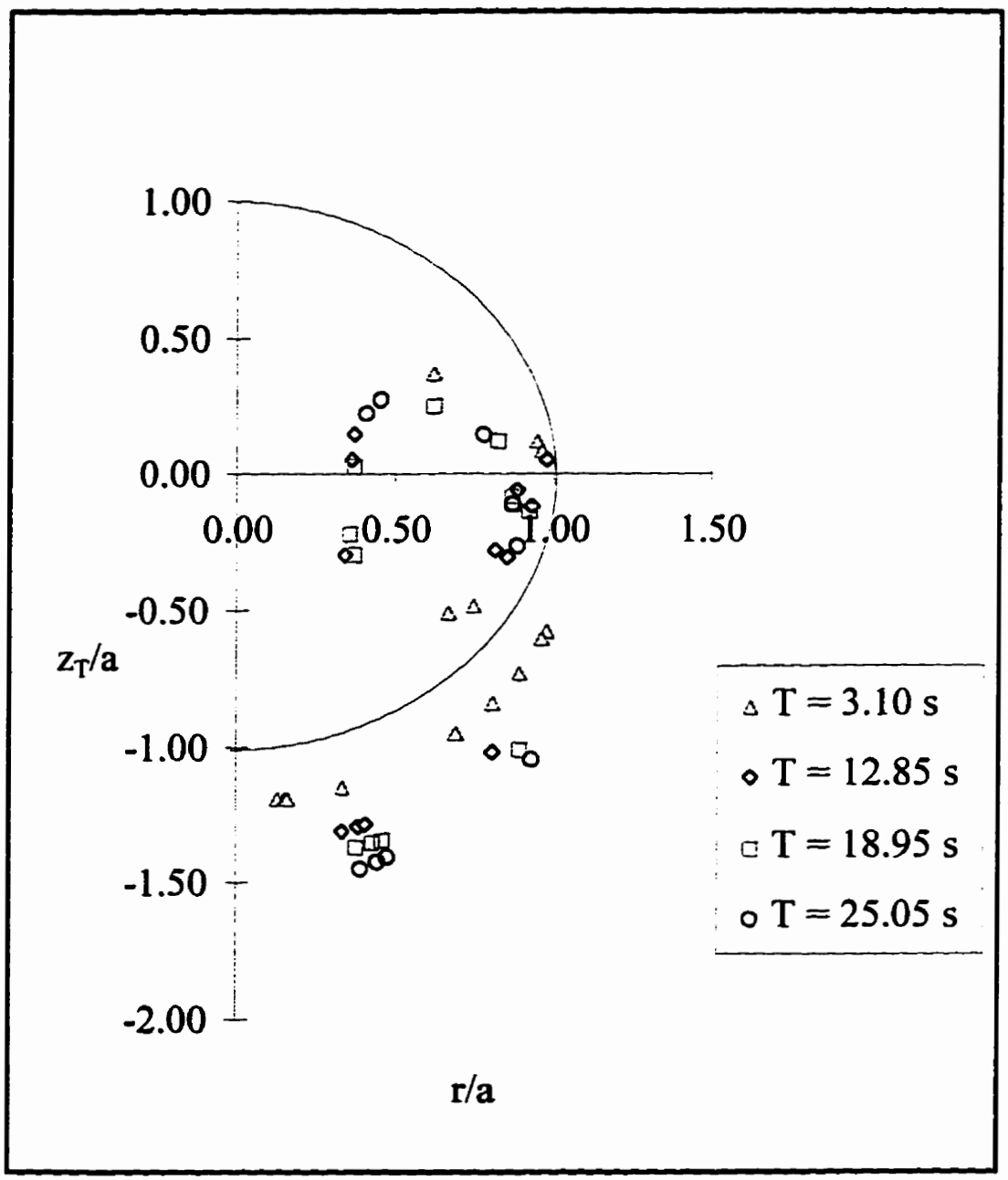

Figure 2.8 A dimensionless plot modelling the behaviour of 14 glass particles (diameter = 0.0274 cm) relative to the behaviour of the thermal. The thermal has a uniform translational velocity (U = -4.05 cm/s) and the experimental duration is 25.05 seconds.

Note: There is some particle overlap at each plotted time interval and there may not appear to be 14 particles.

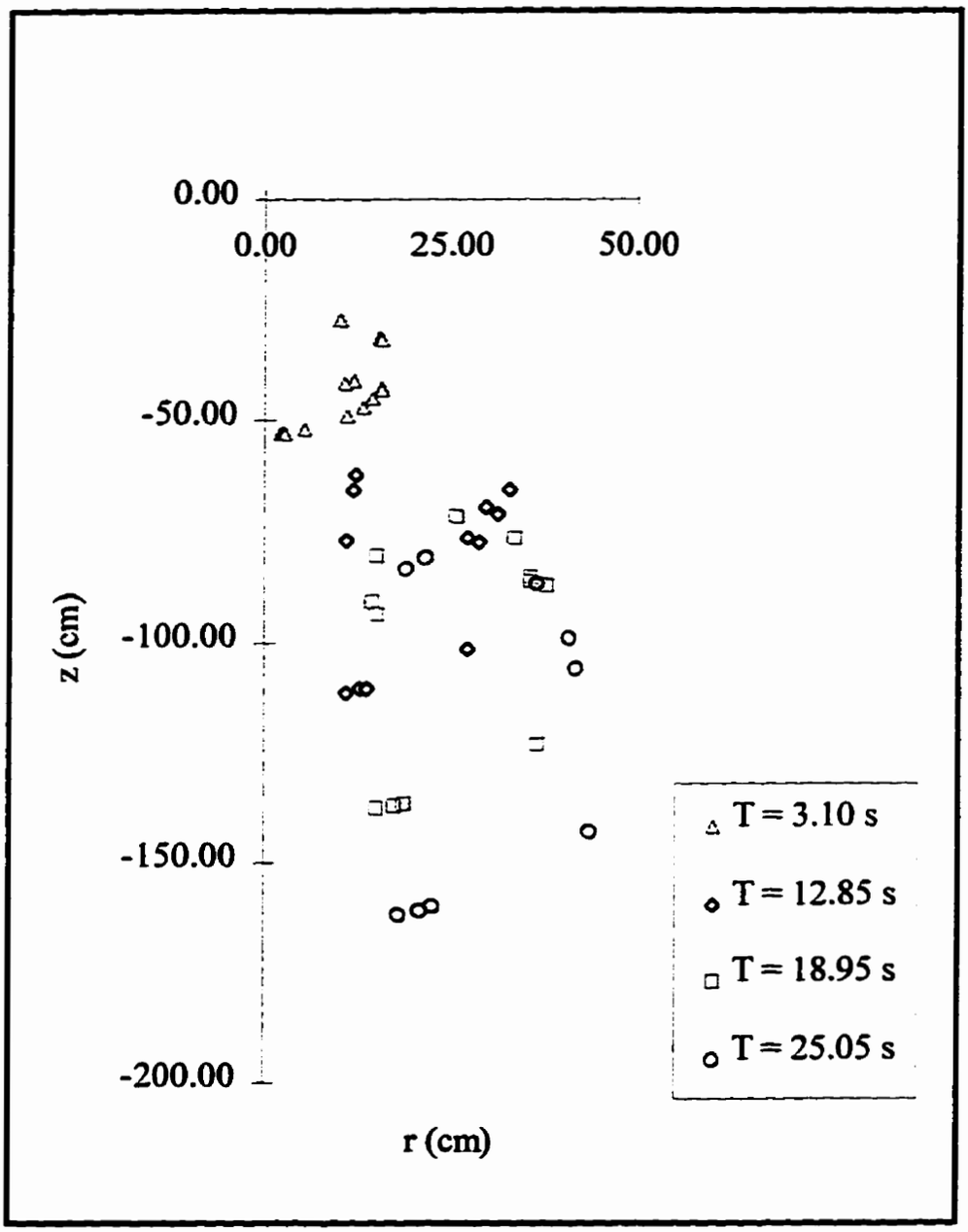

Figure 2.9 A plot modelling the vertical and radial motion of 14 glass particles (diameter = 0.0274 cm). The thermal has a uniform translational velocity (U = -4.05 cm/s) and the experimental duration is 25.05 seconds.

Note: There is some particle overlap at each plotted time interval and there may not appear to be 14 particles.

Chapter 3

Experimental Equipment and Procedure

3.1 Experimental Equipment

3.1.1 Water Tank

A water tank constructed for previous bubble experiments was used to conduct the thermal experiments. The 1.2 m high x 1.13 m wide x 1.13 m long tank was constructed of 1.90 cm thick Plexiglas and was filled with tap water having an average temperature of 5° C (μ=0.0151 g/cm·s). After filling, time was taken for the water to settle before performing experiments. The overall laboratory setup is shown in Figure 3.1.

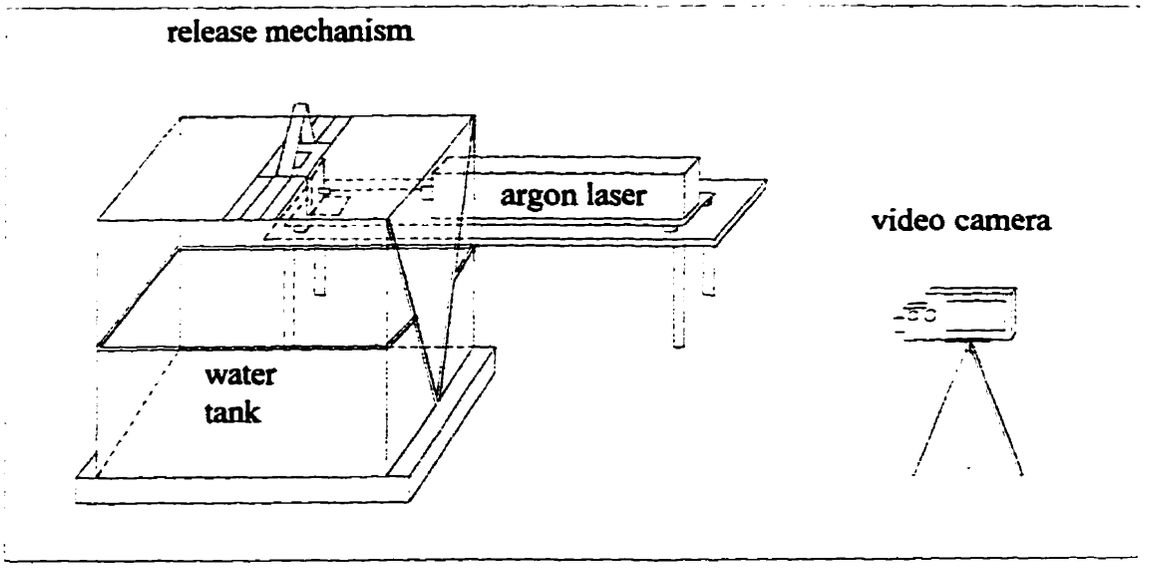

Figure 3.1 Laboratory Setup

3.1.2 Argon Ion Laser

A laser light sheet was used to illuminate a thin cross section of the particle thermal. To create a very thin vertical uniform sheet of light an argon ion laser (5500A) developed by Ion Laser Technology was used. This unit generated a polarized beam in the 457 to 514.5 nm wavelength range. The plasma bore matrix material in the laser is Beryllium Oxide (BeO). This laser model can produce beams ranging in power from 10 to 500 mW, which required three cooling fans due to the tremendous amount of heat produced from its operation. A 220 VAC power source was required.

The argon laser's short wavelengths are an extreme hazard to the eyes and several precautionary measures were required. First, appropriate laser safety goggles, for the 457 to 514.5 nm wavelengths, were worn. The goggles do not provide complete protection

and it is necessary to avoid direct or reflected beams. Second, any exposed skin was covered to prevent tissue damage. Lastly, the laboratory room was locked when the laser was in use to prevent accidental entry into the room. The laser unit has several built in safety features. A key was required in order to operate the laser and once powered up it took approximately 45 seconds for it to produce a beam.

The laser unit was placed on a support to provide stability during operation as well as making it maneuverable. At the opposite end of the support was a 1800 rpm electric motor. The end of the axle connected to the motor was ground to an angle of 45° and a high precision optical mirror (front faced) was placed on the bevelled end. The height and angle of the laser was adjusted so the laser beam lined up with the center of the mirror. By firing the laser onto the spinning mirror, an effective 360° sheet of light was produced. Figure 3.2 shows the laser unit, electric motor, mirror and support mechanism. As a safety precaution, the laser, electric motor and support were enclosed in cardboard to capture reflected laser radiation. To achieve an optimum light sheet, the laboratory lights were dimmed for the experiments.

Fluorescein dye (Uranin, $C_2H_{10}O_5Na_2$) was used to enhance the fluid portion of the particle thermal. The dye became excited by the short wavelengths of the laser beam and the illuminated cross section of the particle thermal fluoresced.

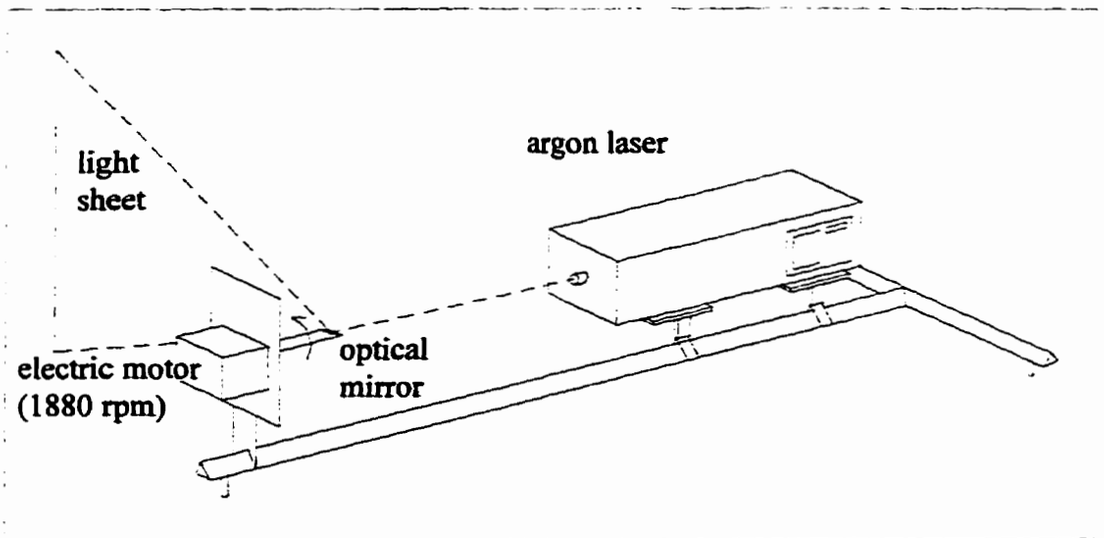

Figure 3.2 Laser Light Sheet Apparatus

3.1.3 Release Mechanism

A small, but important, experimental component was the release mechanism. The purpose of the release mechanism was to release the particle thermal uniformly into the water tank. It was also important not to add any initial impulse to the thermal. To achieve this, a spring loaded release mechanism was used. The main components included a 2 cm radius hemispherical cup, an elastic band, a release pin, torsion springs and a triangular support structure. Figure 3.3 shows a schematic drawing of the release mechanism. To operate the mechanism the elastic band was pulled in tension and the hemispherical cup was forced closed and held in place with the release pin. Next, the particles and dye were loaded into the cup. The release pin was then pulled, forcing the hemispherical cup apart, releasing the particle thermal into the tank.

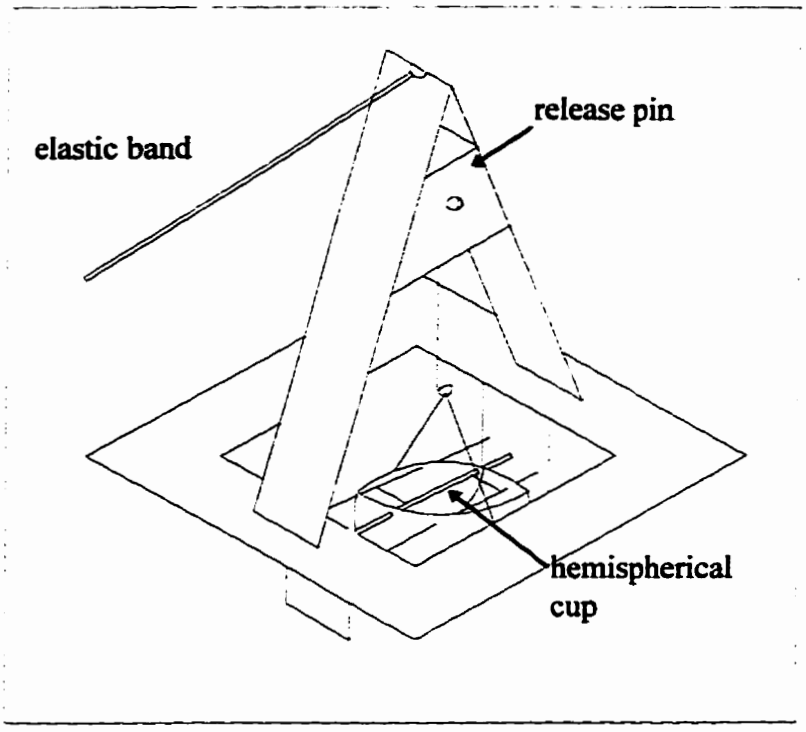

Figure 3.3 Release Mechanism

3.1.4 Video Camera

An Hitachi VM-5400A VHS video camera was used to videotape all of the experiments. The camera was operated manually in order to focus on the descending thermal in the tank. Before videotaping the experiments a removable grid was inserted in the middle of the tank and videotaped. This aided in the analyses of the thermals afterwards. The videotaped grid removed measurement errors due to refraction and parallax effects. The video camera was placed 2.5 metres from the tank.

3.2 Glass Particles

Four sizes of glass particles were used to perform the particle thermal experiments. In previous work by Lee (1992), polystyrene, having a specific gravity of 1.04, was used to perform particle thermal experiments. As an extension to his experimental work, glass particles were chosen because they have a different specific gravity (s.g. = 2.50) and can be found commercially in a wide assortment of sizes. Sieved glass particles were obtained from Canasphere Industries Limited in Calgary, Alberta. The following table shows the different sizes of glass particles used. All the particles have Reynolds numbers in the non-Stokes flow regime (Stokes: Re < 2.0). Glass particles were available in diameters smaller than 0.0274 cm, but they clumped together in water giving poor results. Therefore, 0.0274 cm was the smallest glass particle diameter studied. Note, the grain size is the mean diameter of the particles.

Table 3.1 Glass Particle Sizes with a Specific Gravity = 2.50

Grain Size (cm)	Stokes Terminal Velocity (cm/s)	Stokes Re	Non-Stokes Terminal Velocity (cm/s)	Non-Stokes Re (Terminal Velocity)
0.0548	-16.23	147.10	-6.10	22.12
0.0460	-11.46	87.25	-5.00	15.23
0.0359	-6.96	41.30	-3.76	8.93
0.0274	-4.05	18.34	-2.76	5.00

Water Temperature = 5° C (μ = 0.0151 g/cm·s)
Specific Gravity of Water = 1.0

3.3 Experimental Procedure

The experimental procedure did not change from one glass particle size to another. The laboratory experiments were performed using the following procedure.

1. The tank was filled with tap water to a level just above the hemispherical cup (1.53 m^3 of water).
2. A grid with 1 inch squares was inserted into the center of the tank. The grid was videotaped to aid in the analyses of the thermals afterwards.
3. The tank was allowed to settle for 30 minutes and then the water temperature was recorded.
4. The release mechanism was positioned over the center of the tank.
5. The release mechanism was cocked by pulling the elastic band and then the release pin was inserted.
6. A quantity of glass particles of one size were measured and weighed and loaded into the hemispherical cup. The particles were stirred to prevent clumping and to evenly distribute them in the cup.
7. Approximately 5 mL of fluorescein dye was added to the cup.
8. The laser safety goggles were donned.
9. The argon ion laser and the electric motor rotating the optical mirror were powered up. It took approximately 45 seconds for the laser to warm up.

10. The laser sheet was checked to make sure it sliced through the center of the tank.
11. The video camera was turned on.
12. The release pin was pulled from the release mechanism releasing the particle thermal into the water. With the different glass particle sizes, the duration of the experiments varied from approximately 10 to 25 seconds in length.

Many experiments were performed for each glass particle size and each were examined closely. The five best experiments of each particle size were selected for computer analysis. The data for these runs are contained in Appendix A.

3.4 Computer Analyses

Academic Computing, at the University of Calgary, provided all of the computer equipment and software necessary for the analysis of the laboratory experiments. A Macintosh IIC was used along with a Panasonic VHS VCR. The VCR had frame by frame advance capabilities, which was essential to capture individual frames from the experiments.

Two different software packages were used to analyze the videotape recorded of the glass particle thermal experiments. The first program, "Screenplay", a freeware package was used to capture and digitize frames from the videotape. Frames were captured in 1 second intervals. The second package, "NIH (Version 1.532B)" a utility

program from the National Institute of Health and Science was used to measure the digitized frames of the thermals captured in "Screenplay". The measuring tool used in the program was first calibrated with the digitized frame of the grid in the water tank. Several dimensions of the thermal were measured as well as the distance travelled by the thermal and the particles. Figure 3.4 shows the dimensions and distances measured and recorded.

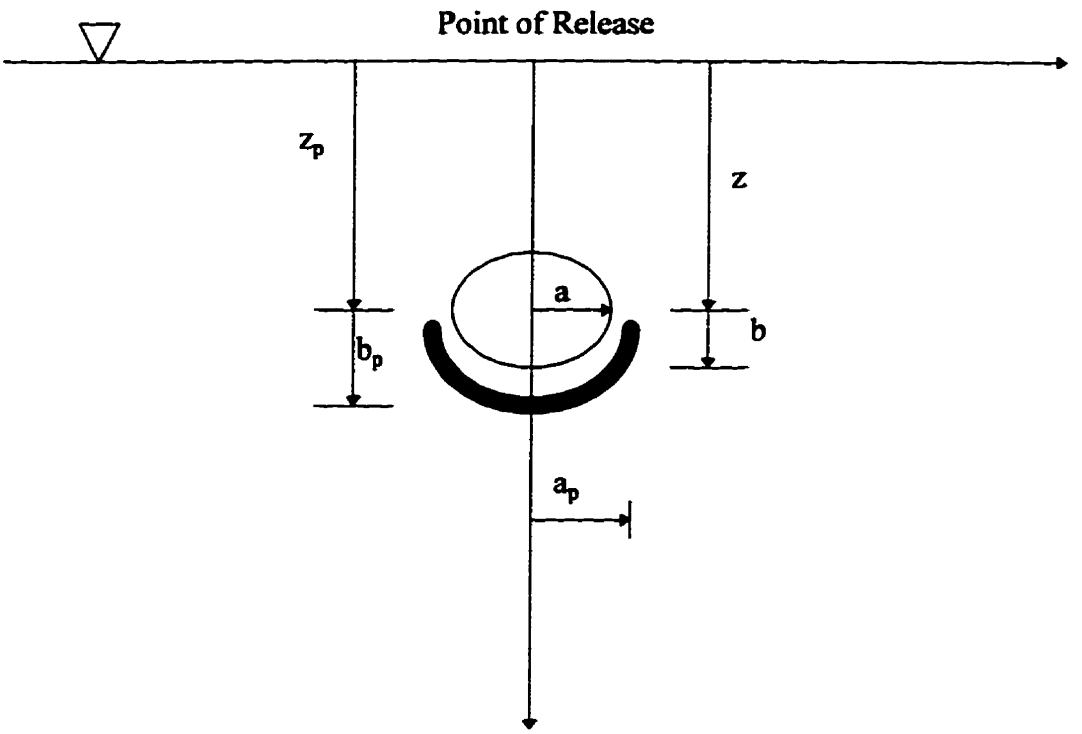

where:

a = the maximum radius of the thermal cloud (dye portion)
a_p = the maximum radius of the particle crescent
z = the vertical distance to the maximum radius of the thermal
z_p = the vertical distance to the maximum radius of the particle crescent
b = the vertical distance from the maximum radius of the thermal to its bottom
b_p = the vertical distance from the top of the particle crescent to its bottom

Figure 3.4 Dimensions and Distances Measured

Chapter 4

Experimental Observations

4.1 Introduction

Particle thermals were released without any deliberate initial impulse into an undisturbed water environment. Upon release the thermal fluid motion was turbulent, which was evident by the rapid mixing of the dye. Theoretically the particle thermal is considered as a perfect sphere in the flow field, but from the experiments it had an elliptical shape resembling a cumulus cloud. Symmetry existed for the fluid (dye) and particle portions of the thermal on good experiments. This was the main criteria used in determining those experiments selected for analysis.

The two phase thermals exhibited several phases as they developed and grew in size. They grew by entraining fluid from their exterior. Altogether there were four different phases displayed by the glass particle thermals. These phases are described below.

i.) Initial Acceleration Phase

Upon release into water the particle thermal accelerated until it reached its maximum attainable velocity. Unfortunately, this was only an observation from the experiments. It was not possible to extract data from the videotape for this phase, because it occurred very quickly with each particle size used.

ii.) Single Phase Behaviour

For a period after release, a particle thermal displayed single phase behaviour. In this phase no distinction could be made between the fluid (dye) and particle portions of the thermal. This behaviour was due to the rapid turbulent mixing and velocity of the initial thermal.

iii.) Two Phase Behaviour

As the thermal decelerated an apparent boundary was observed to form between the particles and the internal fluid. In this phase the particles continued to move in the internal circulation flow of the thermal, but there was an accumulation of particles at the

front end (leading face) of the thermal. There was no particle separation from the thermal when this behaviour was first noticed.

iv.) Particle Separation

Particle separation was observed when the thermal decelerated to a velocity lower than the terminal velocity of the particles. Fluid from the wake of the particles became entrained within the trailing thermal.

4.2 Experimental Observations

As mentioned in the previous chapter, four different sizes of glass particles were used in the laboratory experiments. The 0.0359, 0.0460, and the 0.0548 cm diameter particles displayed the four thermal phases described above while the 0.0274 cm diameter particles appeared to be missing the particle separation phase. However, as noted in Table 4.1 at $t_e = 14.0$ s, it became difficult to see the particles and this phase may not have been visible to the naked eye.

The following series of photographs were digitized from the videotape recorded during the laboratory experiments for the 0.0274 and 0.0548 cm particles. The other two particle sizes displayed all of the same thermal phases, but at progressively different time intervals. Three graphical plots for each particle size are included at the end of the chapter. One verifies the use of 0.25 for the entrainment coefficient α, the second shows

nonuniform velocity behaviour and the third is a velocity profile of the thermals. Raw data for all the laboratory experiments performed can be found in Appendix A.

4.2.1 Smallest Glass Particle Size (Grain Size = 0.0274 cm)

The first series of data and pictures were for laboratory experiment #3 for 0.0274 cm diameter glass particles. Refer to Figure 3.4 for a description of the various parameters in Table 4.1.

Figure 4.1 shows the particle thermal 1 second after release. At this point there was single phase thermal behaviour present, because no distinction can be made between the particles and fluid (dye) portions of the thermal. The thermal had already reached its maximum velocity and was starting to decelerate. In section 2.2.2, assuming non-Stokes flow for a nonuniform speed thermal the theoretical maximum velocity is -23.16 cm/s at t = 0.45 seconds (theoretical time measured from a point source release) for 0.0274 cm diameter particles. It was not possible to validate either of these values from the videotape, but the maximum velocity did occur at $t_e < 1.0$ s. The thermal had a very nice symmetrical shape at $t_e = 8.0$ s. The two bright fluorescing areas on the upper right and left hand sides were the two vortex centers of the thermal. It was difficult to see, but two phase behaviour was first observed within the thermal at this time interval. At 18 seconds the thermal had grown in size and was still in the same phase as in Figure 4.2. Referring to Table 4.1, the particles became increasingly harder to see and did not remain

visible after 18 seconds . It was impossible to predict when particle separation occurred for this particle size.

Table 4.1 Raw Data for 0.0274 cm Diameter Glass Particles (Run #3)

Experiment #3 - 14.6 g of 0.0274 cm Diameter Glass Particles (0.01 g/mL dye)
Date: March 30/94
Time: 2:40 PM

Measurement Scale = 1.57480 pixels/cm

t_c (s)	a (cm)	a_p (cm)	z (cm)	z_p (cm)	b (cm)	b_p (cm)	Observations
0.0	2.0	2.0	0.0	0.0	2.0	2.0	
1.0	6.0	6.0	15.2	15.2	5.1	7.0	Nice spherical thermal on release - single phase behaviour.
2.0	7.6	7.6	22.2	22.2	7.6	7.6	Single phase behaviour.
3.0	10.5	10.5	29.9	29.9	8.3	8.3	Single phase behaviour.
4.0	11.8	11.8	34.3	34.3	9.5	9.5	Single phase behaviour.
5.0	13.3	13.3	38.1	38.1	10.2	10.2	Single phase behaviour.
6.0	14.6	14.6	42.6	42.6	10.8	10.8	Nice symetrical thermal - single phase behaviour.
8.0	16.5	16.5	50.8	50.8	7.0	13.3	Start of two phase behaviour.
10.0	18.1	18.1	51.4	51.4	10.8	16.5	Two phase behaviour.
12.0	21.9	21.9	61.0	61.0	8.9	16.5	Two phase behaviour.
14.0	22.2	22.2	64.8	64.8	12.7	19.7	Harder to see particles.
16.0	23.2	23.2	64.1	64.1	15.9	22.9	Hardly see particles.
18.0	23.5	23.5	68.0	68.0	16.5	16.5	Can't see particles anymore - particle separation?
20.0	23.5	23.5	71.1	71.1	14.0	14.0	
22.0	23.5	23.5	75.6	75.6	19.7	19.7	
24.0	22.9	22.9	78.7	78.7	17.8	17.8	
26.0	22.5	22.5	82.6	82.6	20.3	20.3	
28.0	22.9	22.9	86.4	86.4	21.6	21.6	

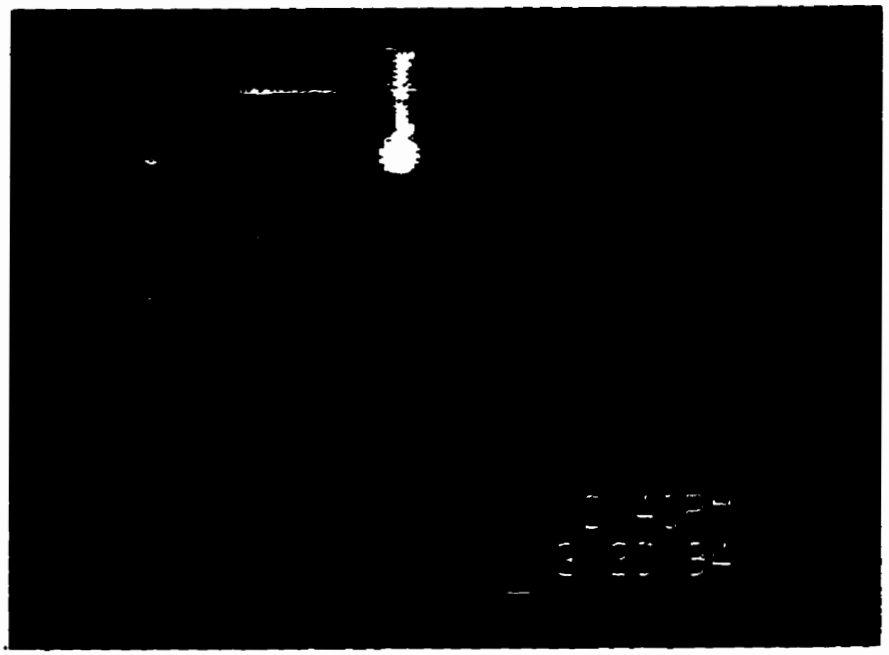

Figure 4.1 Time t_e = 1.0 second
15 g of 0.0274 cm Diameter Glass Particles

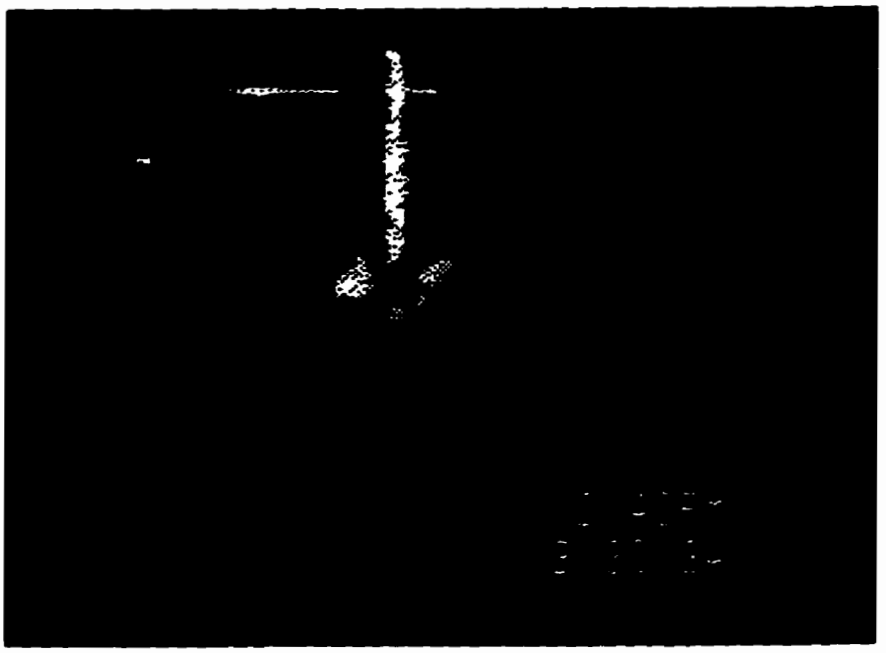

Figure 4.2 Time t_e = 8.0 seconds
15 g of 0.0274 cm Diameter Glass Particles

Figure 4.3 Time t_e = 18.0 seconds
15 g of 0.0274 cm Diameter Glass Particles

4.2.2 Largest Glass Particle Size (Grain Size = 0.0548 cm)

Figures 4.5 through 4.8 were for experiment #16 using the largest glass particles (diameter = 0.0548 cm). The particle thermal developed much more quickly and the four thermal phases could be seen clearly. The raw data for experiment #16 is given below in Table 4.2.

Table 4.2 Raw Data for 0.0548 cm Diameter Glass Particles (Run #16)

Experiment #16 - 22.8 g of 0.0548 cm Diameter Glass Particles (0.01 g/mL dye)
Date: April 14/94
Time: 6:34 PM

Measurement Scale = 1.57480 pixels/cm

t_e (s)	a (cm)	a_p (cm)	z (cm)	z_p (cm)	b (cm)	b_p (cm)	Observations
0.0	2.0	2.0	0.0	0.0	2.0	2.0	
1.0	5.7	5.7	15.9	15.9	5.1	5.1	Nice release- single phase behaviour.
2.0	8.3	8.3	27.9	27.9	7.0	7.0	Single phase behaviour.
3.0	10.8	10.8	35.6	35.6	5.1	7.6	Two phase behaviour.
4.0	10.8	13.3	37.5	47.0	8.3	9.5	Separation.
5.0	12.1	14.9	40.6	50.2	8.9	10.8	
6.0	13.3	16.5	47.0	57.2	7.6	11.4	
7.0	14.3	17.1	50.8	65.4	7.0	9.5	Nice particle crescent.
8.0	16.2	18.7	50.8	72.4	10.8	10.8	
9.0	15.9	20.0	52.7	78.7	12.7	11.4	
10.0	15.9	19.4	56.5	87.0	13.3	10.8	
11.0	17.8	21.0	60.3	94.0	12.7	10.8	

Figure 4.4 shows single phase thermal behaviour 1 second after release. The thermal had reached the point of maximum velocity and was already decelerating. Theoretically, for a nonuniform speed thermal assuming non-Stokes flow the maximum velocity is -25.0 cm/s at t = 0.47 seconds. The initial signs of two phase behaviour

(particles collecting at the front end of the thermal) can be seen in Figure 4.5. In the pictures the particles appear blue and the dye is green. For comparison, the 0.0274 cm diameter particles did not display two phase behaviour until $t_e = 8.0$ s. After 4 seconds, the particles were more visible at the head of the thermal, but were still captured within the thermal boundary. In Figure 4.6 the particles have started to separate from the thermal, and in Figure 4.7 the particles have moved farther in front. All of the pictures show very symmetrical thermal and particle behaviour. The wake of the thermal was missing in Figures 4.6, because the rotational speed of the optical mirror generating the laser light sheet was slower than the frame rate of the video camera.

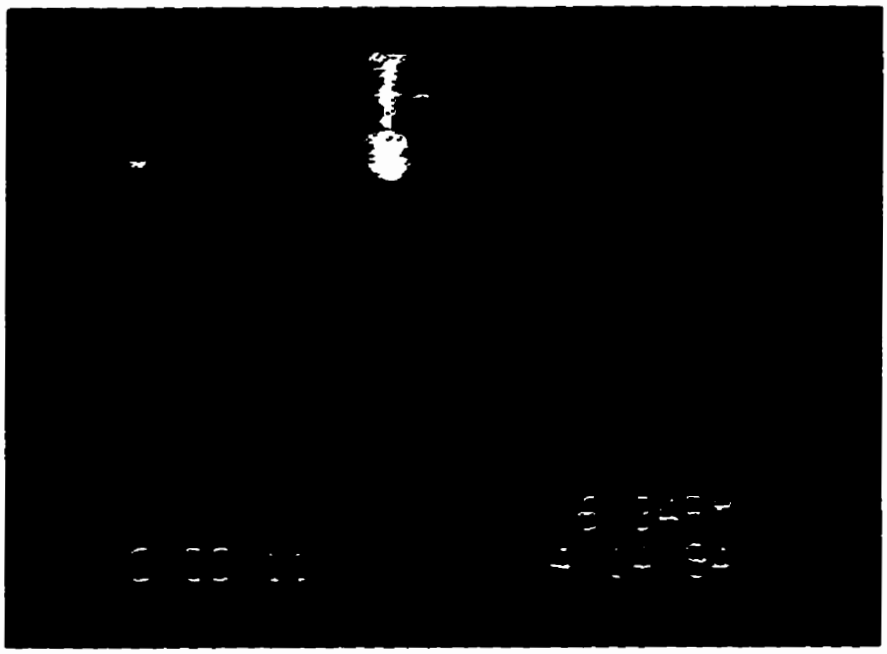

Figure 4.4 Time t_e = 1.0 second
22.5 g of 0.0548 cm Diameter Glass Particles

Figure 4.5 Time t_e = 3.0 seconds (Two Phases)
22.5 g of 0.0548 cm Diameter Glass Particles

Figure 4.6 Time t_e = 4.0 seconds (Close to Separation)
22.5 g of 0.0548 cm Diameter Glass Particles

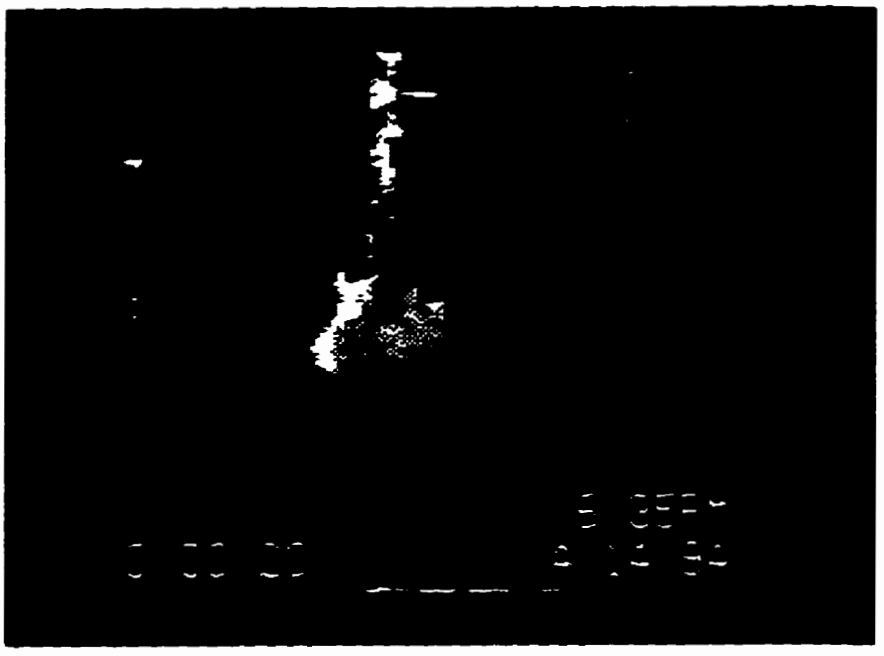

Figure 4.7 Time t_e = 10.0 seconds
22.5 g of 0.0548 cm Diameter Glass Particles

4.3 Thermal Behaviour

The theoretical fluid model uses an entrainment coefficient α which is equal to the tangent of the 1/2 angle of spread in radians. It is widely accepted, that 0.25 is an appropriate value for α for single phase thermals. Figures 4.8 and 4.9 are plots of the thermal radius versus the vertical distance travelled by the dye for experiments #3 and experiment #16. From these figures the entrainment coefficients were calculated to be 0.25 and 0.28. Identical plots were made for all the experimental data recorded and values close to 0.25 were found as well for α. Thus, it is a valid assumption to use 0.25 for the entrainment coefficient α in the theoretical model.

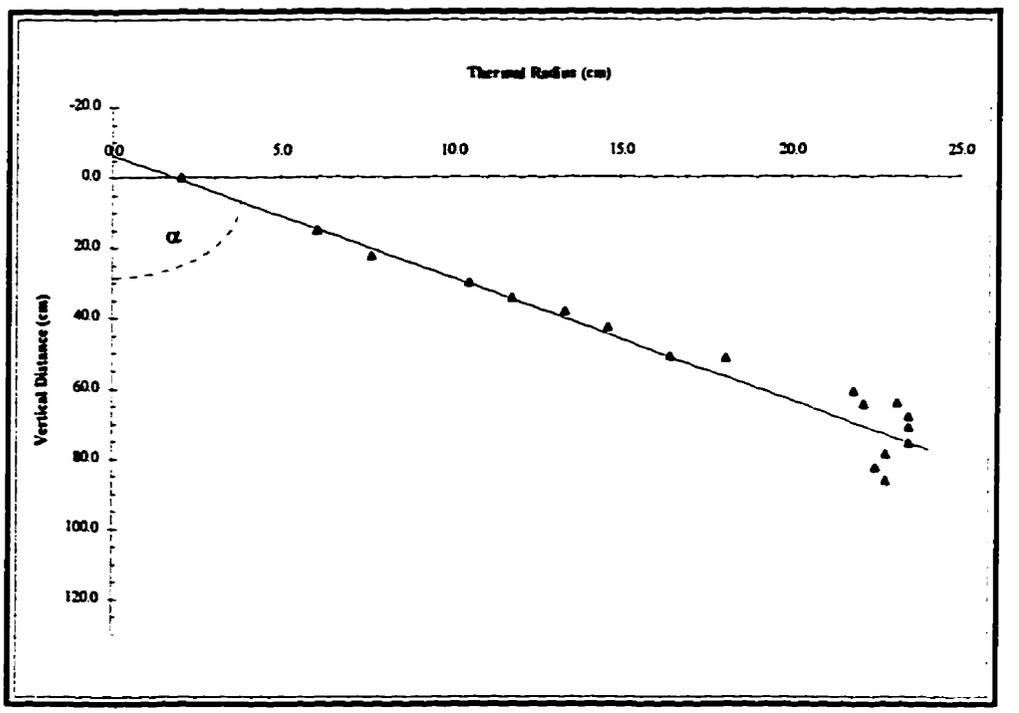

Figure 4.8 Thermal Radius versus Vertical Distance Travelled by Dye for 0.0274 cm Diameter Particle Thermals (Experimental Run #3)

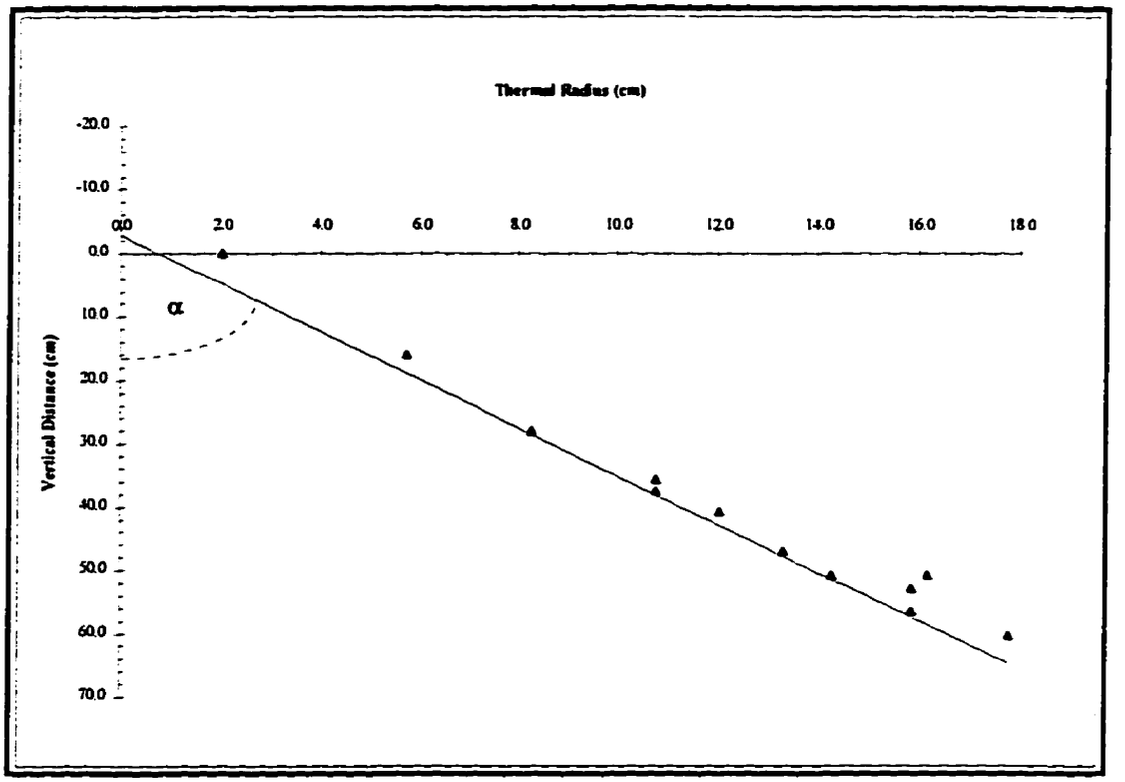

Figure 4.9 Thermal Radius versus Vertical Distance Travelled by Dye for 0.0548 cm Diameter Particle Thermals (Experimental Run #16)

In Figures 4.8 and 4.9 the best fit line is extended back to intersect the y-axis. This roughly corresponds to where a particle thermal would start if it were released from a point source rather than from an initial radius of a = 2 cm.

A linear relationship was observed by Scorer (1978) when he plotted the square of the vertical distance travelled by a single phase thermal versus time. During the glass particle experiments, nonuniform thermal velocities were observed. To verify this observation, the square of the vertical distance travelled by the glass particle thermals were plotted versus time. Figures 4.10 and 4.11 are the plots for experiments #3 and #16.

A linear relationship can clearly be seen in both figures. From the slope of the best fit line the K constant, discussed in Chapter 2, can be found for each experimental run. K is equal to the square root of the slope divided by 2. This value of K is used in the theoretical model for the nonuniform thermal speed case.

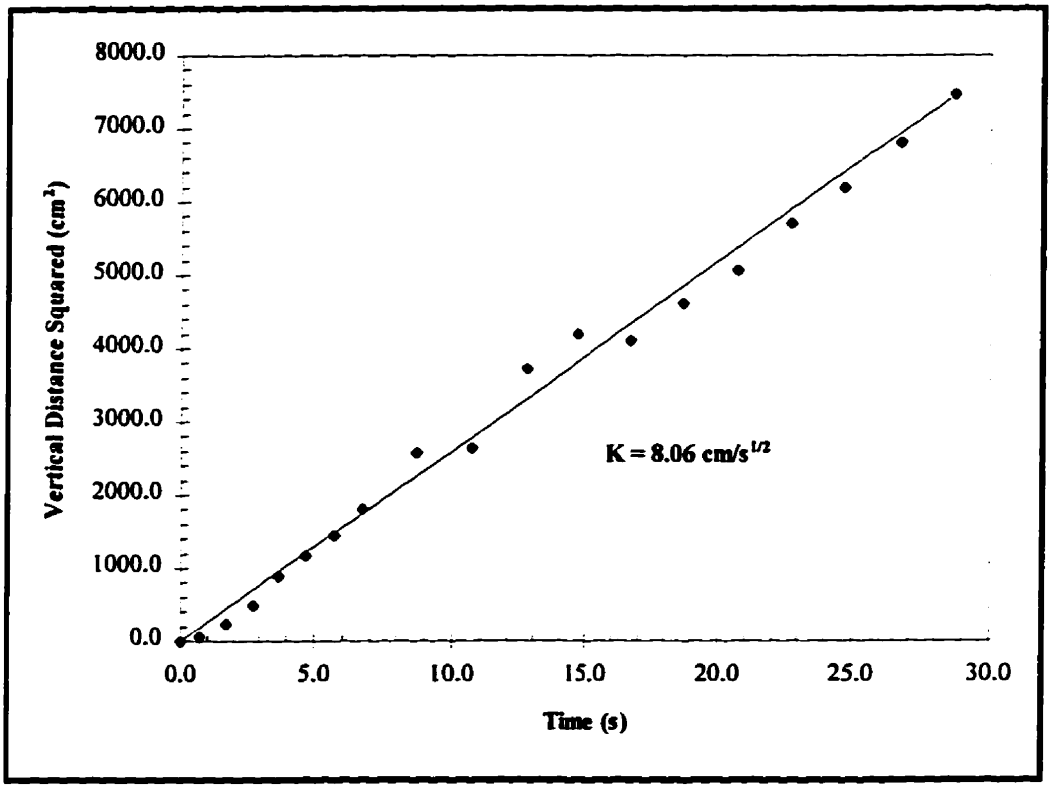

Figure 4.10 Dye Vertical Distance Squared (cm^2) versus Time for 0.0274 cm Diameter Particle Thermals

Figures 4.12 and 4.13 are plots of the velocity profiles for experiments #3 and #16. The vertical distance travelled by the dye portion of the glass particle thermals is plotted versus time. The thermals were decelerating at all of the time intervals. The

thermals experienced a short acceleration period upon release, but this happened very quickly and it was not possible to extract quality data for frames under 1 second in length from the experimental videotape. To illustrate the initial acceleration phase a curve has been drawn to represent this phase. The curves have been drawn according

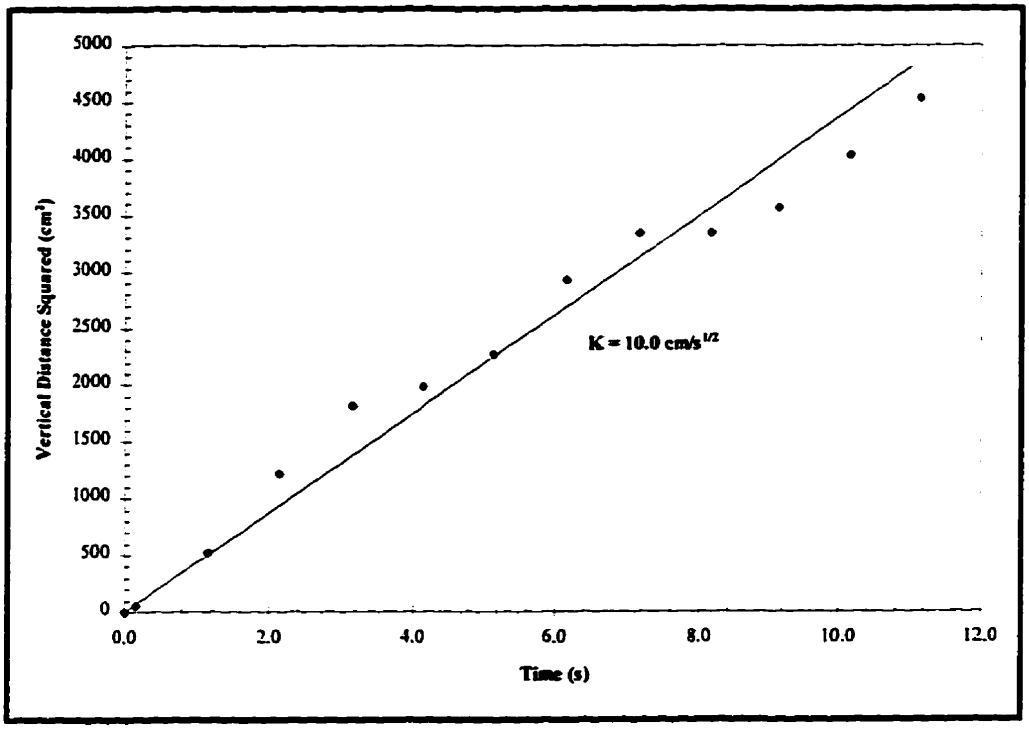

Figure 4.11 Dye Vertical Distance Squared (cm^2) versus Time for 0.0548 cm Diameter Particle Thermals

to what theory dictates for a nonuniform speed thermal assuming non-Stokes flow. The curves fit nicely with the rest of the data. From the two figures, the dye portions of the thermals did not experience any further changes in velocity when two phase behaviour or particle separation occurred. As a particle thermal entrains surrounding fluid and loses particles, it will gradually reach a state of neutral buoyancy. At this infinitesimal point in

time the thermal will come to rest. The travelling distance of the water tank was not long enough for the particle thermals studied here to approach this state. Two phase behaviour was first noticed at $t_e = 8.0$ seconds and at $t_e = 3.0$ seconds for the 0.0274 and the 0.0548 cm diameter particles, respectively. Particle separation occurred at $t_e = 4.0$ seconds for the 0.0548 cm diameter particles.

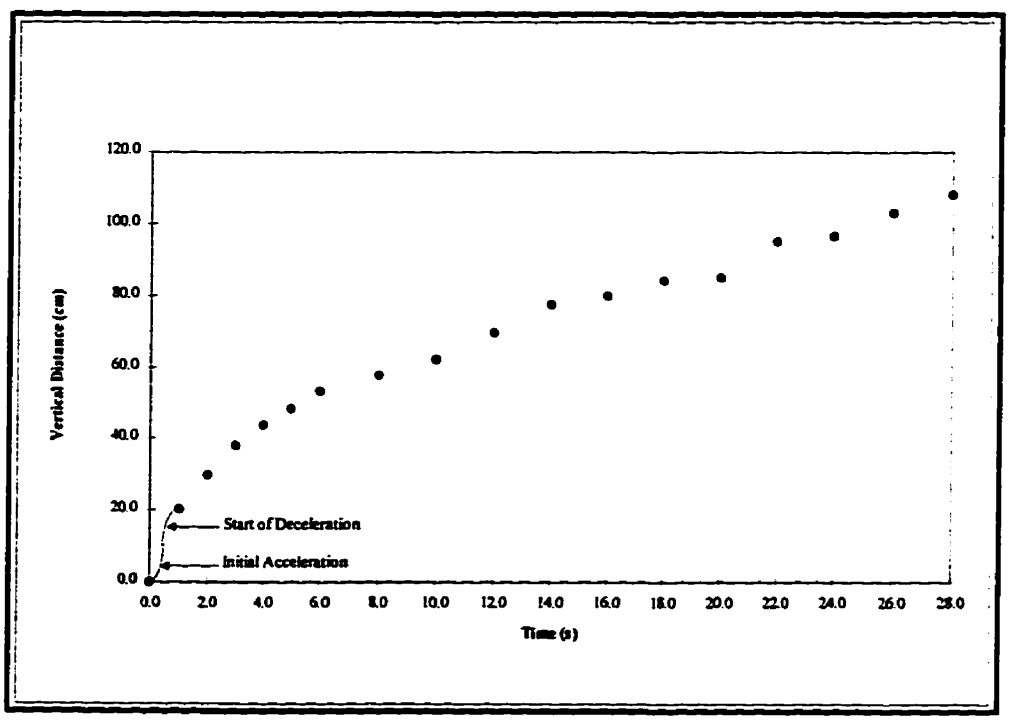

Figure 4.12 Velocity Profile of a 0.0274 cm Diameter Particle Thermal

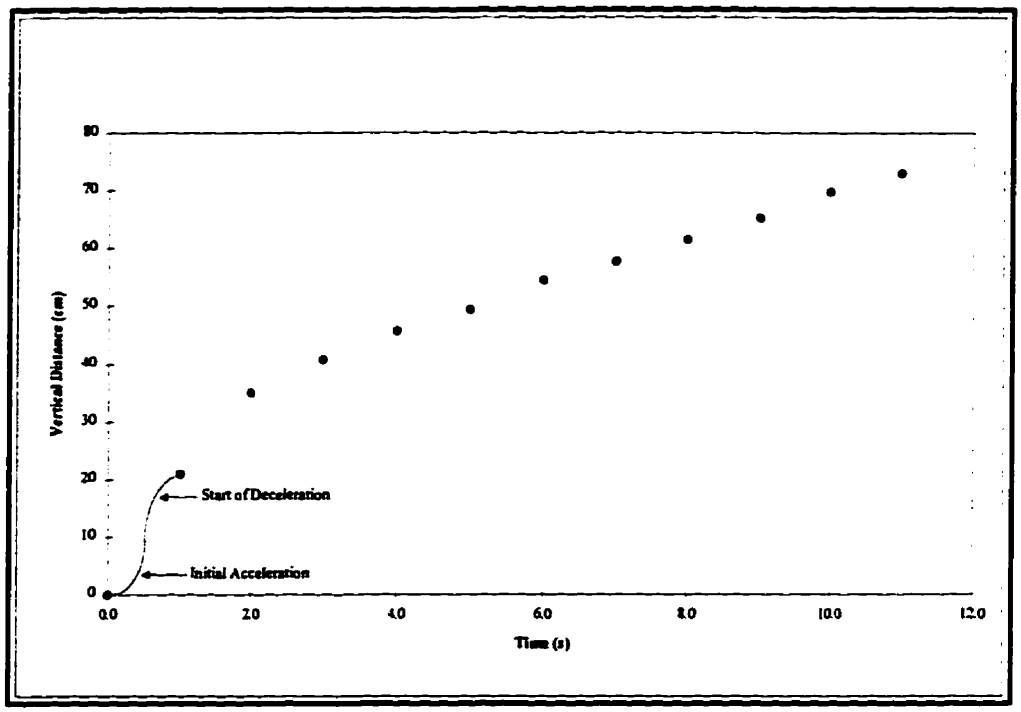

Figure 4.13 Velocity Profile of a 0.0548 cm Diameter Particle Thermal

Chapter 5

Theoretical Results

5.1 Introduction

Particle locations at various time increments were found numerically by solving the particle equations in Chapter 2. This was accomplished using the software package "Scientist" and a 80486DX 33 MHz computer with 8 Mb of RAM. "Scientist" is a Windows™ based program developed by MicroMath Scientific Software. Several numerical integration routines are available in the software including Euler, Fourth-order Runge-Kutta, Error Controlled Runge-Kutta, Bulirsch-Stoer and an Episode package.

The Episode package was used to perform all of the theoretical simulations, which is the program's most advanced integration routine. It can solve both stiff and

non-stiff differential equations using variable error control. The routine was initialized to run all the simulations using the non-stiff option with a relative error size of 1×10^{-5}. The routine in this format gave the most consistent results. "Scientist" requires some computer code, which contains the differential equations for the particle and fluid models in radial and vertical coordinates, a list of variables to solve numerically, values for the constants, initial conditions and the time duration of the simulation. Samples of this code for non-Stokes and Stokes drag relationships for both uniform and nonuniform speed thermals can be found in Appendix D.

The theoretical initial thermal ($a = 2.0$ cm) contains 14 evenly distributed particles. This number of particles gives a good representation of how the particles behave throughout thermal development without making the calculations too cumbersome. Initially, 80 particles were used for the computer generated results. However, calculations became too long and they did not prove to be anymore representative than using 14 particles in the model. Five time intervals are plotted on each graph from the computer results. The time intervals for all the plots are from 0 to 50 s, which encompasses the duration of all the laboratory experiments with the four particle sizes studied.

To avoid repetition, only the 0.0548 cm diameter glass particle size results are presented in sections 5.2 and 5.3 for uniform and nonuniform speed thermals. Results for 0.0274 cm diameter glass particles can be found in section 5.4 and Appendix C. Stokes

and non-Stokes drag relationships are examined for each of these situations. In the uniform case, three different uniform velocities are examined. One velocity is faster than the terminal velocity of the particle, one equals the terminal velocity and the other is slower. Topham et al (1994) presented their results for polystyrene particles in this manner. Thus, by doing the same a comparison can be carried out between the results presented here and those in their paper (section 5.4). For the nonuniform speed thermal, laboratory run #16 was chosen to determine a K value because this experiment exhibited the best ideal thermal behaviour using 0.0548 cm diameter particles. The K value is determined from the slope of the best fit line in Figure 4.11 in the previous chapter.

5.2 Uniform Thermal Speed

5.2.1 Stokes Drag

An example of the starting locations and fluid velocities of the 14 particles in the initial a = 2 cm theoretical thermal using a uniform speed are shown in Table 5.1. The initial conditions are for a thermal having a uniform speed of -25.0 cm/s. This speed is what theory predicts as the maximum velocity for a thermal with this volume of 0.0548 cm diameter glass particles. In the laboratory experiments the particle thermals were released from a hemispherical cup having a radius of 2 cm. Since the particles are not starting from a point source, the initial theoretical starting time t is not equal to zero. For a uniform speed thermal the initial theoretical time is the time for a thermal to grow

to a radius of a = 2.0 cm. The uniform thermal velocity corresponds to U, the initial radial coordinate is r, the initial vertical coordinate relative to the thermal center is z_T, the initial vertical coordinate extrapolated back to the point source release is z, and U_r and U_z correspond to the radial and vertical velocity components of the fluid flow field. The computer program "Scientist" uses the initial conditions of the 14 particles in Table 5.1 to start the computer simulation.

Table 5.1 Initial Starting Conditions for 0.0548 cm Diameter Glass Particles
Uniform Speed Thermal with Stokes Drag
Thermal Speed U = -25.0 cm/s

Particle No.	t (s)	U (cm/s)	r (cm)	z_T (cm)	z (cm)	U_r (cm/s)	U_z (cm/s)
1	0.32	-25.0	0.4	0.1	-7.9	-0.4	-34.7
2	0.32	-25.0	1.5	0.5	-7.5	-7.0	8.1
3	0.32	-25.0	1.0	0.7	-7.3	-6.5	-15.1
4	0.32	-25.0	0.5	0.7	-7.4	-2.9	-29.4
5	0.32	-25.0	0.1	0.4	-7.6	-0.4	-35.9
6	0.32	-25.0	0.5	1.5	-6.5	-7.0	-11.3
7	0.32	-25.0	0.1	1.2	-6.8	-0.6	-24.0
8	0.32	-25.0	0.8	-0.3	-8.3	1.8	-26.1
9	0.32	-25.0	0.3	-0.2	-8.2	0.7	-35.0
10	0.32	-25.0	1.3	-0.9	-8.9	11.4	2.0
11	0.32	-25.0	0.7	-1.0	-9.0	6.5	-19.2
12	0.32	-25.0	0.3	-0.8	-8.8	1.8	-30.9
13	0.32	-25.0	0.1	-0.4	-8.4	0.2	-36.0
14	0.32	-25.0	0.1	-1.6	-9.6	0.8	-13.5

Figure 5.1 is the dimensionless plot of the particle trajectories relative to the thermal from the computer simulation. It shows one half of a symmetrical particle thermal and at all values of time the thermal has a dimensionless radius of unity. The

thermal has a uniform velocity of -25.0 cm/s and the 0.0548 cm diameter glass particles have a terminal velocity of V_T = -16.2 cm/s in water assuming Stokes drag. The vortex center is located where there is a cluster of particles trapped within the thermal at r/a = 0.80 and z_T/a = -0.20. Except for the single particle at r/a = 0.47 and z_T = -1.10, all of the particles remain in the internal flow of the thermal for all the time intervals. Figure 5.2 is for the same flow situation as in Figure 5.1, but shows the radial and vertical positions of the 14 particles. The frame of reference is relative to the location for a point source release. The vortex center is distinguished by the cluster of particles at each time interval.

Figures 5.3 and 5.4 are for a thermal velocity equal to the terminal velocity of the particles (V_T = -16.2 cm/s). Figures 5.5 and 5.6 are for a thermal velocity of -10.30 cm/s. As the thermal speed is lowered, more particles migrate outside the boundary of the thermal. There is permanent particle separation in Figures 5.5 and 5.6 now that the thermal speed is slower than the terminal velocity of the particles.

Figures C.1 to C.6 in Appendix C are the theoretical results for 0.0274 cm diameter particles at several uniform velocities assuming a Stokes drag relationship in the model. They display almost identical behaviour to what is seen with the 0.0548 cm diameter particles. This is expected since the uniform velocities are varied by the same factor as what they are in this section.

5.2.2 Non-Stokes Drag

The non-Stokes Reynolds numbers of the particles used range from 5 to 22 at their respective terminal velocities. For the 0.0548 cm diameter particle size the non-Stokes terminal velocity is -6.10 cm/s. As with the Stokes drag case, there are three separate simulations included in this section. One simulation is at a uniform speed of -9.60 cm/s, the second is at -6.10 cm/s and the third is at -3.90 cm/s.

Figures 5.7 to 5.12 are the results using a non-Stokes drag relationship in the uniform speed thermal model. The dimensionless plots are very similar to the previous plots for Stokes drag. The amount of relative particle separation is almost identical for the three flow situations. For both Stokes and non-Stokes drag, the thermal speeds above and below the two respective terminal velocities are varied by the same factor. This is the same factor as that used by Topham et al to vary their thermal speeds. The radial and vertical spread of the particles is substantially less than that for Stokes drag. This is due to the lower simulation speeds and the lower non-Stokes terminal velocity. As before, Figures C.7 to C.12 for 0.0274 cm diameter particles show very similar behaviour to the plots for 0.0548 cm diameter particles with a non-Stokes drag relationship in the model.

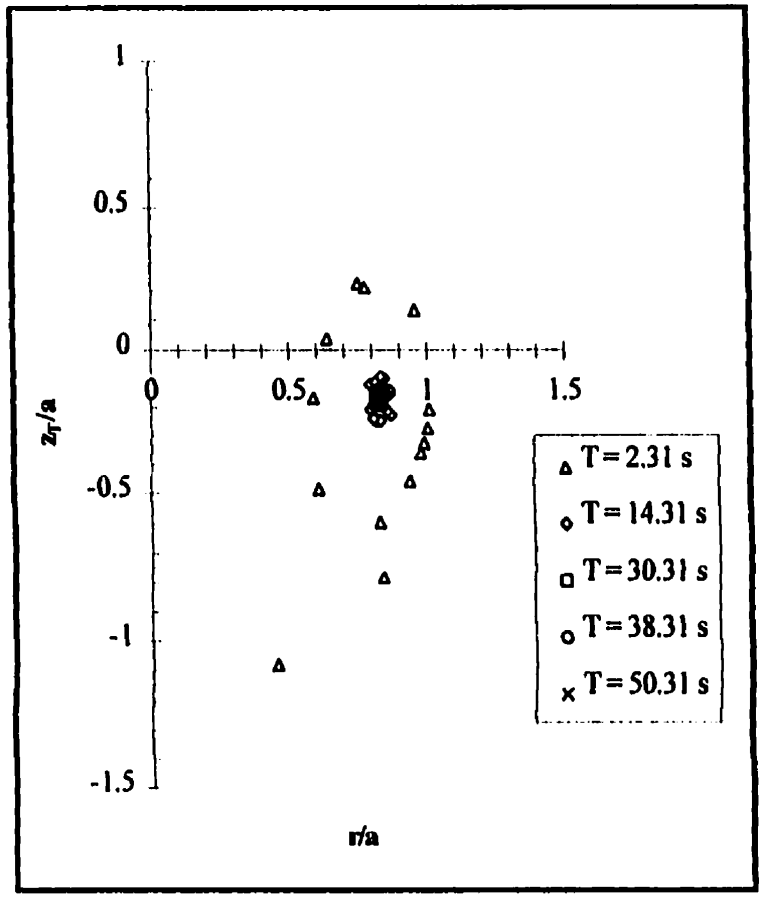

Figure 5.1

Dimensionless plot for 0.0548 cm diameter particles. Uniform speed thermal at the maximum theoretical velocity with Stokes drag (U = -25.0 cm/s).

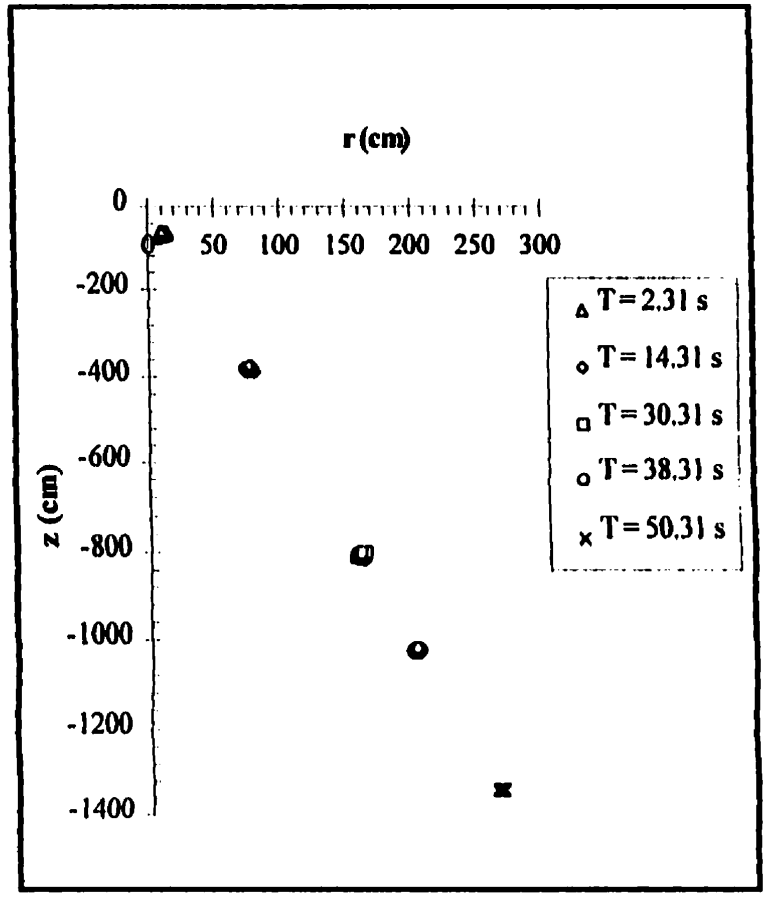

Figure 5.2

Vertical and radial particle positions for 0.0548 cm diameter particles. Uniform speed thermal at the theoretical maximum velocity with Stokes drag (U = -25.0 cm/s).

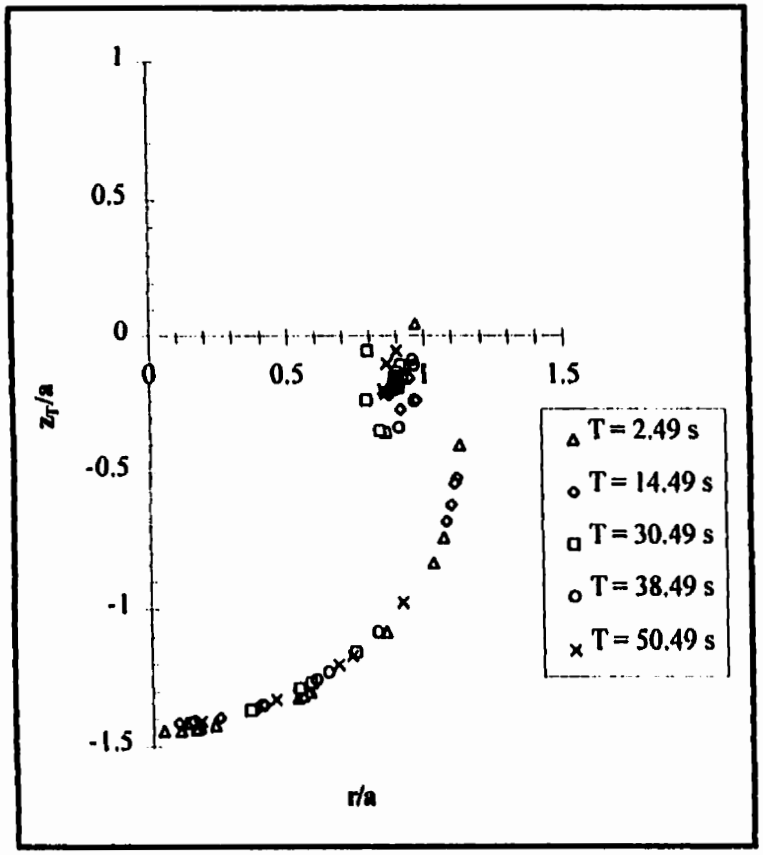

Figure 5.3

Dimensionless plot for 0.0548 cm diameter particles. Uniform speed thermal at the terminal velocity with Stokes drag (U = -16.23 cm/s).

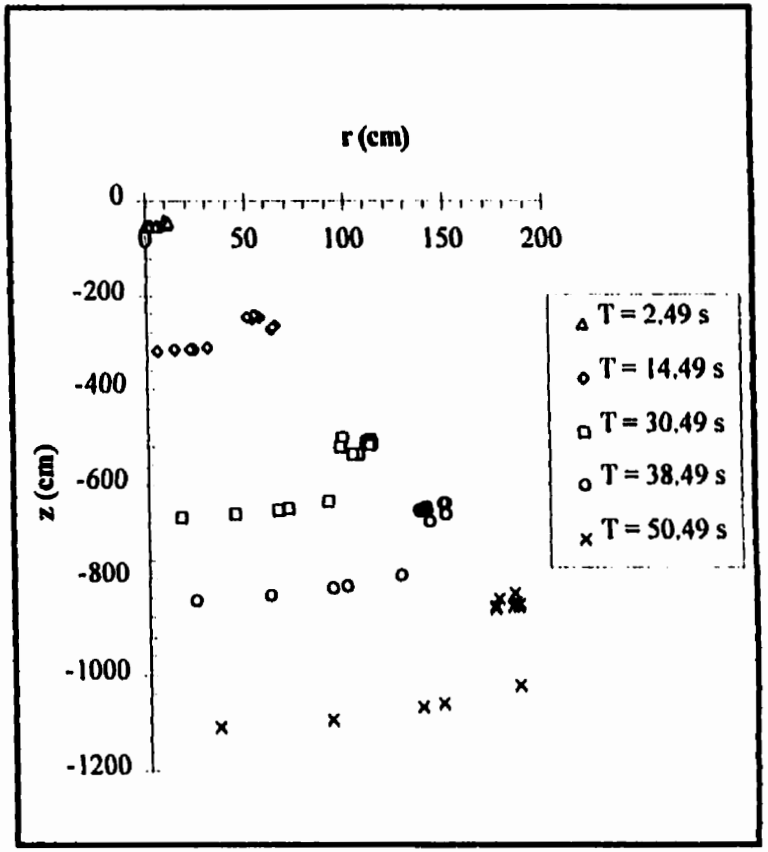

Figure 5.4

Vertical and radial particle positions for 0.0548 cm diameter particles. Uniform speed thermal at the terminal velocity with Stokes drag (U = -16.23 cm/s).

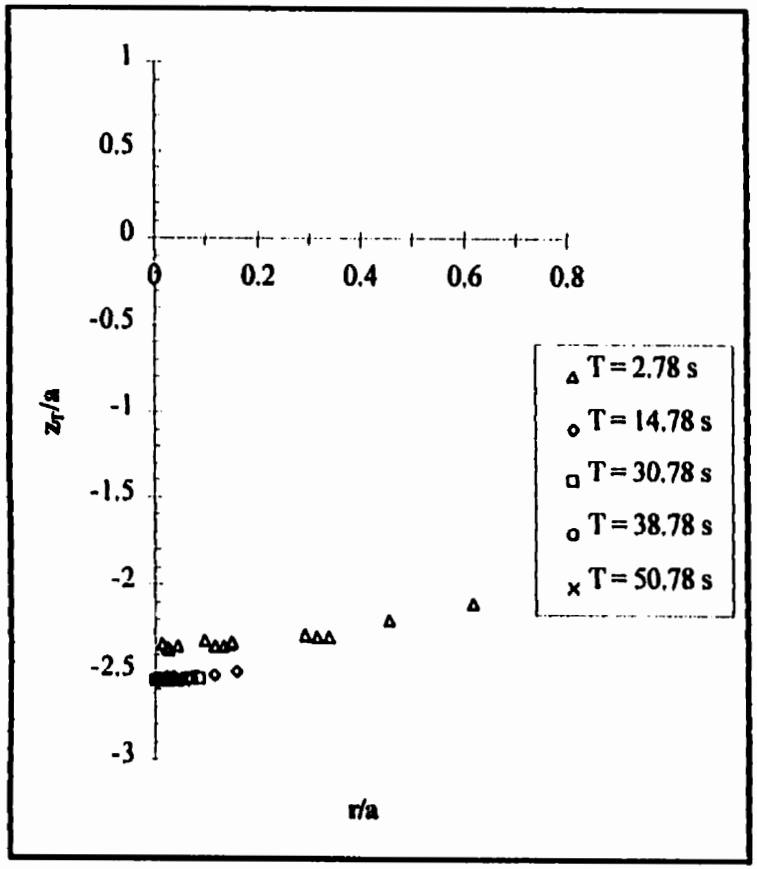

Figure 5.5

Dimensionless plot for 0.0548 cm diameter particles. Uniform speed thermal below the terminal velocity with Stokes drag (U = -10.30 cm/s).

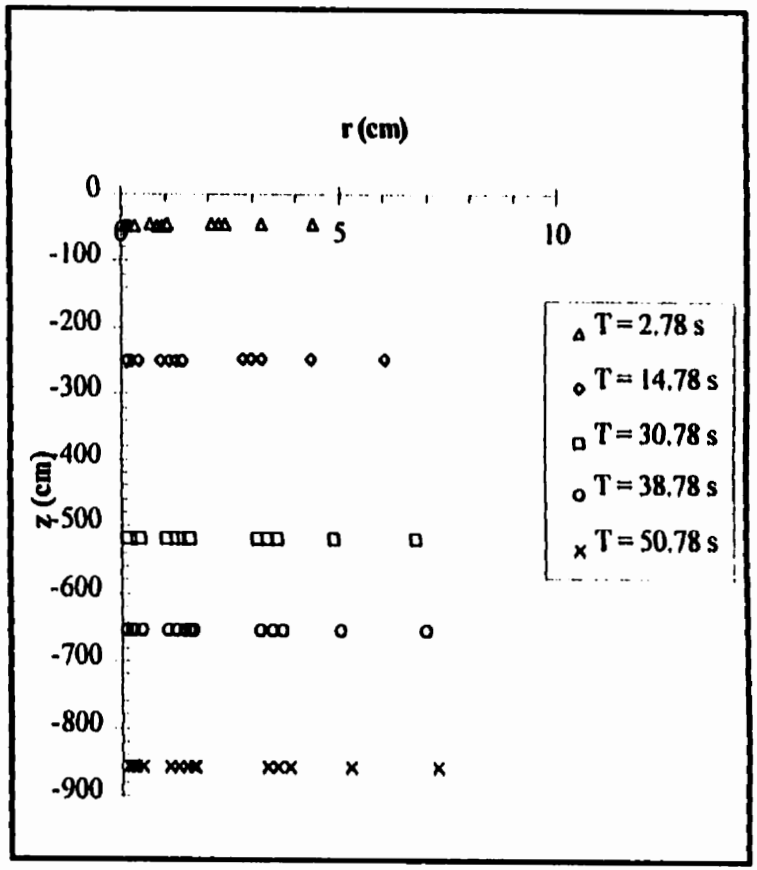

Figure 5.6

Vertical and radial particle positions for 0.0548 cm diameter particles. Uniform speed thermal below the terminal velocity with Stokes drag (U = -10.30 cm/s).

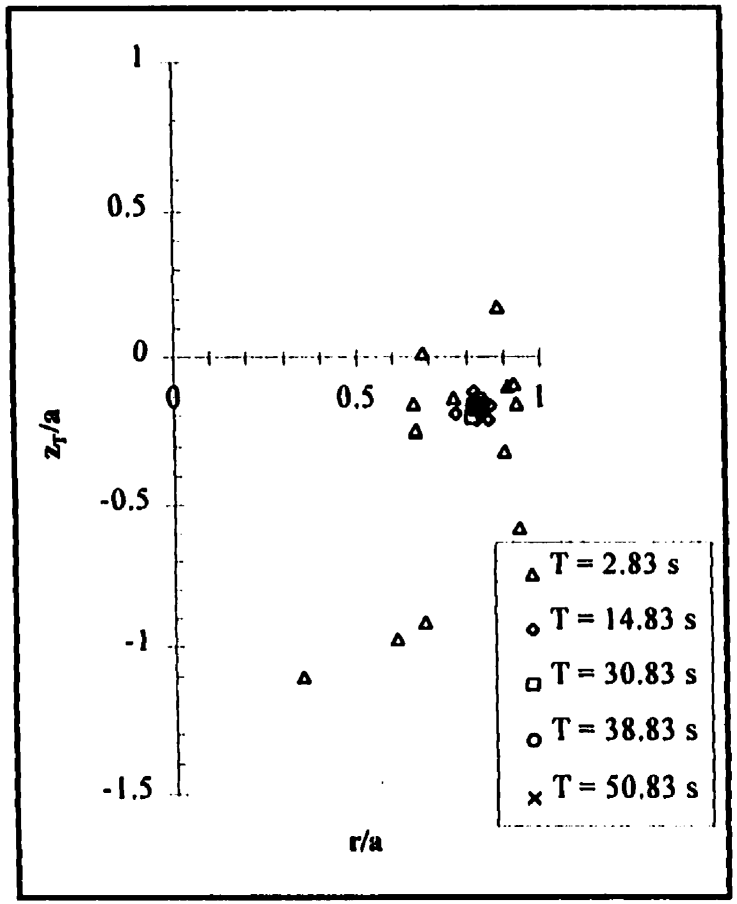

Figure 5.7

Dimensionless plot for 0.0548 cm diameter particles. Uniform speed thermal above the terminal velocity with Non-Stokes drag (U = -9.62 cm/s).

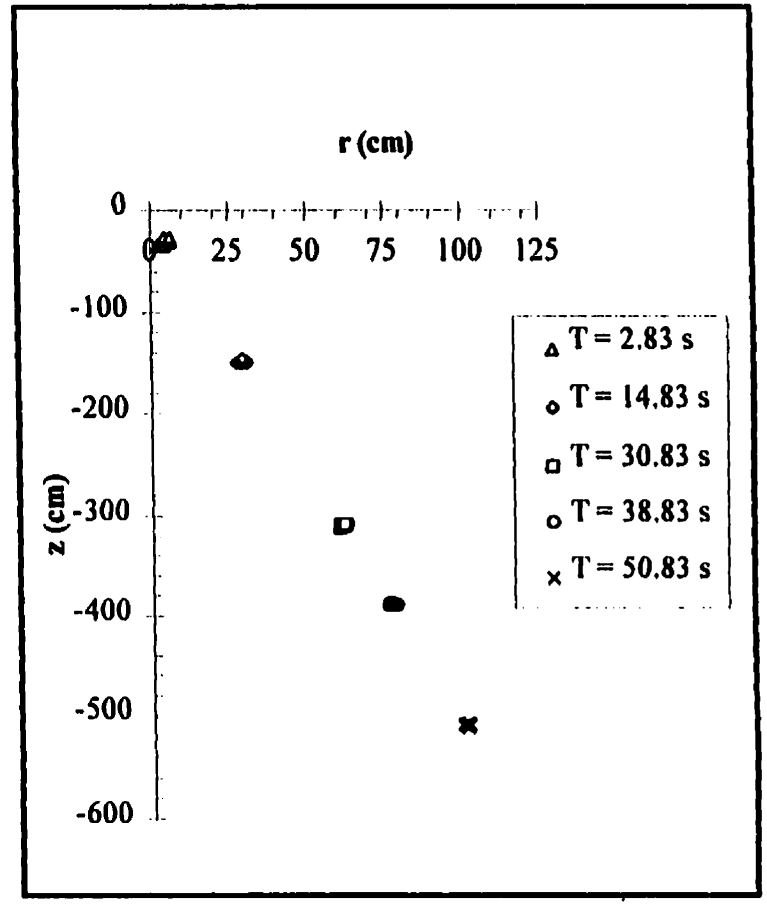

Figure 5.8

Vertical and radial particle positions for 0.0548 cm diameter particles. Uniform speed thermal above the terminal velocity with Non-Stokes drag (U = -9.62 cm/s).

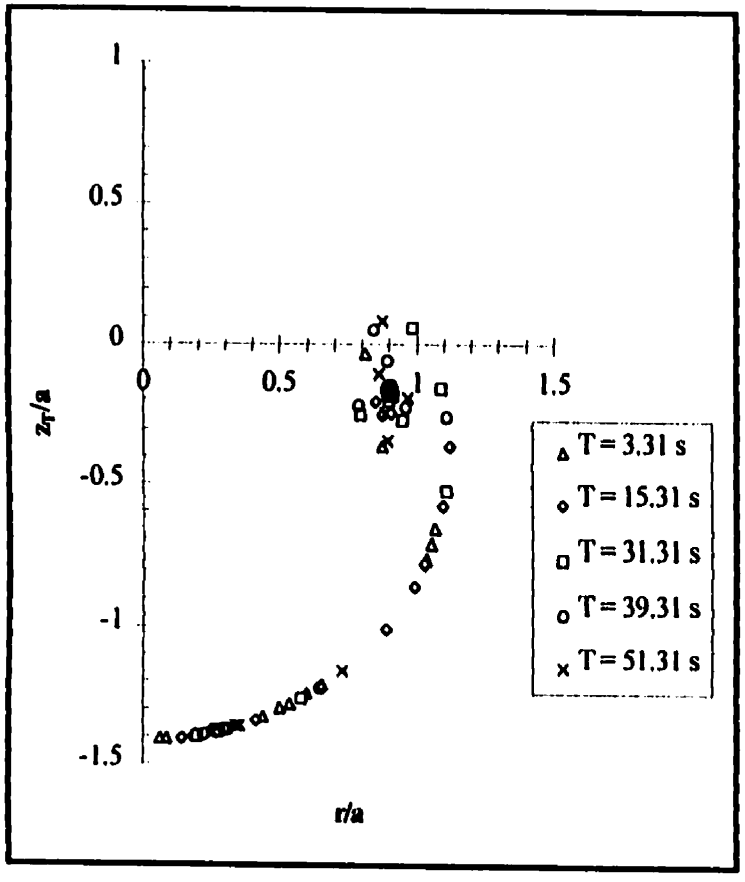

Figure 5.9

Dimensionless plot for 0.0548 cm diameter particles. Uniform speed thermal at the terminal velocity with Non-Stokes drag (U = -6.10 cm/s).

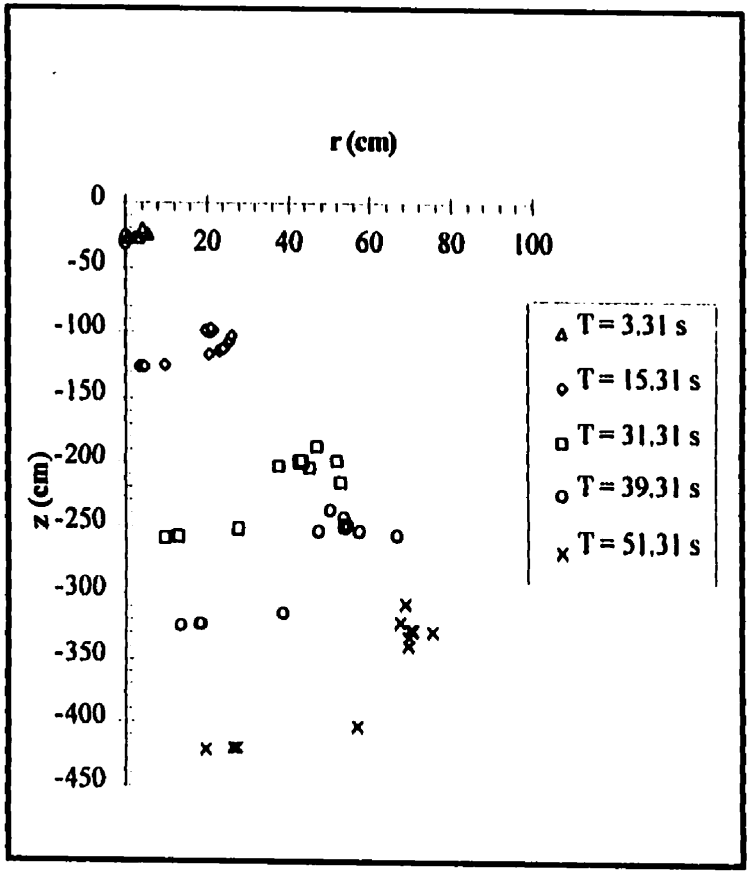

Figure 5.10

Vertical and radial particle positions for 0.0548 cm diameter particles. Uniform speed thermal at the terminal velocity with Non-Stokes drag (U = -6.10 cm/s).

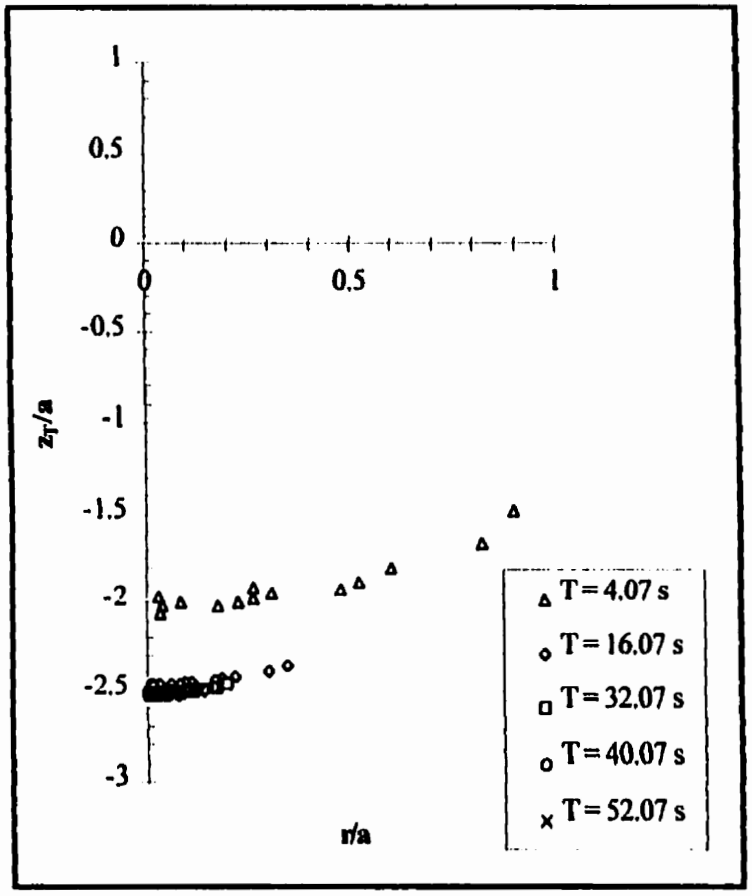

Figure 5.11

Dimensionless plot for 0.0548 cm diameter particles. Uniform speed thermal below the terminal velocity with Non-Stokes drag (U = -3.87 cm/s).

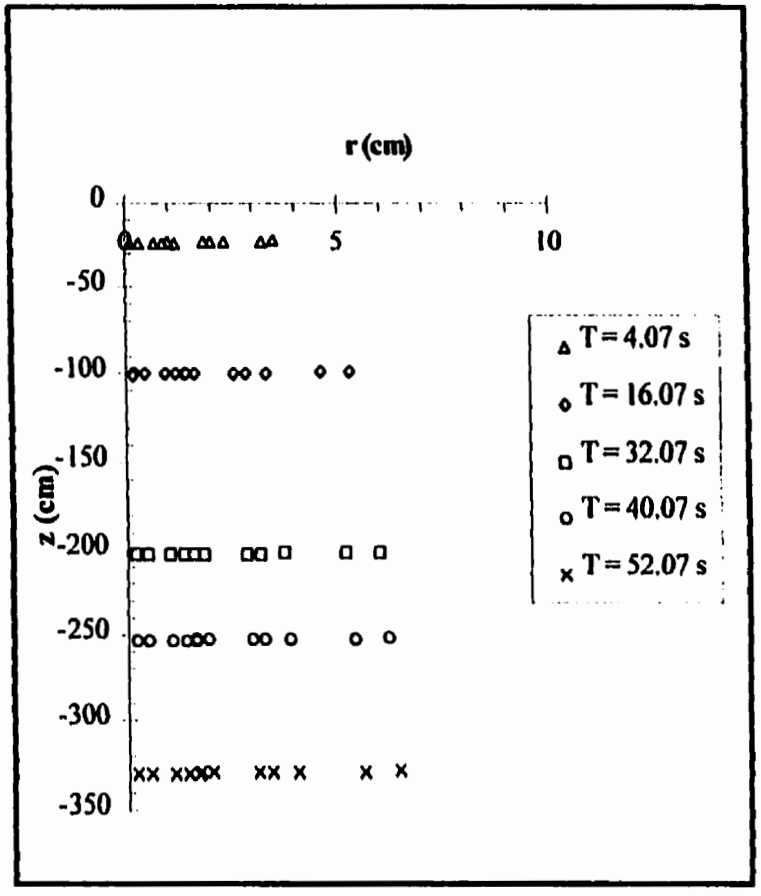

Figure 5.12

Vertical and radial particle positions for 0.0548 cm diameter particles. Uniform speed thermal below the terminal velocity with Non-Stokes drag (U = -3.87 cm/s).

5.3 Nonuniform Thermal Speed

At the onset of this thesis project the intention was only to consider a uniform speed thermal in the model. However, after performing some experiments it became apparent that a nonuniform speed should also be examined. As with the uniform speed case only results from the 0.0548 cm diameter particle size are shown in this section. These results are organized a bit differently than the previous uniform speed results. Since the thermal velocity decays with time, it is necessary to assume a starting velocity for the simulations. Therefore, simulations were performed with Stokes and non-Stokes drag relationships with initial velocities corresponding to the velocity of the experimental thermals at $t_e = 1.0$ s. Reasons for this are that this is the first recorded data point from the experiments and all the particle thermals are already decelerating at this point in time. This is necessary since expression (2.15), for thermal velocity, only decays with time.

As with the uniform case, Table 5.2 provides an example of the initial starting conditions of the 0.0548 cm diameter glass particles from laboratory run #16. There are a few differences. For instance, the starting time t is now the time at which the thermal reaches the selected initial velocity to start the simulation and not the time when a thermal reaches a radius of a = 2 cm. Accordingly, the starting velocity U is the selected initial velocity of the thermal. The thermal velocity decreases inversely with the square root of time. By using a nonuniform thermal velocity, the theoretical simulations are now specific to individual laboratory runs, which is laboratory run #16 for Table 5.2. From

the laboratory experiments a constant K is found for each experiment. Sections 2.1.4 and 2.1.5 discuss how the K values are determined. This constant is required in order to calculate the nonuniform thermal velocity. Tables similar to 5.2 were developed for the other particle sizes. The initial conditions for nonuniform speed thermals remain the same for Stokes and non-Stokes drag for each particle size.

Table 5.2 Initial Conditions for 0.0548 cm Diameter Glass Particles
Nonuniform Speed Thermal with K = 10.0 $cm/s^{1/2}$
Laboratory Run #16

Particle No.	t (s)	U (cm/s)	r (cm)	z_T (cm)	z (cm)	U_r (cm/s)	U_z (cm/s)
1	1.16	-9.28	1.0	0.3	-21.2	-0.2	-22.1
2	1.16	-9.28	4.1	1.3	-20.2	-2.6	-6.3
3	1.16	-9.28	2.6	1.9	-19.6	-2.4	-14.9
4	1.16	-9.28	1.3	1.8	-19.8	-1.1	-20.2
5	1.16	-9.28	0.3	1.0	-20.5	-0.2	-22.6
6	1.16	-9.28	1.3	4.1	-17.5	-2.6	-13.5
7	1.16	-9.28	0.1	3.2	-18.3	-0.2	-18.2
8	1.16	-9.28	2.0	-0.7	-22.2	0.7	-19.0
9	1.16	-9.28	0.9	-0.6	-22.2	0.3	-22.3
10	1.16	-9.28	3.5	-2.5	-24.1	4.2	-8.5
11	1.16	-9.28	1.9	-2.6	-24.2	2.4	-16.4
12	1.16	-9.28	0.7	-2.0	-23.6	0.7	-20.8
13	1.16	-9.28	0.1	-1.1	-22.6	0.1	-22.6
14	1.16	-9.28	0.1	-4.3	-25.9	0.3	-14.3

5.3.1 Stokes Drag

For the first results assuming Stokes drag, the thermal is starting at a theoretical time of t = 1.16 s. This time corresponds to a velocity of -9.28 cm/s and an initial thermal size of a = 5.39 cm. Figures 5.13 and 5.14 show a dimensionless plot and a plot of the absolute particle positions for five time intervals. It is quite clear that there is permanent separation for all five time intervals. For comparison, the uniform speed model with U = V_T and assuming Stokes drag, there is no permanent separation for the duration of the simulation. With the 0.0274 cm diameter particles in Figures C.13 and C.14, there is only permanent particle separation for the last four time intervals.

5.3.2 Non-Stokes Drag

The non-Stokes drag case, along with a nonuniform speed thermal, is more indicative of actual flow. These results are organized in the same manner as the Stokes drag results for a nonuniform speed thermal. The non-Stokes terminal velocity is -6.10 cm/s for 0.0548 cm diameter particles versus a Stokes terminal velocity of -16.2 cm/s. Particles do not separate from the thermal as quickly with a lower terminal velocity.

These results are for laboratory run #16 with an initial thermal speed of -9.28 cm/s. As before, this corresponds to an initial thermal radius of a = 5.39 cm and an initial theoretical starting time of t = 1.16 s. These results are shown in Figures 5.15 and 5.16. The first time interval of t = 2.16 s already shows permanent particle separation

from the thermal. The plots show very nice half moon crescent formations, which are very similar to the observations from the laboratory experiments. Very similar results are shown for the 0.0274 cm diameter particles in Figures C.15 and C.16, with permanent particle separation for the latter four time intervals. However, it appears that there are some particles trapped within the thermal vortex for the first two time intervals. In figures such as C.15 the thermal boundary at all values of time has a dimensionless radius of $z_T/a = r/a = 1.0$.

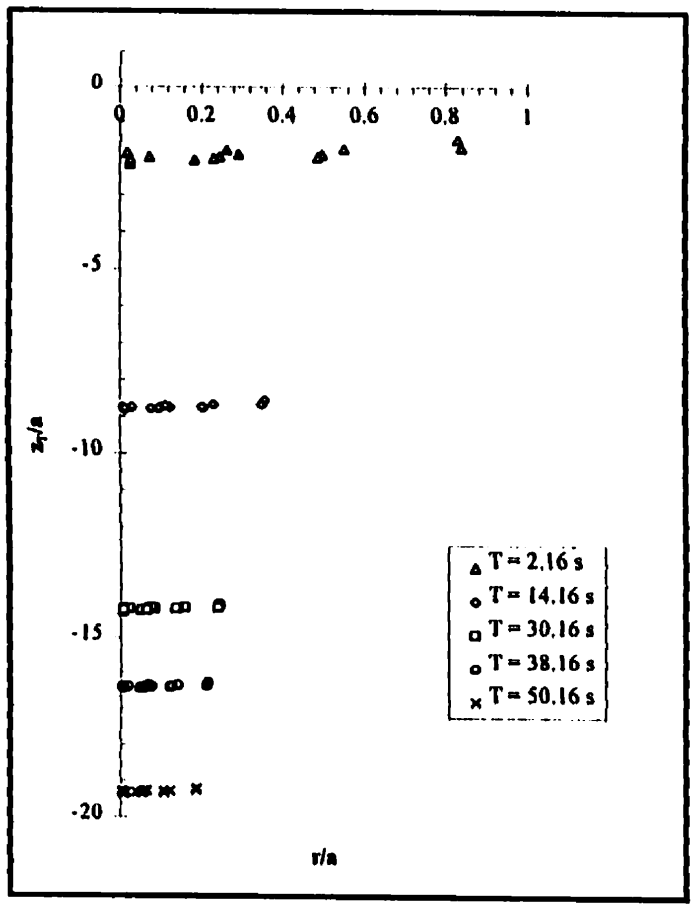

Figure 5.13

Dimensionless plot for 0.0548 cm diameter particles. Nonuniform speed thermal starting at U = -9.28 cm/s with Stokes drag.

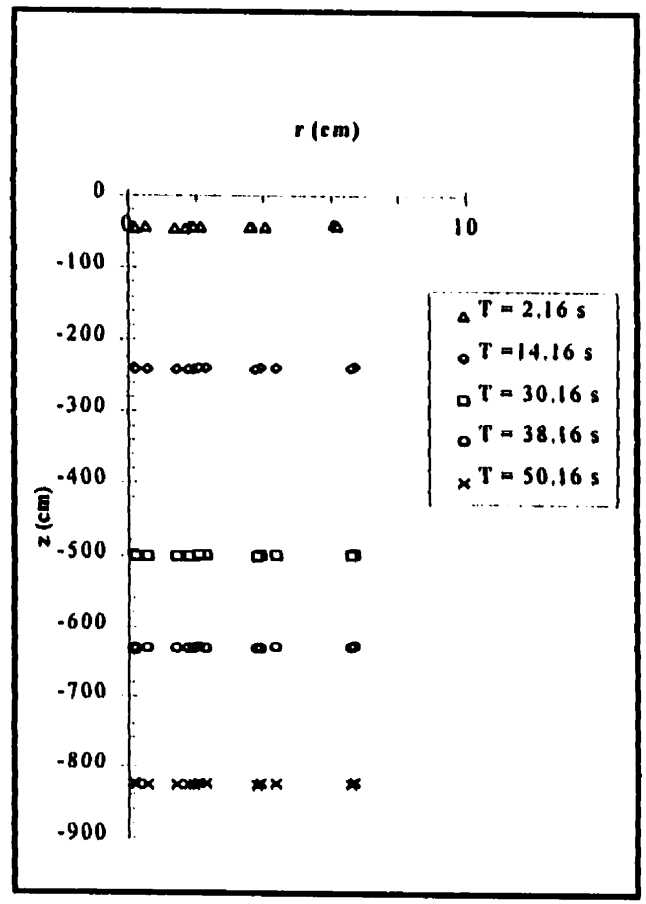

Figure 5.14

Vertical and radial particle positions for 0.0548 cm diameter particles. Nonuniform speed thermal starting at U = -9.28 cm/s with Stokes drag.

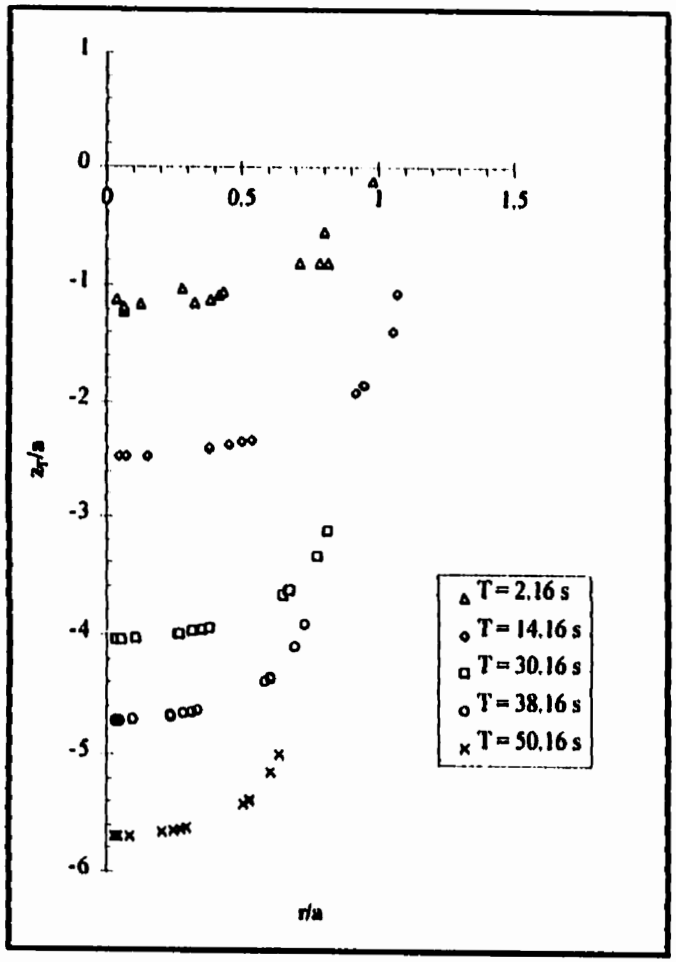

Figure 5.15

Dimensionless plot for 0.0548 cm diameter particles. Nonuniform speed thermal starting at U = -9.28 cm/s with Non-Stokes drag.

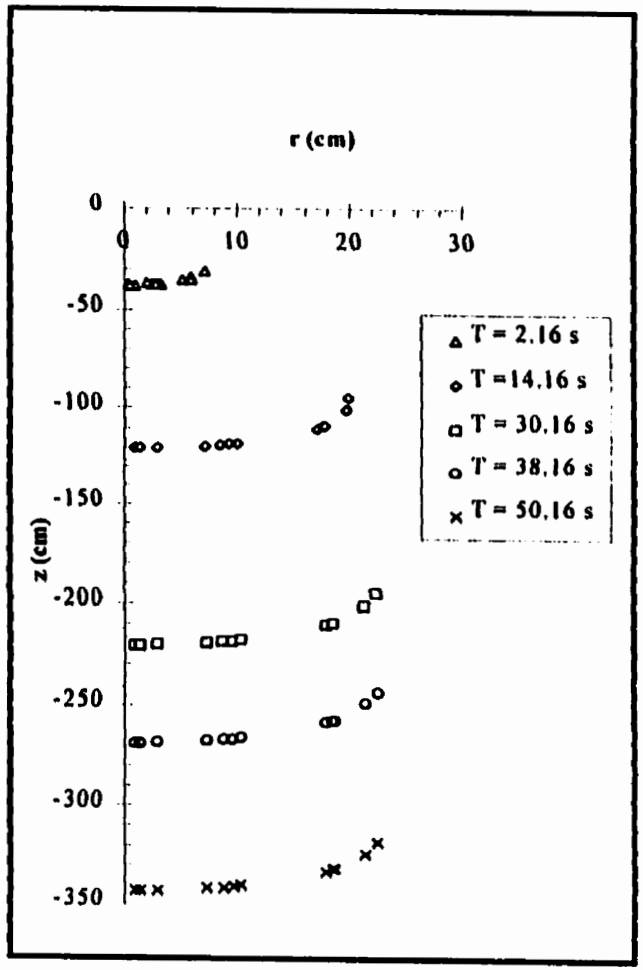

Figure 5.16

Vertical and radial particle positions for 0.0548 cm diameter particles. Nonuniform speed thermal starting at U = -9.28 cm/s with Non-Stokes drag.

5.4 Comparison with Topham et al

Topham et al looked at the theoretical behaviour of polystyrene particles considering a uniform speed thermal in their model. Their work along with Lee's thesis (1992), spawned this thesis into using another particle type with a larger specific gravity. Glass was chosen because it has a larger specific gravity and can be obtained commercially in very accurate sizes.

Topham et al examined four different uniform thermal speeds using polystyrene particles having a diameter of 0.054 cm and a specific gravity of 1.04. Two of the uniform speeds were lower than the terminal velocity of the polystyrene particles, another was equal to the terminal velocity and the fourth was faster. There were several notable results from these simulations. First, when the speed of the thermal was faster than the terminal velocity of the polystyrene particles there was no permanent particle separation from the thermal. There was some particle separation at small values of time, but the particles eventually migrated back to the vortex center of the thermal. Second, when the speed of the thermal approached the terminal velocity of the particles there was partial particle separation from the thermal. However, at larger values of time all the particles migrated to the vortex center again. Third, at speeds below the terminal velocity the particles permanently separated from the thermal. At small values of time the particles were still part of the internal flow of the thermal.

Earlier in Chapter 5 results were presented for 0.0548 cm diameter glass particles using the same theoretical thermal model Topham et al used for polystyrene particles (Uniform thermal model with a Stokes drag relationship). Figures 5.17 through 5.22 display Topham et al's results alongside the 0.0274 cm diameter glass results. The 0.0274 cm diameter results are shown because the 0.0548 cm diameter glass results were shown previously.

Figures 5.17 and 5.18 compare the two sets of results at comparable uniform thermal speeds greater than the terminal velocities of the respective particles. The vortex center is located approximately in the same position, relative to the position of the thermal, in each figure ($z_T/a \approx -0.2$ and $r/a \approx 0.8$). The center is below the horizontal axis because of the influence of gravity and due to particle slip. Note, y/a and x/a are the same dimensionless quantities as z_T/a and r/a. Both particle types exhibit the same behaviour at the smallest time interval and maximum particle separation relative to the thermal for each figure is $z_T/a \approx 1.2$. Lastly, the rest of the time intervals show the particles clustered at the vortex center. There is a higher density of particles in the Topham et al simulations because 80 particles were used in their model whereas only 14 are used here.

In Figures 5.19 and 5.20, the two sets of results are at a uniform speed equal to the terminal velocity of the two particle types. The location of the vortex center remains unchanged from before for both sets of results. Both results show partial particle

separation for all time intervals. The amount of particle separation is the same in each case ($z_T/a \approx -1.4$).

In Figures 5.21 and 5.22, the two sets of results are at a uniform speed lower than the respective terminal velocities of the particles. Permanent particle separation is shown in both figures. Relative particle separation is equal in both cases.

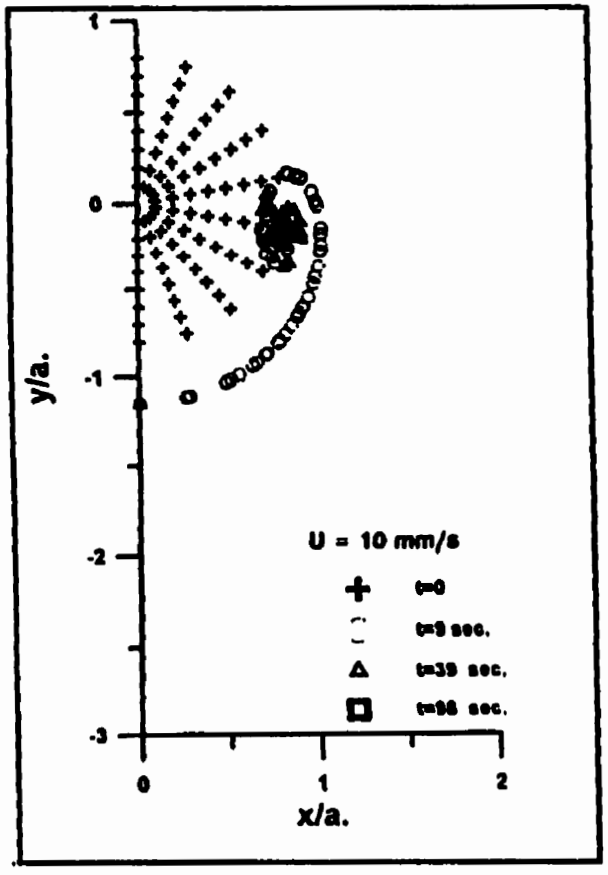

Figure 5.17

Dimensionless plot for 0.054 cm diameter polystyrene particles (from Topham et al). Uniform speed thermal above the terminal velocity with Stokes drag **(U = -1.0 cm/s).**

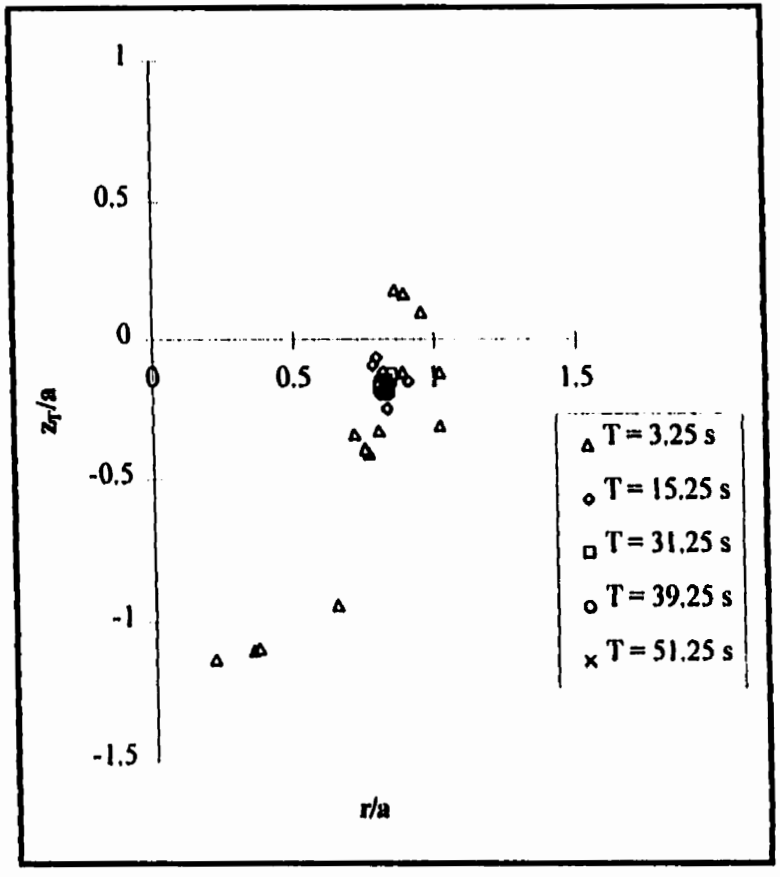

Figure 5.18

Dimensionless plot for 0.0274 cm diameter glass particles. Uniform speed thermal above the terminal velocity with Stokes drag **(U = -6.38 cm/s).**

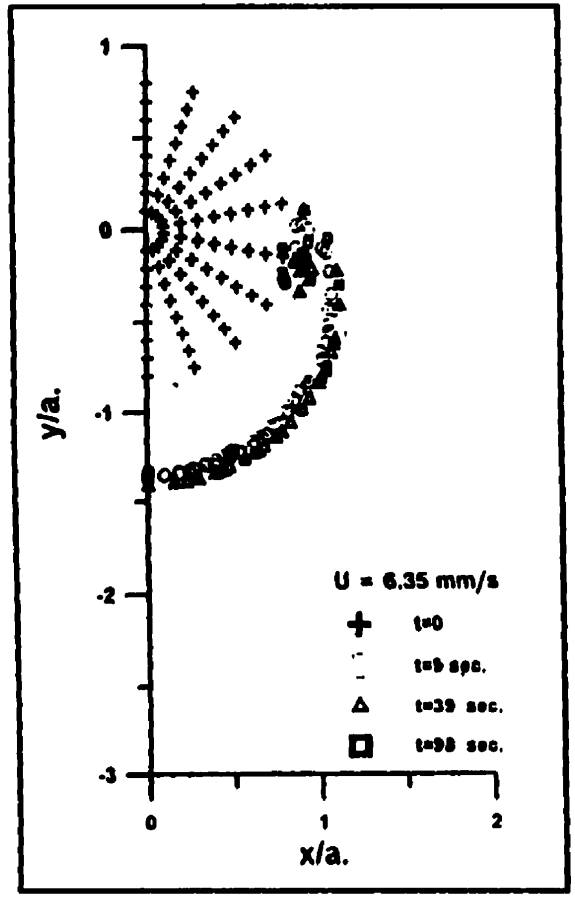

Figure 5.19

Dimensionless plot for 0.054 cm diameter polystyrene particles (from Topham et al). Uniform speed thermal at the terminal velocity with Stokes drag (**U = -0.635 cm/s**).

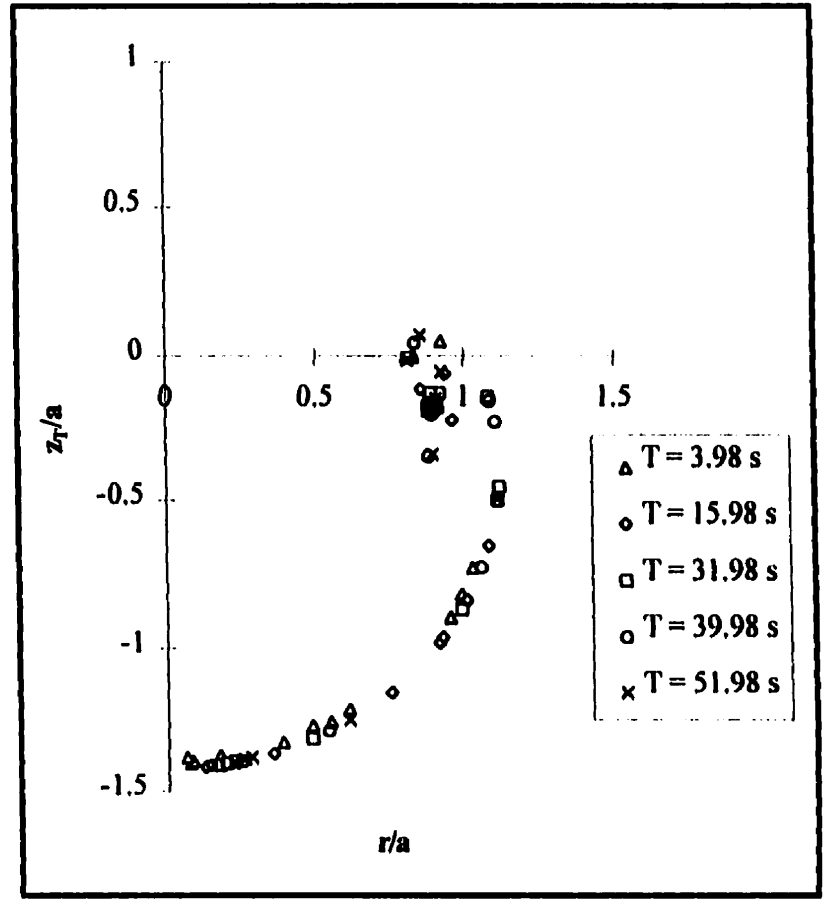

Figure 5.20

Dimensionless plot for 0.0274 cm diameter glass particles. Uniform speed thermal at the terminal velocity with Stokes drag (**U = -4.05 cm/s**).

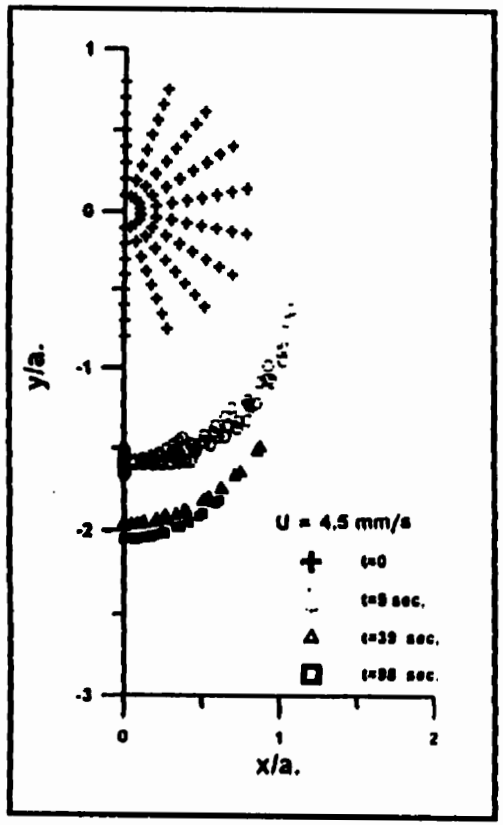

Figure 5.21

Dimensionless plot for 0.054 cm diameter polystyrene particles (from Topham et al). Uniform speed thermal below the terminal velocity with Stokes drag **(U = -0.45 cm/s).**

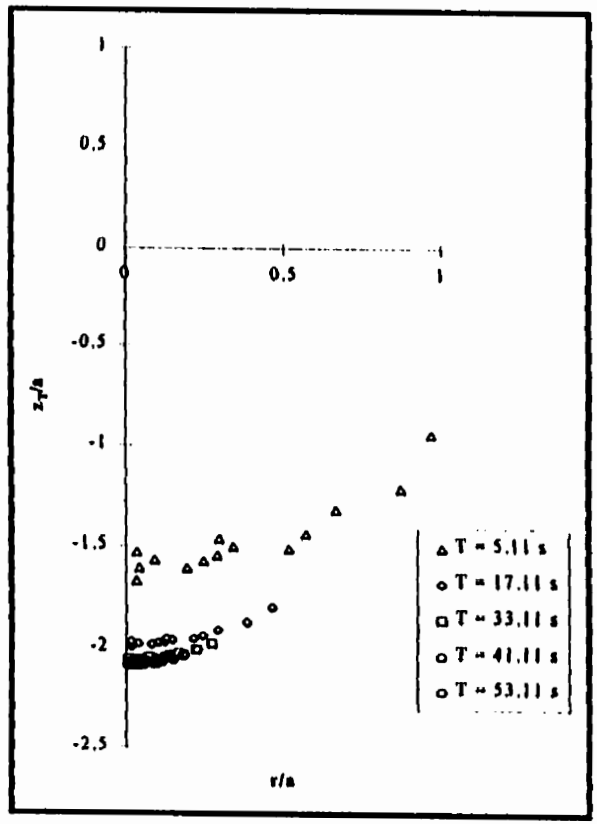

Figure 5.22

Dimensionless plot for 0.0274 cm diameter glass particles. Uniform speed thermal below the terminal velocity with Stokes drag **(U = -2.87 cm/s).**

Chapter 6

Analyses of Theoretical and Laboratory Results

6.1 Introduction

The previous chapters have shown results from the theoretical simulations and the laboratory experiments. The purpose of this chapter is to compare and analyze some of these results. The theoretical results shown in Chapter 5 were for uniform and nonuniform speed thermals using Stokes and non-Stokes drag relationships. After a preliminary comparison of laboratory and theoretical results, it was found that non-Stokes drag compared more closely with the laboratory results. This was expected since the settling behaviour of the glass particles falls in the non-Stokes flow regime.

Data from the results are compared in several ways. The parameters used to analyze the results are the:

- Thermal radius, a
- Thermal depth, z
- Maximum particle radius, r
- Maximum particle depth, z
- Maximum particle separation from thermal (measured from center of thermal), z_T
- Thickness of the particle crescent (difference between the depth where the maximum radius occurs and the maximum depth of the particles in the crescent), b

The parameters are compared at five different time intervals, which are chosen so that there is correlation between the theoretical and the laboratory intervals. The next two sections contain figures and tables comparing both theoretical and laboratory results for uniform and nonuniform speed thermals. The tables included in these sections show the difference between theoretical and laboratory values along with percent differences. A negative difference indicates that the laboratory result is larger than the theoretical, whereas the percent differences are absolute values. The figures in these sections contain plots of the theoretical results with the laboratory results superimposed. The laboratory results are represented by bolded symbols for each time interval and a connecting arc. A small assumption is made in representing the laboratory results in this manner. Since the laboratory data does not have the same detail as the theoretical, it is assumed that a radial arc can represent the particle distribution between data points.

6.2 Uniform Speed Thermal Comparison

The next two sub-sections show results using Stokes and non-Stokes drag relationships in the thermal model for 0.0548 and 0.0274 cm diameter glass particles. These two sizes represent the largest and smallest glass particles used in the laboratory experiments and theoretical model. The theoretical time is referenced in Tables 6.1 to 6.4 and Figures 6.1 to 6.4. The theoretical time for a thermal to grow to a 2 cm radius from a point source release is found from equation $a = \alpha Ut$ (2.4), assuming a uniform speed thermal. Therefore, the laboratory time is offset by this amount (Δt) because the laboratory thermals were not released from a point source, but from an initial radius of $a = 2$ cm. The difference between theoretical and laboratory values of time vary with each simulation, because the uniform thermal speed is different in each case.

6.2.1 Stokes Drag

The first analysis in Table 6.1 and Figure 6.1 show the comparison for 0.0548 cm diameter particles assuming Stokes drag. As mentioned in Chapter 2, the Stokes Reynolds number is 58.8 for this particle size at terminal velocity. Since the Reynolds number is greater than 2.0, the settling behaviour of the particles fall in the non-Stokes flow regime. This explains why the differences increase with time for most of the parameters.

Table 6.1 Comparison between Theoretical and Laboratory Results for 0.0548 cm diameter Particles (Run #16). Uniform Speed Thermal (U = -16.23 cm/s) and Stokes Drag.

Time	Thermal Radius, a		Maximum Particle Radius, r		Thermal Depth, z		Maximum Particle Depth, z		Particle Crescent Thickness, b		Maximum Particle Separation, z_T	
(s)	Diff. (cm)	(%)	Diff. (cm)	(%)	Diff. (cm)	(%)	Diff. (cm)	(%)	Diff. (cm)	(%)	Diff. (cm)	(%)
2.49	2.5	24.6	3.1	27.2	-4.5	11.2	-12.1	22.0	3.6	33.9	-7.6	52.0
4.49	8.7	47.7	6.9	34.0	-27.5	37.6	-34.5	34.8	11.9	55.6	-7.0	26.9
6.49	15.9	60.2	12.9	43.9	-50.4	47.8	-66.3	46.4	14.6	56.1	-15.9	42.5
8.49	21.0	60.8	17.4	48.2	-79.0	57.3	-95.6	51.2	36.3	77.1	-16.6	33.9
11.49	31.4	67.3	28.3	57.4	-118.2	63.4	-139.9	55.4	21.7	66.7	-21.7	32.8

The next analysis in Table 6.2 and Figure 6.2 is for 0.0274 cm diameter particles using Stokes drag in the model. The Stokes Reynolds number is 7.3 at the terminal velocity of the particles, which is still greater than 2.0, but is eight times less than the corresponding Reynolds number for 0.0548 cm diameter particles. This is evident in the analysis. Comparison between theoretical and laboratory results is very good. The largest differences are found for the first time interval of 4.98 s, while the next two intervals are lower. The rise in the percent differences after this point may be attributed to measurement error in the laboratory results. At the latter time intervals it became increasingly difficult to see and measure the glass particles. From the laboratory data, it was noted that it became difficult to see the particles at an experimental time of t_e = 14.0 s. This also explains why the laboratory particle crescents at t = 15.98 s and t = 21.98 s almost overlap.

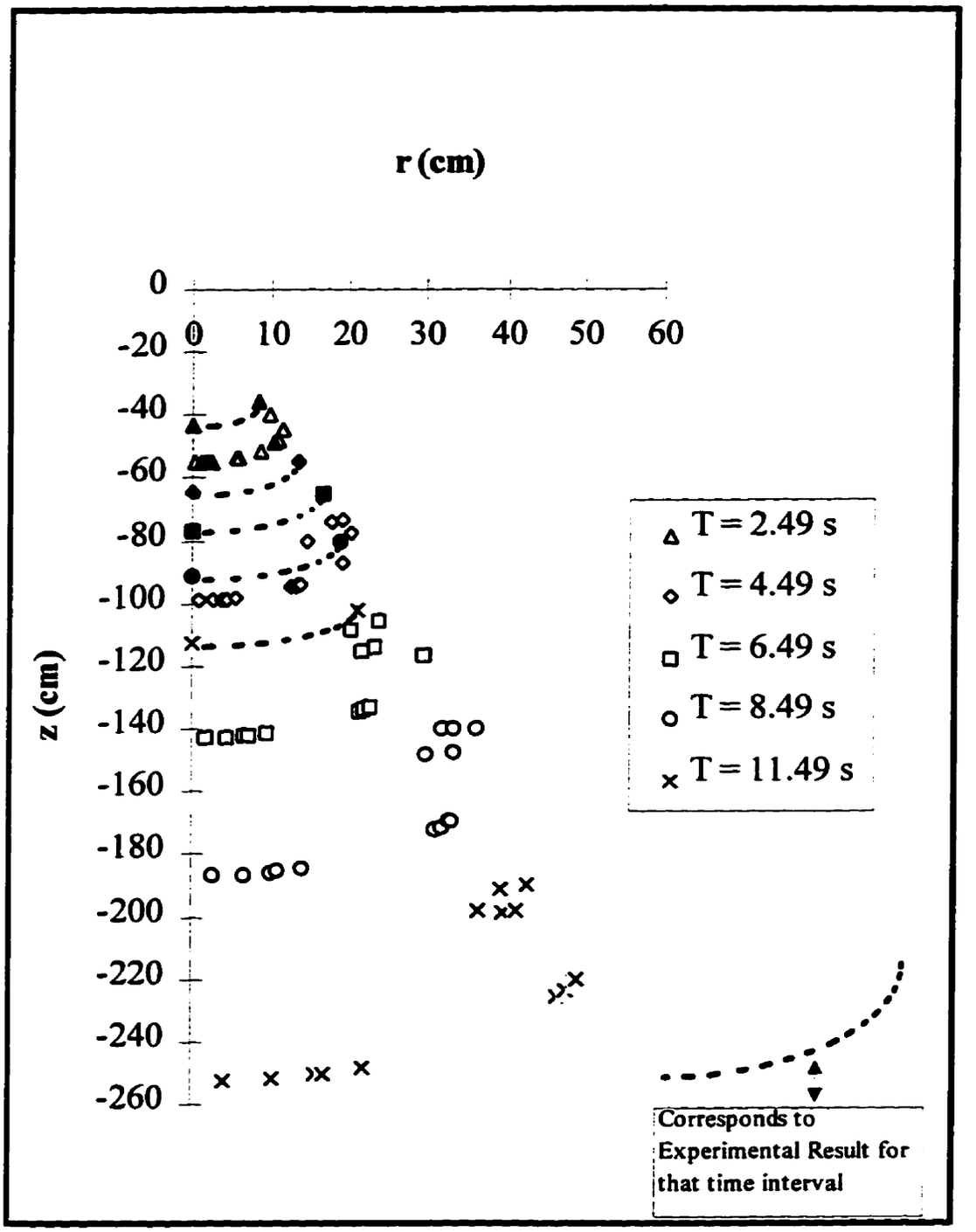

Figure 6.1 Comparison between theoretical and laboratory results for 0.0548 cm diameter particles (Run #16). Uniform speed thermal (U = -16.23 cm/s) and Stokes drag.

Table 6.2 Comparison between Theoretical and Laboratory Results for 0.0274 cm diameter Particles (Run #3). Uniform Speed Thermal (U = -4.05 cm/s) and Stokes Drag.

Time	Thermal Radius, a		Maximum Particle Radius, r		Thermal Depth, z		Maximum Particle Depth, z		Particle Crescent Thickness, b		Maximum Particle Separation, z_r	
(s)	Diff. (cm)	(%)	Diff. (cm)	(%)	Diff. (cm)	(%)	Diff. (cm)	(%)	Diff. (cm)	(%)	Diff. (cm)	(%)
4.98	-4.3	86.0	-5.0	90.0	17.7	87.8	18.9	69.2	-3.8	86.0	1.2	16.3
7.98	-4.6	57.3	-5.6	62.6	18.3	56.5	17.6	40.3	-1.8	19.7	-0.6	5.4
15.98	-1.3	8.0	-4.8	27.4	8.1	12.5	4.9	5.6	-7.4	59.9	-3.2	13.8
21.98	3.5	15.7	1.3	5.3	-9.9	11.1	-27.3	22.6	10.3	42.3	-17.4	55.4
27.98	6.9	24.3	9.1	28.7	-22.7	20.1	-42.3	27.6	10.2	33.5	-19.5	49.0

Also from the laboratory data, two phase flow was first noticed at $t_e = 8.0$ s. In the theoretical results, two phase behaviour occurs at the first time interval of $t = 4.98$ s. The cluster of particles at $r \approx 5$ cm and $z \approx -23$ cm indicate particles contained within the vortex flow of the thermal. The other particles at a slightly lower depth of $z \approx -27$ cm are ones that have separated from the thermal.

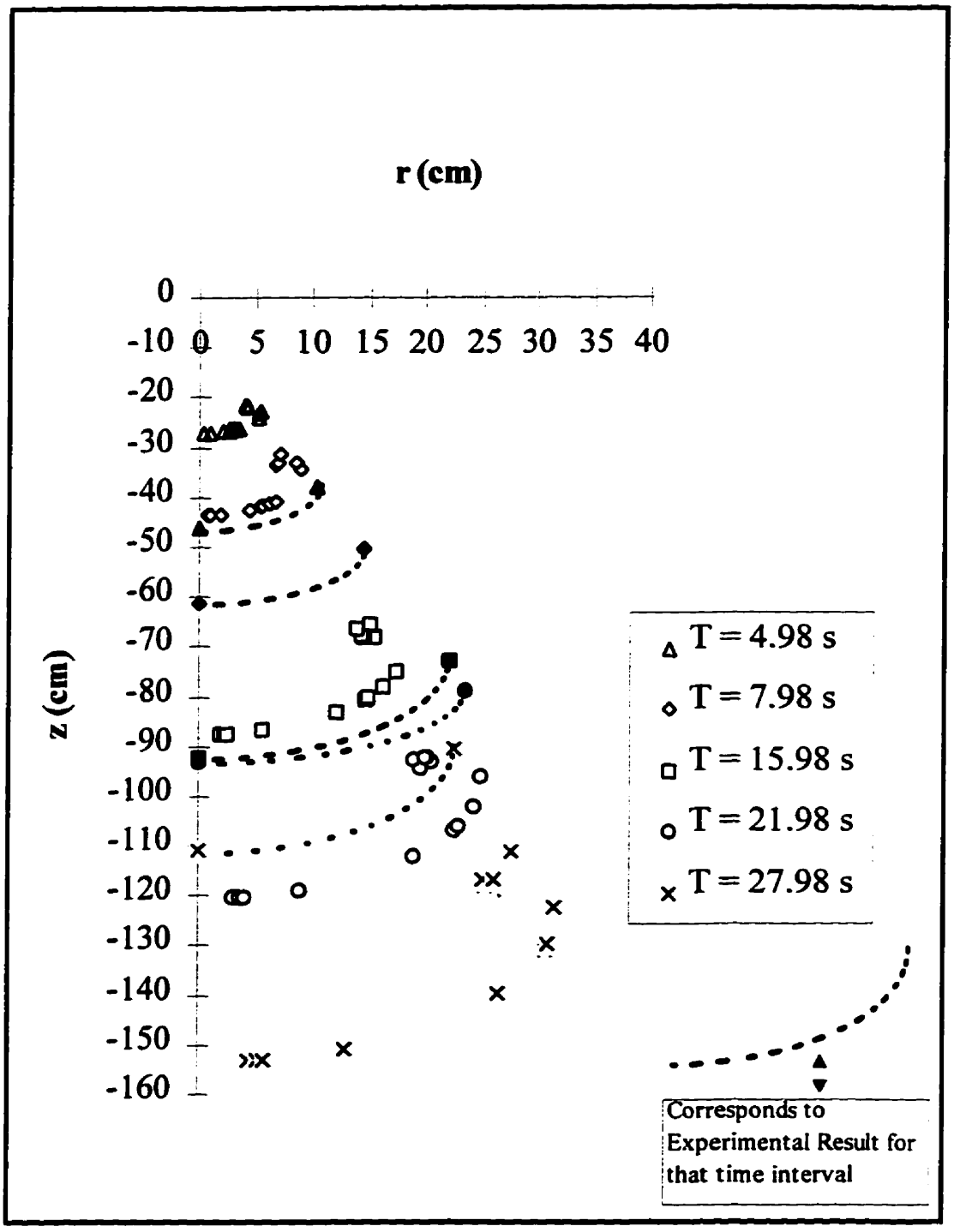

Figure 6.2 Comparison between theoretical and laboratory results for 0.0274 cm diameter particles (Run #3). Uniform speed thermal (U = -4.05 cm/s) and Stokes drag.

6.2.2 Non-Stokes Drag

The first non-Stokes analysis is for 0.0548 cm diameter particles, which have a non-Stokes Reynolds number of 22.1 at terminal velocity. The analysis shows that non-Stokes drag compares much better than the analysis using a Stokes drag relationship in the model, which is expected since the Reynolds number is greater than 2.0. Most of the percent differences progressively get less as time increases. The last time interval has differences of 18.8% for thermal radius, 2.2% for particle radius, 9.0% for thermal depth, 11.1% for particle depth, 29.2% for particle crescent thickness and 68.0% for maximum particle separation. The last two parameters, b and z_T, have higher percent differences than the others, but this is evident with most of the other analyses in this chapter.

Table 6.3 Comparison between Theoretical and Laboratory Results for 0.0548 cm diameter Particles (Run #16). Uniform Speed Thermal (U = -6.10 cm/s) and Non-Stokes Drag.

Time	Thermal Radius, a		Maximum Particle Radius, r		Thermal Depth, z		Maximum Particle Depth, z		Particle Crescent Thickness, b		Maximum Particle Separation, z_T	
(s)	Diff. (cm)	(%)	Diff. (cm)	(%)	Diff. (cm)	(%)	Diff. (cm)	(%)	Diff. (cm)	(%)	Diff. (cm)	(%)
3.31	-2.6	51.0	-2.9	53.6	15.7	77.9	15.6	57.1	-3.2	84.5	-0.1	1.9
5.31	-1.4	17.6	-4.3	48.0	13.1	40.4	20.7	47.1	-0.5	5.5	7.6	66.4
7.31	0.7	6.0	-6.1	59.1	10.4	23.3	16.2	26.9	2.8	19.7	5.8	37.0
9.31	0.7	4.9	-4.4	30.4	2.0	3.5	14.3	18.7	-2.3	27.3	12.3	61.6
12.31	3.5	18.8	-0.5	2.2	-6.8	9.0	11.2	11.0	4.5	29.2	18.0	68.0

Theory predicts smaller particle radii and shallower particle depths than what was seen in the laboratory. Theory also shows two phase behaviour for all five time intervals, which was observed in the laboratory at t_e = 3.0 s.

The parameter z_T, the maximum particle separation from the thermal, is found by

translating the frame of reference of the particles relative to the center of the thermal ($z = z_T + Ut$). Since the model predicts the maximum depth reached by the particles for larger values of time very well it appears that the translational thermal speed U is causing some inconsistencies. One observation from the laboratory experiments is that the particle thermals exhibit acceleration and deceleration stages, indicating a nonuniform thermal velocity.

The last analysis for uniform speed thermals is for 0.0274 cm diameter particles assuming non-Stokes drag. Like the previous analysis for non-Stokes drag for 0.0548 cm diameter particles, theory and laboratory results compare very well. The non-Stokes analysis compares a little better than the Stokes drag analysis. This was expected since the non-Stokes Reynolds number is 5.0 at the terminal velocity of the particles. As before, the percent differences lessen as time increases. The differences for the last time interval are quite close, even for the particle crescent thickness. Theory also displays two phase behaviour for all the plotted intervals.

The thermal radius exhibits high percent differences for time intervals of $t = 4.90$ s and $t = 8.90$ s. The thermal radius is a function of the entrainment coefficient α, the thermal's translational velocity U and time t. The use of 0.25 as the value of the entrainment coefficient was validated in Chapter 4 and, therefore, it seems the value of the thermal velocity U maybe a contributing factor for this error.

Table 6.4 Comparison between Theoretical and Laboratory Results for 0.0274 cm diameter Particles (Run #3). Uniform Speed Thermal (U = -2.76 cm/s) and Non-Stokes Drag.

Time	Thermal Radius, a		Maximum Particle Radius, r		Thermal Depth, z		Maximum Particle Depth, z		Particle Crescent Thickness, b		Maximum Particle Separation, z_r	
(s)	Diff. (cm)	(%)	Diff. (cm)	(%)	Diff. (cm)	(%)	Diff. (cm)	(%)	Diff. (cm)	(%)	Diff. (cm)	(%)
4.90	-4.2	125.4	-4.1	119.5	16.7	123.6	19.7	108.4	-3.6	87.5	3.0	64.2
8.90	-6.6	106.8	-7.8	113.8	26.0	105.8	28.1	84.7	-4.6	75.2	2.2	24.9
14.90	-5.1	49.8	-12.0	121.3	27.8	67.7	29.9	53.7	-11.2	213.1	2.0	13.9
20.90	-5.6	38.7	-8.0	52.1	18.3	31.7	14.5	18.6	-5.8	54.4	-3.8	18.7
26.90	-1.8	9.5	-2.1	10.3	12.5	16.8	4.2	4.2	0.5	3.0	-8.3	31.9

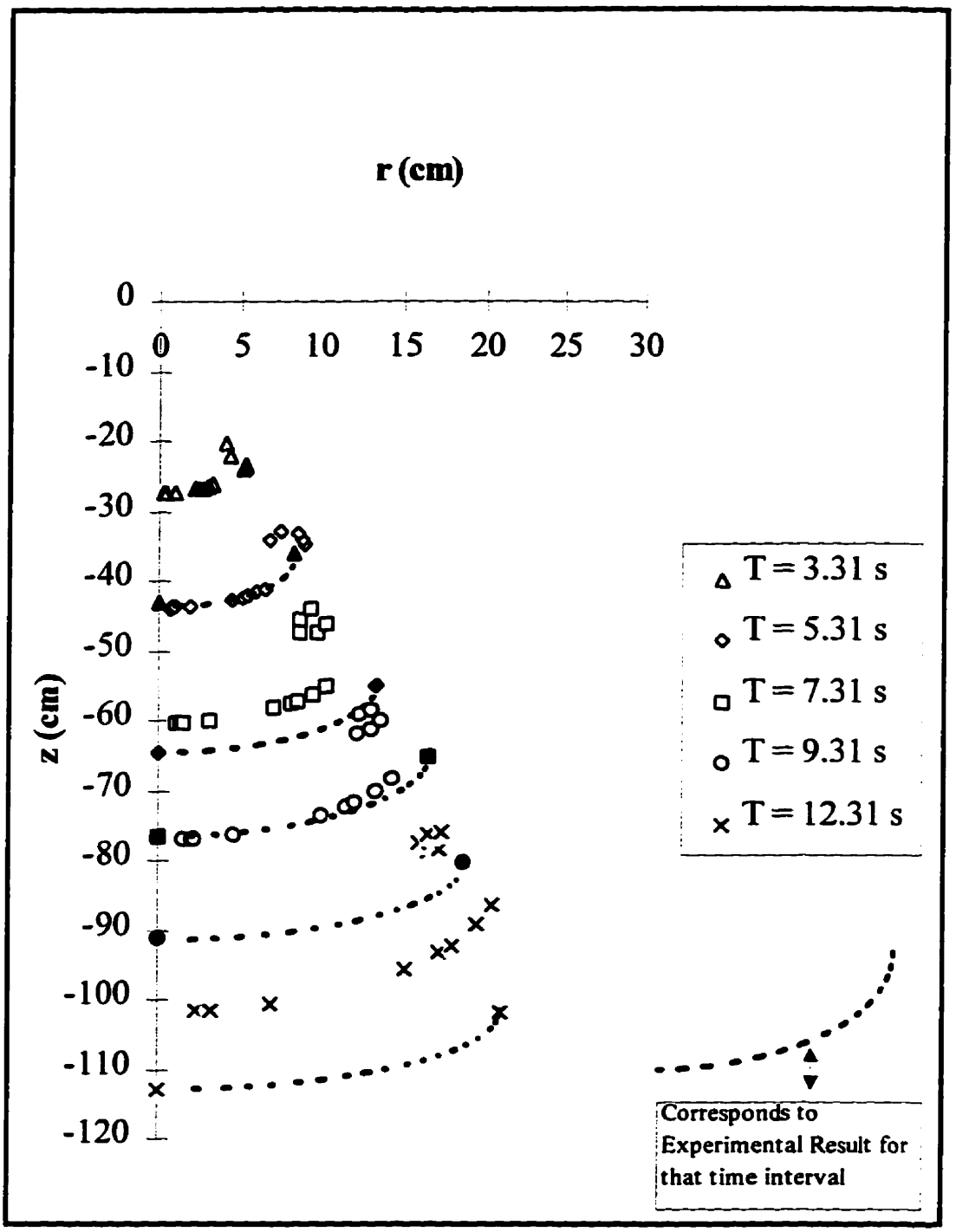

Figure 6.3 Comparison between theoretical and laboratory results for 0.0548 cm diameter particles (Run #16). Uniform speed thermal (U = -6.10 cm/s) and non-Stokes drag.

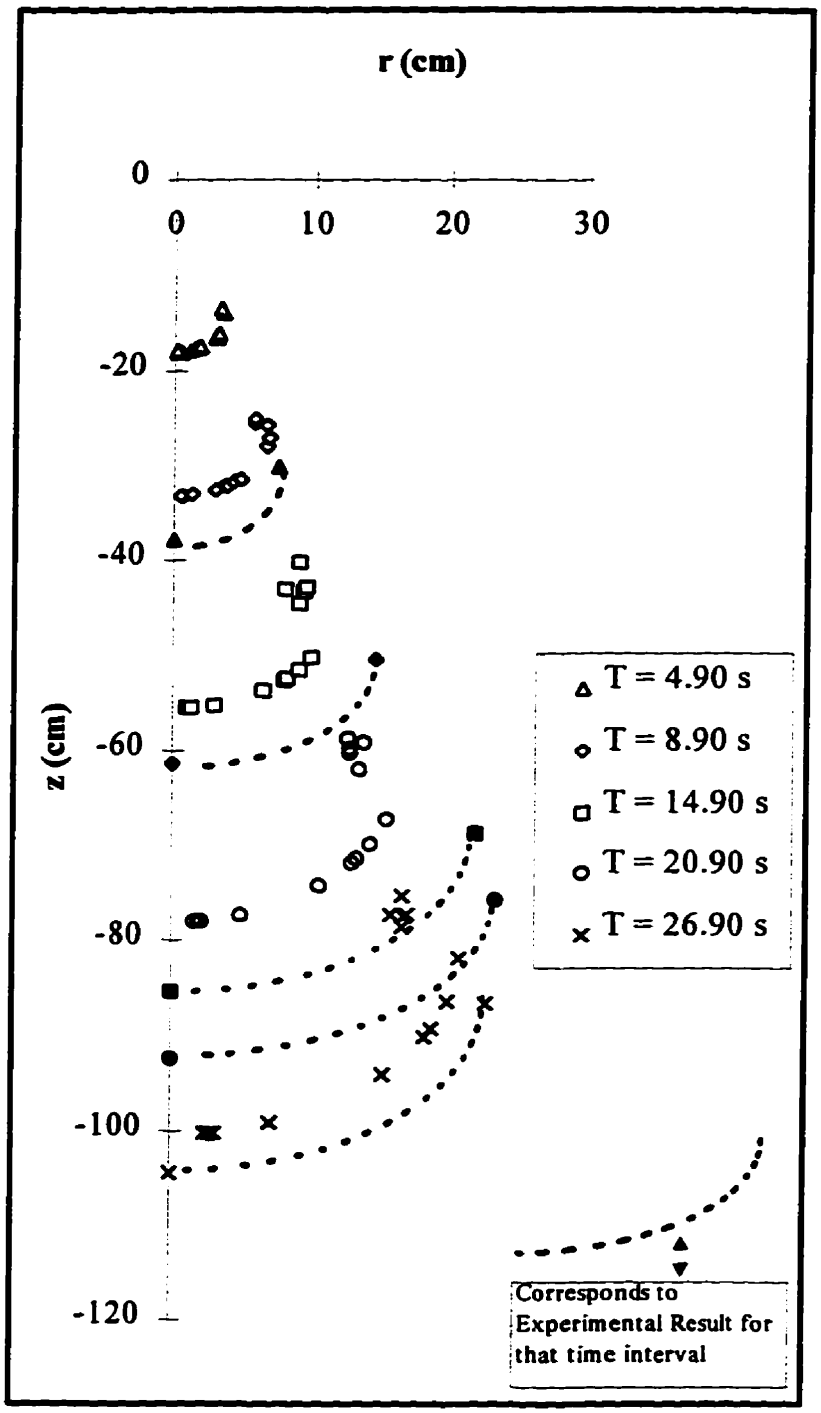

Figure 6.4 Comparison between theoretical and laboratory results for 0.0274 cm diameter particles (Run #3). Uniform speed thermal (U = -2.76 cm/s) and non-Stokes drag.

6.3 Nonuniform Speed Thermal Comparison

Nonuniform thermal speeds were observed in the many laboratory experiments performed. Thermal acceleration and deceleration was clearly seen with all the particle sizes studied. In order to compare the nonuniform theoretical simulations with the laboratory experiments the acceleration phase of a thermal is neglected. Acceleration occurs very quickly and in the laboratory experiments with 0.0274 and 0.0548 cm diameter particles the thermals both began to decelerate before the first recorded data point at t_e = 1.0 s (Refer to Figures 4.13 and 4.14). Theory estimates that both particle sizes will begin to decelerate after 0.5 s for a point source release. Therefore, there should be very little error in neglecting this phase in the nonuniform speed model.

Referring back to section 4.3, Figures 4.10 and 4.11, a linear relationship was found to exist for the particle thermals when the square of the vertical distance was plotted versus time. This implies that the thermal velocity varies inversely with the square root of time. From equations $U = \frac{K}{t^{\frac{1}{2}}}$ (2.14) and $a = 2\alpha K t^{\frac{1}{2}}$ (2.13), in section 2.1.4, velocity and thermal growth relationships were derived which also indicates this same behaviour. Constant K can be determined from the slope (square root of slope divided by two) of Figures 4.10 and 4.11, which directly relates the theoretical simulations to the laboratory experiments. K constants were determined for all 20 of the laboratory experiments included in Appendix A with constants varying from 8.0 to

12.0 $cm/s^{1/2}$ in value.

K can also be found theoretically from the equation for constant Q in section 2.1.4. Q is a function of the initial thermal and external fluid densities. Assuming that the internal thermal density is equal to the density of the glass particles initially, then a thermal having an initial radius of a = 2 cm has a constant K equal to 17.5 $cm/s^{1/2}$, which is the same value for the all glass particle sizes. Thus, there is reasonable agreement between the theoretical and laboratory K values (43% error for the K value from laboratory experiment #16 using 0.0548 cm particles).

From Figures 4.8 and 4.9, plots of the radial growth of the particle thermals for laboratory experiments #3 and #16, the best fit line was extended back to intersect the y-axis. Neglecting the initial acceleration phase of a thermal, this intersection corresponds to the location of a point source release. Thus, by knowing constant K, the theoretical time when a particle thermal grows to a radius of a = 2 cm, starting point for laboratory experiments, can be calculated. This is how much time offset (Δt) there is between laboratory and theoretical time intervals. The first data point recorded in the laboratory experiments was at t_e = 1.0 s in all experiments. Therefore, theoretical simulations are performed with an initial theoretical time of $t = t_e + \Delta t$, which corresponds to the first laboratory data point. Thus, a direct comparison can be done with the results.

For the nonuniform thermal speed analyses only a non-Stokes drag relationship is considered for the 0.0274 and 0.0548 cm diameter particles sizes since this compared the best in section 6.2. One theoretical simulation was performed and compared to

laboratory experiments #3 and #16. It is not necessary to compare more laboratory results with the theoretical model because each simulation is normalized to the laboratory result with the K constant. Other simulations with different K values would show identical behaviour.

6.3.1 0.0548 cm Diameter Particles - Non-Stokes Drag

The 0.0548 cm diameter particle analysis is for an initial velocity of -9.28 cm/s (initial condition of t = 1.0 s + 0.16 s). The K constant was determined from Figure 4.11 and is equal to 10.0 cm/s$^{1/2}$. The theoretical time is the time referenced in Figure 6.5. Equivalent laboratory time intervals can be found by subtracting 0.16 seconds from the theoretical time.

Table 6.5 Comparison between Theoretical and Laboratory Results for 0.0548 cm diameter Particles (Run #16). Nonuniform Speed Thermal (Initial Speed U = -9.28 cm/s) and Non-Stokes Drag.

Time	Thermal Radius, a		Maximum Particle Radius, r		Thermal Depth, z		Maximum Particle Depth, z		Particle Crescent Thickness, b		Maximum Particl Separation, z_T	
(s)	Diff. (cm)	(%)	iff. (cm	(%)	iff. (cm	(%)	Diff. (cm)	(%)	Diff. (cm	(%)	iff. (cm	(%)
1.16	0.0	-0.2	-1.6	-39.7	-5.7	26.3	-4.9	18.9	0.6	9.8	0.8	-17.6
3.16	0.9	10.1	-1.8	-20.4	0.2	-0.7	-3.9	8.3	1.3	15.0	-4.1	35.2
6.16	1.8	14.9	-3.1	-23.2	-2.2	4.6	-0.8	1.2	-1.3	-13.1	1.4	-7.0
9.16	0.7	4.8	-3.7	-22.5	-7.3	12.2	0.9	-1.0	7.9	41.0	8.2	-28.0
11.16	1.3	7.9	-2.8	-15.7	-5.9	8.9	2.8	-2.8	9.3	46.2	8.7	-24.4

The particle and thermal depths and radii compare very well to the laboratory results. Except for the first time interval for some parameters the percent differences remain fairly low for all the other intervals. This is a promising indication that the model

is valid for longer values of time to predict particle and thermal behaviour. The particle crescent thickness b and particle separation z_T compare better using a nonuniform speed versus a uniform speed in the model. Overall, for an initial speed of -9.28 cm/s the nonuniform results in Table 6.5 compare better to the laboratory results than the uniform thermal speed analysis. Referring to Figures 6.3 and 6.5, the uniform and nonuniform speed plots display thermal behaviour that is visually quite similar to the laboratory data. They both show two phase behaviour, i.e., particles located in clusters and particles in a crescent for each time interval. The clusters indicate particles trapped within the vortex flow of the thermal and the crescents indicate particles that have separated from the thermal.

6.3.2 0.0274 cm Diameter Particles - Non-Stokes Drag

The 0.0274 cm diameter analysis is with an initial speed of -7.22 cm/s (initial condition of t = 1.0 s + 0.25 s). The comparison between theoretical and laboratory results are shown in Table 6.6 and Figure 6.6. As before, the theoretical time is the one referenced in the table and figure. The laboratory time can be found by subtracting 0.25 s from the theoretical value. A K constant equal to 8.06 $cm/s^{1/2}$ was found from Figure 4.10 and is used for the theoretical simulation.

The analysis in Table 6.6 shows similar results to those in Table 6.5. Considering all time intervals the nonuniform model predicts thermal and particle parameters better than the uniform speed model. However, the uniform speed model does predict better

particle and thermal behaviour for the last time interval. Figures 6.4 and 6.6 visually

Table 6.6 Comparison between Theoretical and Laboratory Results for 0.0274 cm diameter Particles (Run #3). Nonuniform Speed Thermal (Initial Speed U = -7.22 cm/s) and Non-Stokes Drag.

Time	Thermal Radius, a		Maximum Particle Radius, r		Thermal Depth, z		Maximum Particle Depth, z		Particle Crescent Thickness, b		Maximum Particle Separation, z_T	
(s)	Diff. (cm)	(%)	Diff. (cm)	(%)	Diff. (cm)	(%)	Diff. (cm)	(%)	Diff. (cm)	(%)	Diff. (cm)	(%)
1.25	-1.1	-23.5	-2.6	-76.5	0.2	-0.9	3.6	-16.6	-2.3	-48.9	3.4	-94.7
8.25	-0.2	-1.6	-4.7	-39.2	7.4	-16.1	6.1	-10.0	0.3	2.0	-1.4	9.2
14.25	-2.3	-14.8	-5.5	-32.7	6.9	-11.3	4.4	-5.2	-4.6	-30.7	-2.5	11.2
20.25	-0.6	-3.4	-3.1	-15.4	1.5	-2.1	-14.5	14.1	5.6	28.5	-16.0	53.4
26.25	-0.8	-3.8	0.7	3.1	2.9	-3.5	-15.1	12.5	1.5	7.0	-18.0	47.0

display particle behaviour similar to the laboratory experiments. They show particles trapped within the vortex as well as particles that have separated from the thermal.

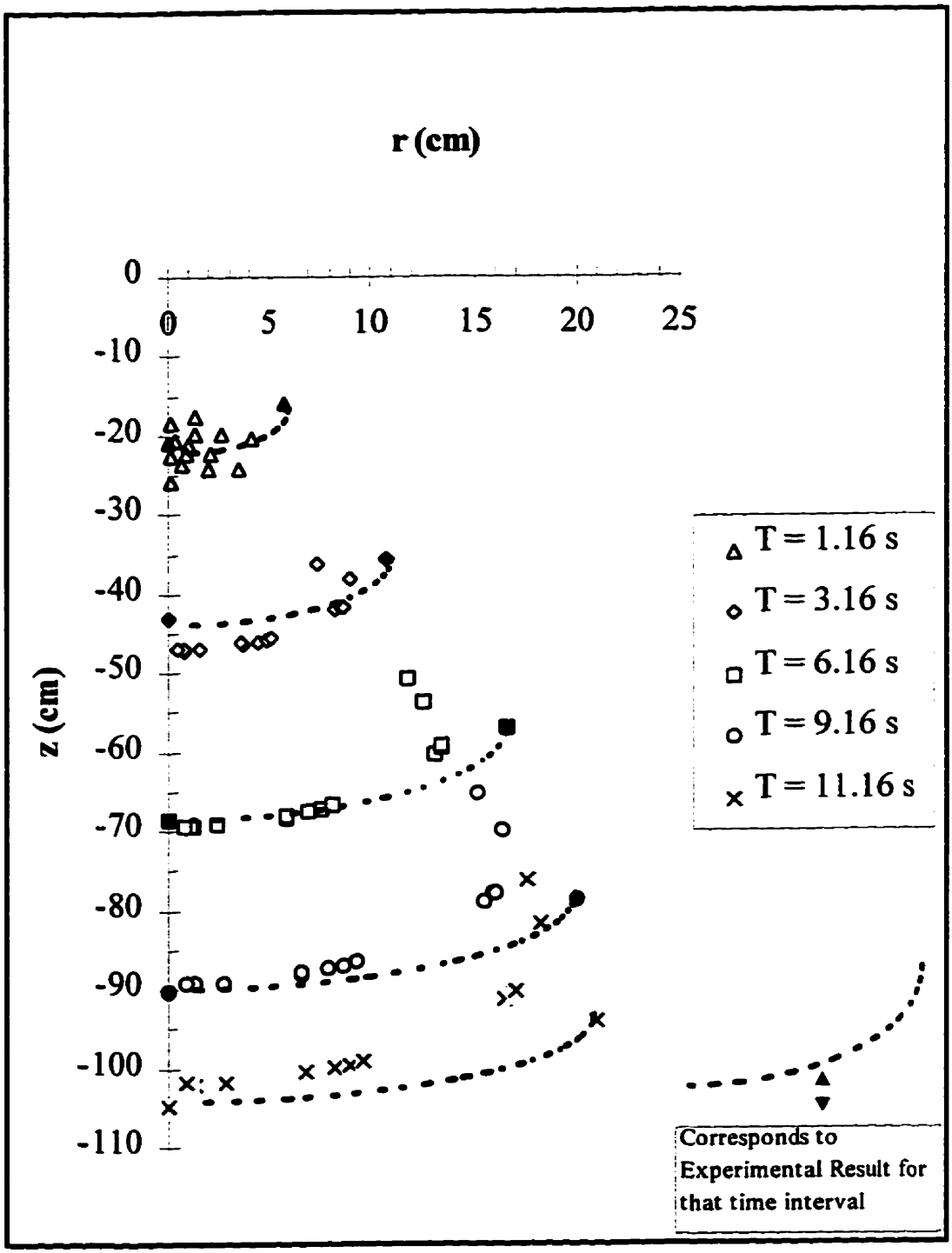

Figure 6.5 Comparison between theoretical and laboratory results for 0.0548 cm diameter particles (Run #16). Nonuniform speed thermal (initial speed U = -9.28 cm/s) and non-Stokes drag.

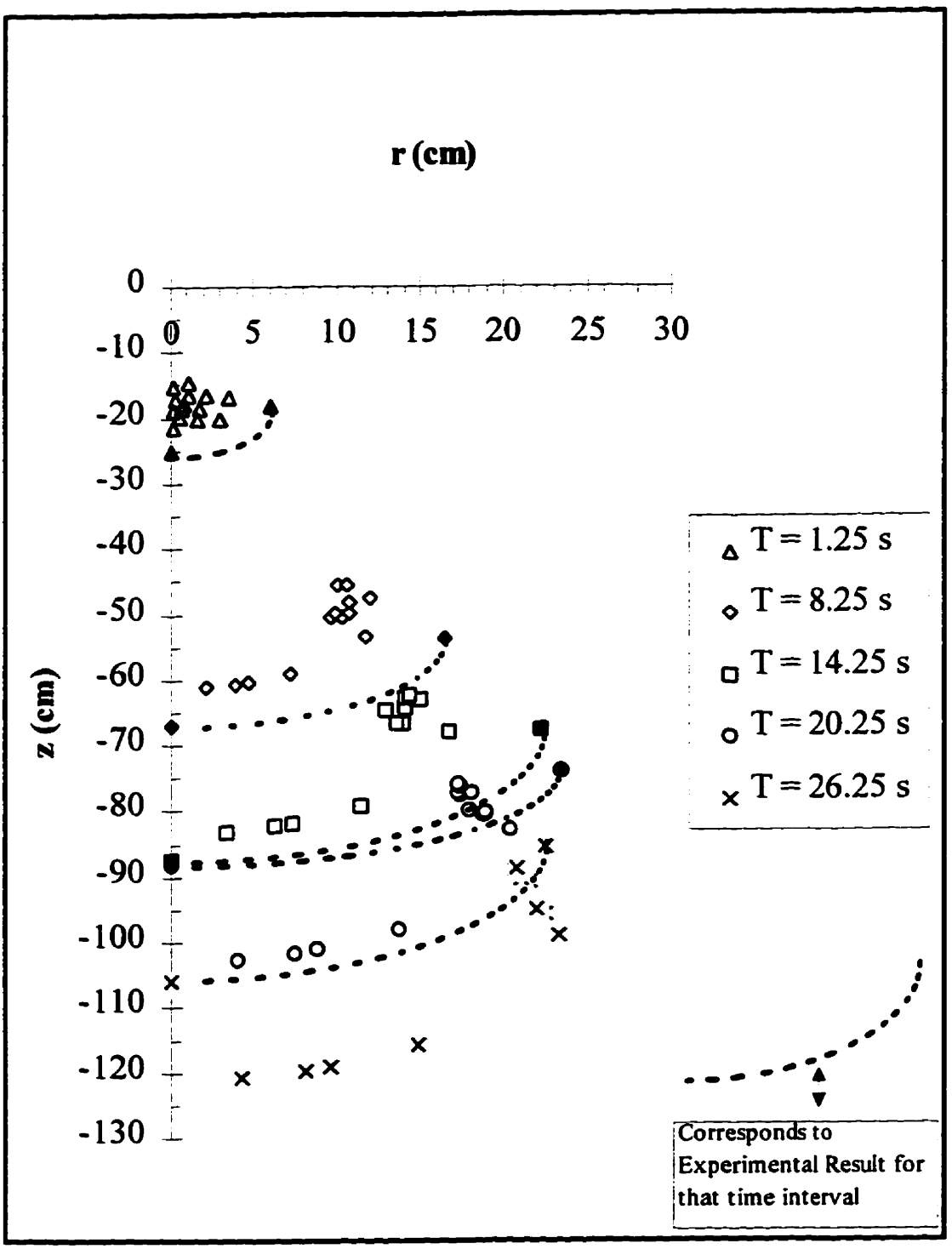

Figure 6.6 Comparison between theoretical and laboratory results for 0.0274 cm diameter particles (Run #3). Nonuniform speed thermal (initial speed U = -7.22 cm/s) and non-Stokes drag.

Chapter 7

Conclusions and Recommendations

7.1 Conclusions

1. Excellent agreement was found from the comparison carried out in Chapter 5 between Topham et al's theoretical thermal model using polystyrene particles and the same model using glass particles. A uniform thermal velocity with a Stokes drag relationship were used in the theoretical model. In Topham et al's paper (1994), they roughly compared their theoretical model with laboratory experiments performed by Lee (1992) and Laureschen (1992), whereas a detailed comparison was performed here.

2. The assumed fluid flow field in the thermal model consisted of an expanding Hill's spherical vortex and potential flow theory. Both flow fields modelled thermal and particle behaviour very well. The dimensionless plots in Chapter 5 visually display very similar behaviour to the pictures of the laboratory experiments included in Chapter 4. The detailed comparison of theoretical and laboratory results in Chapter 6 helped verify that this type of flow field effectively describes the fluid motions of a solid particle thermal.

3. Originally, this thesis project was only going to consider a particle thermal model travelling at a uniform velocity, but after performing some laboratory experiments it became apparent particle thermals travel at nonuniform velocities. They initially accelerate until they reach their maximum velocity and then decelerate. A nonuniform velocity relationship was proposed in Chapter 2 for use in the theoretical thermal model. This relationship ignores the initial acceleration phase of the thermal and only considers the deceleration phase. Initial velocities were selected at values less than the theoretical maximum velocity. In Chapter 5 and 6 simulations were performed with initial velocities corresponding to the first data point from each laboratory experiment at $t_e = 1.0$ s.

4. The nonuniform thermal model with a non-Stokes drag relationship predicted particle thermal behaviour that compared the best with the laboratory experiments. The theoretical results display particle behaviour that is very similar to observations from the laboratory experiments. For the 0.0548 cm diameter glass particles, they were observed to separate quickly from the thermal and then settle in a crescent shape moon formation. The nonuniform model predicted very similar behaviour at similar time intervals. The 0.0274 cm diameter glass particles were observed to stay in the internal flow of the thermal for a longer period of time. Again, the model reasonably predicted this behaviour.

5. Even though nonuniform thermal velocities were observed in the laboratory experiments, the uniform speed thermal model predicted glass particle thermal behaviour quite well when using a non-Stokes drag relationship and a uniform translational velocity equal to the terminal velocity of the glass particles.

6. The glass particles used in this thesis project all have terminal velocities in the non-Stokes flow regime, which led to the use of a linear drag law (non-Stokes drag) in the theoretical model. Results compared very well for both uniform and nonuniform thermal speeds using a non-Stokes drag relationship. Stokes drag also was used in the model for comparison purposes. Only the 0.0274 cm diameter glass particle size

compared reasonably well to the laboratory experiments. This was expected since this was the smallest particle size studied and it's Reynolds number at terminal velocity lies just outside the Stokes flow regime.

7. The K constant can be determined two ways. First, experimentally from the square root of the slope divided by a factor of two from the laboratory plots of the vertical distance squared versus time. Second, theoretically from the initial buoyancy of the solid particle thermal. The first method was used in the thermal model in Chapters 5 and 6, in order to carry out a detail comparison between theoretical and laboratory results. However, the theoretical K constant was tested in the various forms of the model as well and the results also compared very well to the laboratory experiments. The theoretical K constant is the same value for all sizes of particles, because it is only dependent on the specific gravity of the glass particles, whereas the experimental K is specific to each experimental run. Experimental K constants varied in value from 8.0 - 12.0 $cm/s^{1/2}$ and the theoretical K was equal to 17.5 $cm/s^{1/2}$ assuming that the initial thermal at release has a specific gravity equal to the glass particles.

8. The theoretical particle motion equations only model the behaviour of a single glass particle. Therefore, for each theoretical simulation the equations were numerically integrated for 14 different particles with different initial locations in the initial

thermal. The 14 separate results were then combined to produce a summary result which described the behaviour of multiple particles in a thermal flow field. Thus, it was assumed that the particle motions of each single particle has negligible impact on the motions of other particles. Since the laboratory experiments compare very well to the theoretical simulations, this seems to be a valid assumption.

9. The initial velocity of the particles in the theoretical model was assumed to have a value equal to the Hill's spherical vortex at that location and time. This assumption is adequate, but it does introduce some unrealistic initial particle accelerations when predicting the behaviour of particles at small values of time ($t < 1.0$ s). However, for longer periods of time ($t > 1.0$ s) this assumption does not introduce any substantial error.

10. Solid particle thermals do not experience a change in vertical or radial growth after the transition point, when particles permanently separate from the thermal. This observation was also noted by Noh and Fernando (1993). It is thought that turbulence from the particle wakes is entrained in the trailing thermal.

11. The value of $\alpha = 0.25$ for the entrainment coefficient was validated. In other research, values of the entrainment coefficient are often assumed to be either 0.25 or

0.30. By plotting the radial spread versus distance from the laboratory data, entrainment coefficients were found in this range.

12. A spring loaded release mechanism, as shown in Chapter 3, is an effective way to release a solid particle thermal cloud into a water tank. The mechanism added little or no initial impulse to the particle thermal and generally produced a very symmetrical thermal cloud.

13. The laser light sheet effectively illuminated a thin cross-sectional area of the experimental thermal, which greatly aided in the subsequent computer analysis of the experimental videotape. The light sheet was generated with a 500 mW argon ion laser and a rotating front-faced mirror.

7.2 Recommendations

The theoretical model used to predict the behaviour of glass particle thermals consisted of a particle model with an assumed fluid flow field. The model was simplified in several ways in order to solve numerically. Areas worth further development with regards to the model are outlined below.

- Investigate the effect of the Basset history and lift force terms in the particle model.

- Examine the initial particle velocity in the model. Is another initial velocity appropriate, rather than making it equal to the initial velocity of the background fluid flow field?

- Study the small time behaviour of solid particle thermals. The Basset history term will have more impact at smaller values of time.

The laboratory experiments were executed smoothly, due in part, to the use of an argon laser, a large water tank and an efficient release mechanism. However, there are a few areas where future laboratory work can be done.

- Rework the raw laboratory data for polystyrene particles from Lee's research (1992) and see how they compare with the theoretical models introduced in this thesis project. It might be worthwhile performing more laboratory experiments with another particle type with the present apparatus. Lee's experiments were performed with a slightly different apparatus.

- Obtain laboratory data for the acceleration phase of a thermal ($t_e < 1.0$ s). This would require a few changes to the present laboratory apparatus. The argon laser setup

would require a higher speed motor to spin the mirror, which generates the laser light sheet (a multifaceted mirror would also work). The one used only rotated at 1880 rpm and, therefore, would not generate a light sheet of sufficient frequency for a high speed video camera. A high speed camera would aid in the study of the small time behaviour of particle thermals.

References

Auton, T.R., Hunt, J.C.R. & Prud'homme, M., 1988, The Force Exerted on a Body in Inviscid Unsteady Non-uniform Rotational Flow, J. Fluid Mech., Vol. 197, pp. 241-257.

Ayotte, B.A., and Fernando, H.J.S., 1994, The Motion of a Turbulent Thermal in the Presence of Background Rotation, J. Atmos. Sci., Vol. 51, pp. 1989-1994.

Batchelor, G.K. 1954, Heat Convection and Buoyancy Effects in Fluids, Quart. J. Roy. Met. Soc., Vol. 80, pp. 339-358.

Boras, A., 1996, Cutting CO_2 emissions painful, Calgary Herald, Dec. 12 edit.

Davidson, G.A., 1989, Simultaneous Trajectory and Dilution Predictions From a Simple Integral Plume Model, Atmos.Envir., Vol. 23, pp. 341-349.

Edmonton Journal, 1996, Swan Hills - Correcting leak to cost a bundle, Calgary Herald, Dec. 12 edit.

Escudier, M.P. and T. Maxworthy 1973, On the Motion of Turbulent Thermals, J.Fluid Mech., Vol. 61, pp. 541-552.

Heinke, G.W. and Henry, J.G., 1989, Environmental Science and Engineering, Prentice-Hall Inc., Englewood Cliffs, New Jersey, U.S.A., pp. 372-398.

Hellums, J.D. and S.W. Churchill 1961, Dimensional Analysis and Natural Circulation, Chemical Engineering Progress Symposium.

Johari, H., 1992, Mixing in Thermals with and without Buoyancy Reversal, Amer. Meteor. Society, vol. 49, pp. 1412-1426.

Krishnappan, B.G., 1975, Dispersion of Granular Material Dumped in Deep Water, Scientific Series No. 55, Information Canada, Ottawa, Canada.

Lee, Y.G., 1992, An Investigation of the Dynamics of Solid Particle Thermals, M.Sc. Thesis, Department of Mechanical Engineering, The University of Calgary, Calgary, Canada.

Luketina, D., and Wilkinson, D., 1994, Particle Clouds in Density Stratified Environments, Fourth International Symposium on Stratified Flows, Vol. 2 of the preprints.

Maxey, M.R. and Riley, J.J., 1983, Equations of Motion for a Small Rigid Sphere in a Non-uniform Flow, Phys. Fluids, pp. 883-889.

Milne and Thomson,1967, Theoretical Hydrodynamics, 5th edit., Macmillan, pp. 554-555.

Morton, B.R., Taylor, Sir Geoffrey. and Turner, J.S., 1956, Turbulent Gravitational Convection from Maintained and Instantaneous Sources, Proc. Roy. Soc. A, Vol. 234.

Nelson, B., 1996, Bid to cut greenhouse has emissions failing, Calgary Herald, Dec. 12 edit.

Noh, Y. and Fernando, H.J.S., 1993, The transition in the sedimentation pattern of a particle cloud, Phys. Fluids, pp. 3049-3055.

Ramalho, R.S., 1983, Introduction to Wastewater Treatment Processes, 2nd edit., Academic Press Inc., San Diego, CA, U.S.A., pp. 80-85.

Reeks, M.W. and McKee, S., 1984, The dispersive effects of Basset history forces on particle motion in a turbulent flow, Phys. Fluids, Vol. 27, pp. 1573-1582.

Ruetsch, G.R. and Meiberg, E., 1993, On the Motion of Small Spherical Bubbles in Two-Dimensional Vortical Flow, Phys. Fluids, Vol. 5, pp. 2326-2341.

Saffman, P.G., 1965, The lift on a small sphere in a slow flow, J. Fluid Mech., Vol. 22, pp. 385-400.

Schatzmann, M., 1979, An Integral Model of Plume Rise, Atmos. Envir., Vol. 13, pp. 721-731.

Scorer, R.S., 1978, Environmental Aerodynamics, Halsted Press, John Wiley & Sons, Chichester, England, pp. 276-303.

Sene, K.J., Hunt, J.C.R. and Thomas, N.H., 1994, The role of coherent structures in bubble transport by turbulent shear flows, J. Fluid Mech., Vol. 259, pp. 219-240.

Thomas, D., 1996, Oil Cleanup far from complete, Calgary Herald, Dec. 12 edit.

Tio, K-K., Linan, A., Lasheras, J.C. and Ganan-Calvo, A.M, 1993, On the Dynamics of Buoyant and Heavy Particles in a Periodic Stuart Vortex Flow, J. Fluid Mech., Vol. 254, pp. 671-208.

Topham, D.R., Laureshen, C.J., Lee, Y.G., and Rowe, R.D., 1994, The Dynamics of Particle Thermals, Proceedings of the 10th International Heat Transfer Conference, Vol. 6, Brighton, England, pp. 283-288.

Tritton, D.J., 1988, Physical Fluid Dynamics, 2nd edit., Oxford University Press, New York, U.S.A., pp. 48-69.

Turner, J.S., 1964, The Flow into an Expanding Spherical Vortex, J. Fluid Mech., Vol. 18, pp. 195-208.

Turner, J.S., 1973, Buoyancy Effects in Fluids, Cambridge University Press, Cambridge, England, pp. 165-207.

Appendix A - Raw Data from Laboratory Experiments

Table A.1 Experimental Run #1 - 14.6 g of 0.0274 cm Diameter Glass Particles
Date: March 25/94
Time: 1:00 PM

Measurement Scale = 1.57480 pixels/cm

Time (s	a (cm)	a_p (cm)	z (cm)	z_p (cm)	b (cm)	b_p (cm)	Observations
0.0	2.0	2.0	0.0	0.0	2.0	2.0	
1.0	5.4	5.4	12.7	12.7	8.3	8.3	
2.0	8.3	8.3	25.4	25.4	7.0	7.0	
3.0	9.2	9.2	29.2	29.2	10.2	10.2	
4.0	11.4	11.4	36.8	36.8	9.5	9.5	
5.0	12.4	12.4	41.9	41.9	12.7	12.7	
6.0	14.0	14.0	47.6	47.6	13.3	13.3	
7.0	15.9	15.9	50.8	50.8	9.5	15.2	
8.0	17.8	17.8	52.7	52.7	12.7	18.4	
9.0	17.8	17.8	55.9	55.9	14.0	19.7	Partial separation at 9 sec
10.0	17.8	17.8	59.7	72.4	12.7	8.9	
11.0	17.8	17.8	61.6	76.8	12.1	6.4	
12.0	19.1	19.1	64.1	80.6	11.4	5.7	
13.0	19.7	19.7	64.8	64.8	12.7	12.7	Particles no longer visible
14.0	20.0	20.0	67.3	67.3	13.3	13.3	
15.0	20.3	20.3	71.1	71.1	12.7	12.7	
16.0	21.3	21.3	74.3	74.3	10.8	10.8	
17.0	22.9	22.9	74.9	74.9	14.0	14.0	
18.0	24.1	24.1	76.8	76.8	14.6	14.6	
19.0	25.7	25.7	77.5	77.5	15.2	15.2	
20.0	23.8	23.8	77.5	77.5	12.1	12.1	Effects of tank bottom start
21.0	24.8	24.8	77.5	77.5	18.4	18.4	
22.0	26.7	26.7	78.1	78.1	20.3	20.3	
24.0	25.4	25.4	83.2	83.2	22.2	22.2	

Table A.2 Experimental Run #2 - 14.6 g of 0.0274 cm Diameter Glass Particles
Date: March 28/94
Time: 12:17 PM

Measurement Scale = 1.57480 pixels/cm

Time (s	a (cm)	a_p (cm)	z (cm)	z_p (cm)	b (cm)	b_p (cm)	Observations
0.0	2.0	2.0	0.0	0.0	2.0	2.0	
1.0	5.7	5.7	12.7	12.7	7.0	7.0	
2.0	8.9	8.9	26.7	26.7	4.5	4.5	
3.0	11.1	11.1	29.9	29.9	5.7	5.7	
4.0	13.0	13.0	33.7	33.7	9.5	9.5	
5.0	13.0	13.0	36.2	36.2	12.1	12.1	
6.0	14.3	14.3	41.3	41.3	12.2	12.2	
8.0	18.4	18.4	52.7	52.7	9.5	9.5	Start of two phase behaviour
10.0	22.5	22.5	59.7	59.7	8.9	12.7	Two phase behaviour
12.0	24.1	24.1	60.3	60.3	14.6	18.4	
14.0	26.0	26.0	60.3	60.3	17.8	23.5	Particles in front dispersing
16.0	27.3	27.3	66.0	66.0	12.1	12.1	Can't see particles out front
18.0	27.0	27.0	71.8	71.8	14.6	14.6	
20.0	26.7	26.7	76.8	76.8	14.0	14.0	
22.0	28.6	28.6	78.7	78.7	14.6	14.6	
24.0	28.9	28.9	80.0	80.0	14.6	14.6	
26.0	28.6	28.6	83.2	83.2	14.0	14.0	

Table A.3 Experimental Run #3 - 14.6 g of 0.0274 cm Diameter Glass Particles
Date: March 30/94
Time: 2:40 PM

Measurement Scale = 1.57480 pixels/cm

Time (s	a (cm)	a_p (cm)	z (cm)	z_p (cm)	b (cm)	b_p (cm)	Observations
0.0	2.0	2.0	0.0	0.0	2.0	2.0	
1.0	6.0	6.0	15.2	15.2	5.1	7.0	Nice release
2.0	7.6	7.6	22.2	22.2	7.6	7.6	Single phase behaviour
3.0	10.5	10.5	29.9	29.9	8.3	8.3	Single phase behaviour
4.0	11.8	11.8	34.3	34.3	9.5	9.5	Single phase behaviour
5.0	13.3	13.3	38.1	38.1	10.2	10.2	Single phase behaviour
6.0	14.6	14.6	42.6	42.6	10.8	10.8	Nice symmetrical thermal
8.0	16.5	16.5	50.8	50.8	7.0	13.3	Start of two phase behaviour
10.0	18.1	18.1	51.4	51.4	10.8	16.5	Two phase behaviour
12.0	21.9	21.9	61.0	61.0	8.9	16.5	Two phase behaviour
14.0	22.2	22.2	64.8	64.8	12.7	19.7	Harder to see particles
16.0	23.2	23.2	64.1	64.1	15.9	22.9	Hardly see particles
18.0	23.5	23.5	68.0	68.0	16.5	16.5	Can't see particles anymore
20.0	23.5	23.5	71.1	71.1	14.0	14.0	
22.0	23.5	23.5	75.6	75.6	19.7	19.7	
24.0	22.9	22.9	78.7	78.7	17.8	17.8	
26.0	22.5	22.5	82.6	82.6	20.3	20.3	
28.0	22.9	22.9	86.4	86.4	21.6	21.6	

Table A.4 Experimental Run #4 - 14.6 g of 0.0274 cm Diameter Glass Particles
Date: March 30/94
Time: 5:22 PM

Measurement Scale = 1.57480 pixels/cm

Time (s	a (cm)	a_p (cm)	z (cm)	z_p (cm)	b (cm)	b_p (cm)	Observations
0.0	2.0	2.0	0.0	0.0	2.0	2.0	
1.0	7.3	7.3	12.7	12.7	7.0	7.0	Nice release
2.0	7.0	7.0	25.4	25.4	6.4	6.4	
3.0	10.2	10.2	30.5	30.5	7.0	7.0	
4.0	11.1	11.1	36.2	36.2	8.3	8.3	
5.0	11.4	11.4	39.4	39.4	10.2	10.2	
6.0	13.7	13.7	42.6	42.6	10.8	12.7	
7.0	14.3	14.3	47.0	47.0	10.8	12.7	
8.0	15.2	15.2	50.8	50.8	8.9	12.7	
9.0	17.1	17.1	55.3	55.3	13.3	13.3	Can still see two phases
10.0	17.5	17.5	55.9	55.9	14.6	14.6	
12.0	20.3	20.3	62.9	62.9	14.6	14.6	
14.0	22.2	22.2	68.6	68.6	13.3	13.3	
16.0	22.9	22.9	73.7	73.7	12.7	12.7	
18.0	26.7	26.7	80.7	80.7	14.6	14.6	
20.0	25.4	25.4	80.0	80.0	17.2	17.2	
22.0	26.7	26.7	81.9	81.9	20.3	20.3	
24.0	26.7	26.7	81.9	81.9	16.5	16.5	
26.0	27.0	27.0	81.3	81.3	19.7	19.7	

Table A.5 Experimental Run #5 - 14.6 g of 0.0274 cm Diameter Glass Particles
Date: March 31/94
Time: 11:01 AM

Measurement Scale = 1.57480 pixels/cm

Time (s	a (cm)	a_p (cm)	z (cm)	z_p (cm)	b (cm)	b_p (cm)	Observations
0.0	2.0	2.0	0.0	0.0	2.0	2.0	
1.0	7.6	7.6	15.9	15.9	5.7	5.7	
2.0	9.5	9.5	20.3	20.3	11.4	11.4	
3.0	9.8	9.8	24.1	24.1	15.2	15.2	
4.0	10.8	10.8	36.8	36.8	8.9	8.9	
5.0	12.7	12.7	40.0	40.0	12.7	12.7	
6.0	14.0	14.0	43.2	43.2	14.6	14.6	
7.0	14.6	14.6	50.2	50.2	12.7	12.7	
8.0	15.9	15.9	54.0	54.0	11.4	13.3	Particles visible out front
9.0	17.1	17.1	55.3	55.3	12.7	16.5	Some particles curling back
10.0	17.5	19.1	61.0	61.0	10.2	14.0	
12.0	17.8	21.6	66.0	66.0	14.6	16.5	
14.0	17.5	21.9	69.9	69.9	14.0	16.5	
16.0	19.4	23.2	73.0	73.0	14.6	NA	Can't see separated particles
18.0	21.6	25.4	81.3	81.3	11.4	NA	
20.0	21.9	NA	85.1	85.1	12.7	NA	
22.0	23.2	NA	86.4	86.4	14.0	NA	
26.0	24.8	NA	90.2	NA	19.1	NA	

Table A.6 Experimental Run #6 - 10 mL 0.0359 cm Diameter Glass Particles
Date: April 8/94
Time: 12:04 PM

Measurement Scale = 1.57480 pixels/cm

Time (s	a (cm)	a_p (cm)	z (cm)	z_p (cm)	b (cm)	b_p (cm)	Observations
0.0	2.0	2.0	0.0	0.0	2.0	2.0	
1.0	6.0	6.0	15.2	15.2	8.9	8.9	Nice release
2.0	7.0	7.0	27.9	27.9	8.9	8.9	
3.0	8.9	8.9	37.5	37.5	8.3	8.3	Nice and spherical thermal
4.0	9.5	9.5	47.0	47.0	7.0	7.0	
5.0	12.7	12.7	49.5	49.5	8.3	9.5	Two phase behaviour
6.0	14.6	14.6	55.3	55.3	8.9	10.8	
7.0	16.2	16.2	60.3	60.3	6.4	12.1	On verge of separation
8.0	15.2	17.1	60.3	64.8	13.3	13.3	Separation
9.0	16.2	18.4	63.5	71.1	15.9	12.1	
10.0	15.6	19.1	65.4	73.0	17.2	NA	Can't see separated particles

Table A.7 Experimental Run #7 - 10 mL 0.0359 cm Diameter Glass Particles
Date: April 8/94
Time: 2:17 PM

Measurement Scale = 1.57480 pixels/cm

Time (s	a (cm)	a_p (cm)	z (cm)	z_p (cm)	b (cm)	b_p (cm)	Observations
0.0	2.0	2.0	0.0	0.0	2.0	2.0	
1.0	5.4	5.4	14.6	14.6	10.2	10.2	
2.0	7.0	7.0	29.2	29.2	6.4	6.4	
3.0	8.6	8.6	35.6	35.6	8.3	8.3	Nice thermal
4.0	10.5	10.5	41.3	41.3	8.9	8.9	
5.0	13.0	13.0	45.1	45.1	7.6	11.4	Two phase behaviour
6.0	13.3	15.2	47.0	56.5	12.1	7.6	
7.0	14.0	16.2	50.2	59.1	10.8	8.3	Separation
8.0	14.0	17.1	51.4	63.5	13.3	8.9	
9.0	16.8	18.7	60.3	69.9	7.6	10.2	Nice particle crescent
10.0	16.5	19.4	61.0	75.6	10.8	8.89	
11.0	17.5	20.6	62.2	NA	14.0	NA	
12.0	17.8	NA	61.6	81.9	12.7	11.4	
13.0	18.7	21.9	64.8	87.6	19.7	9.53	

Table A.8 Experimental Run #8 - 10 mL 0.0359 cm Diameter Glass Particles
Date: April 9/94
Time: 1:03 PM

Measurement Scale = 1.57480 pixels/cm

Time (s	a (cm)	a_p (cm)	z (cm)	z_p (cm)	b (cm)	b_p (cm)	Observations
0.0	2.0	2.0	0.0	0.0	2.0	2.0	
1.0	7.9	7.9	16.5	16.5	5.1	5.1	
2.0	11.4	11.4	25.4	25.4	7.6	7.6	
3.0	12.4	12.4	30.5	30.5	8.9	8.9	Nice and symmetrical
4.0	14.3	14.3	33.7	33.7	12.1	12.1	
5.0	12.4	14.6	40.0	41.3	7.6	11.4	Two phase behaviour
6.0	14.9	15.6	43.8	47.6	8.3	10.8	Partial separation
7.0	14.9	17.1	46.4	52.1	8.9	12.1	Slanted crescent
8.0	13.3	18.4	51.4	52.1	5.7	17.2	Total separation
9.0	14.9	19.4	53.3	59.1	8.9	15.2	
10.0	15.9	19.7	55.9	63.5	12.7	17.78	
11.0	16.8	21.0	61.6	70.5	9.5	15.9	
12.0	16.8	20.6	61.6	73.0	11.4	15.9	
13.0	16.5	22.5	66.7	86.4	8.3	8.89	
14.0	16.8	23.2	69.9	91.4	8.3	8.89	

Table A. 9 Experimental Run #9 - 15 mL 0.0359 cm Diameter Glass Particles
Date: April 9/94
Time: 2:40 PM
Measurement Scale = 1.57480 pixels/cm

Time (s	a (cm)	a_p (cm)	z (cm)	z_p (cm)	b (cm)	b_p (cm)	Observations
0.0	2.0	2.0	0.0	0.0	2.0	2.0	
1.0	6.7	6.7	21.6	21.6	3.2	3.2	
2.0	9.8	9.8	28.6	28.6	7.0	7.0	
3.0	11.8	11.8	33.7	33.7	9.5	9.5	
4.0	13.7	13.7	38.7	38.7	11.4	11.4	
5.0	15.9	15.9	47.0	47.0	12.1	12.1	
6.0	15.6	18.1	45.7	47.0	9.5	15.9	Two phase behaviour
7.0	16.2	17.5	48.3	50.8	12.1	16.5	
8.0	15.6	18.4	47.6	54.6	17.2	19.1	Close to separation
9.0	16.5	18.1	50.8	57.8	15.9	21.6	Separation
10.0	16.5	18.7	52.1	63.5	17.8	21.59	
11.0	16.5	19.1	52.7	65.4	21.6	24.8	
12.0	16.2	20.0	53.3	71.1	26.0	23.5	Elongated thermal
13.0	16.2	21.3	54.0	73.7	27.3	25.4	

Table A.10 Experimental Run #10 - 15 mL 0.0359 cm Diameter Glass Particles
Date: April 9/94
Time: 2:45 PM

Measurement Scale = 1.57480 pixels/cm

Time (s	a (cm)	a_p (cm)	z (cm)	z_p (cm)	b (cm)	b_p (cm)	Observations
0.0	2.0	2.0	0.0	0.0	2.0	2.0	
1.0	5.7	5.7	17.8	17.8	7.0	7.0	
2.0	7.9	7.9	26.7	26.7	8.3	8.3	
3.0	7.9	7.9	36.2	36.2	7.6	7.6	
4.0	10.5	10.5	43.8	43.8	7.0	7.0	
5.0	13.0	12.1	44.5	50.8	10.8	7.6	Two phase behaviour
6.0	15.6	14.6	48.9	55.3	10.2	8.3	
7.0	17.1	15.9	53.3	59.7	9.5	8.9	Separation
8.0	17.1	17.5	54.0	64.8	12.1	9.5	
9.0	18.4	18.7	54.6	69.2	17.2	10.8	
10.0	18.7	18.7	55.3	71.1	17.2	10.8	
11.0	19.7	18.1	59.1	73.7	17.2	12.1	
12.0	20.0	19.7	60.3	78.1	19.7	13.3	
13.0	20.3	20.3	60.3	83.2	22.2	17.78	

Table A.11 Experimental Run #11 - 15 mL 0.0460 cm Diameter Glass Particles
Date: April 12/94
Time: 12:06 PM

Measurement Scale = 1.57480 pixels/cm

Time (s	a (cm)	a_p (cm)	z (cm)	z_p (cm)	b (cm)	b_p (cm)	Observations
0.0	2.0	2.0	0.0	0.0	2.0	2.0	
1.2	6.4	6.4	21.6	21.6	5.7	5.7	
2.2	8.6	8.6	36.8	36.8	4.5	4.5	
3.2	12.1	12.1	41.9	41.9	10.2	10.2	Very symmetrical thermal
4.2	14.0	14.0	48.9	48.9	10.8	10.8	Two phase behaviour
5.2	13.3	15.6	50.8	55.9	10.8	13.3	Small amount of separation
6.2	15.6	17.1	54.6	61.0	12.7	14.6	Nice symmetrical crescent
7.2	16.5	18.7	55.9	68.6	18.4	14.6	
8.2	16.2	19.4	58.4	71.1	18.4	15.9	
9.2	14.9	20.3	59.1	79.4	21.6	14.6	
10.2	16.2	22.2	64.8	85.1	21.6	15.24	
11.2	15.2	21.6	66.0	89.5	24.8	15.2	

Table A.12 Experimental Run #12 - 15 mL 0.0460 cm Diameter Glass Particles
Date: April 12/94
Time: 12:10 PM

Measurement Scale = 1.57480 pixels/cm

Time (s	a (cm)	a_p (cm)	z (cm)	z_p (cm)	b (cm)	b_p (cm)	Observations
0.0	2.0	2.0	0.0	0.0	2.0	2.0	
1.0	7.0	7.0	16.5	16.5	6.4	6.4	
2.0	8.9	8.9	23.5	23.5	12.1	12.1	
3.0	10.2	10.2	36.2	36.2	9.5	9.5	Two phase behaviour
4.0	12.4	12.4	43.8	43.8	9.5	11.4	
5.0	13.3	14.3	45.7	52.1	13.3	13.3	Separation
6.0	13.7	16.5	52.7	57.2	10.2	13.3	Nice particle crescent
7.0	14.3	17.8	55.9	63.5	10.8	12.7	
8.0	16.2	19.1	57.8	69.2	11.4	14.6	
9.0	15.2	20.3	64.8	74.9	10.2	14.0	
10.0	17.5	21.0	68.6	81.3	10.2	13.34	
11.0	19.1	21.9	69.2	90.2	13.3	10.2	

Table A.13 Experimental Run #13 - 15 mL 0.0460 cm Diameter Glass Particles
Date: April 13/94
Time: 10:40 AM

Measurement Scale = 1.57480 pixels/cm

Time (s	a (cm)	a_p (cm)	z (cm)	z_p (cm)	b (cm)	b_p (cm)	Observations
0.0	2.0	2.0	0.0	0.0	2.0	2.0	
1.0	5.1	5.1	18.4	18.4	7.6	7.6	
2.0	7.3	7.3	30.5	30.5	8.9	8.9	
3.0	9.8	9.8	37.5	37.5	12.7	12.7	
4.0	12.7	12.7	50.2	50.2	5.7	8.9	Two phase behaviour
5.0	14.9	14.3	53.3	56.5	8.9	10.2	
6.0	16.2	15.9	55.3	59.7	10.8	13.3	Separation
7.0	17.1	17.8	59.7	66.7	11.4	15.2	
8.0	18.1	19.1	59.1	72.4	14.6	14.6	
9.0	18.4	19.4	60.3	78.1	17.8	14.6	
10.0	16.8	20.3	65.4	83.2	18.4	17.78	
11.0	18.4	21.3	69.9	90.2	12.1	17.2	

Table A.14 Experimental Run #14 - 15 mL 0.0460 cm Diameter Glass Particles
Date: April 13/94
Time: 10:43 AM

Measurement Scale = 1.57480 pixels/cm

Time (s	a (cm)	a_p (cm)	z (cm)	z_p (cm)	b (cm)	b_p (cm)	Observations
0.0	2.0	2.0	0.0	0.0	2.0	2.0	
1.0	7.3	7.3	14.0	14.0	9.5	9.5	
2.0	8.3	8.3	26.7	26.7	8.3	8.3	
3.0	9.5	9.5	35.6	35.6	11.4	11.4	
4.0	12.7	12.7	41.3	41.3	10.2	12.7	Two phase behaviour
5.0	15.2	15.2	47.0	47.0	12.7	15.9	
6.0	15.9	15.9	50.2	53.3	10.8	15.9	Separation (barely)
7.0	16.8	17.1	52.7	63.5	11.4	11.4	
8.0	18.1	17.8	55.9	69.2	12.1	11.4	
9.0	20.0	19.7	55.9	74.3	15.9	15.9	
10.0	20.0	20.3	55.3	79.4	21.0	17.78	
11.0	21.3	NA	60.3	NA	17.8	NA	

Table A.15 Experimental Run #15 - 15 mL 0.0460 cm Diameter Glass Particles
Date: April 14/94
Time: 11:13 AM

Measurement Scale = 1.57480 pixels/cm

Time (s	a (cm)	a_p (cm)	z (cm)	z_p (cm)	b (cm)	b_p (cm)	Observations
0.0	2.0	2.0	0.0	0.0	2.0	2.0	
1.0	7.0	7.0	14.6	14.6	9.5	9.5	
2.0	7.3	7.3	27.9	27.9	6.4	6.4	
3.0	9.5	9.5	36.8	36.8	8.3	8.3	
4.0	11.4	11.4	43.2	43.2	7.6	10.8	Two phase behaviour
5.0	13.3	13.3	51.4	51.4	6.4	10.8	Close to separation
6.0	14.3	14.6	54.0	56.5	8.3	12.7	Separation
7.0	15.9	17.1	55.3	63.5	12.1	15.9	
8.0	16.5	17.8	62.9	73.7	8.9	14.0	
9.0	16.5	18.1	62.2	13.7	12.1	15.2	
10.0	16.8	19.4	64.6	82.6	15.2	14.61	
11.0	15.9	21.0	66.0	88.9	15.9	13.3	

Table A.16 Experimental Run #16 - 23 g 0.0548 cm Diameter Glass Particles
Date: April 14/94
Time: 6:34 PM
Measurement Scale = 1.57480 pixels/cm

Time (s	a (cm)	a_p (cm)	z (cm)	z_p (cm)	b (cm)	b_p (cm)	Observations
0.0	2.0	2.0	0.0	0.0	2.0	2.0	
1.0	5.7	5.7	15.9	15.9	5.1	5.1	Nice release
2.0	8.3	8.3	27.9	27.9	7.0	7.0	Single phase behaviour
3.0	10.8	10.8	35.6	35.6	5.1	7.6	Two phase behaviour
4.0	10.8	13.3	37.5	47.0	8.3	9.5	Separation
5.0	12.1	14.9	40.6	50.2	8.9	10.8	
6.0	13.3	16.5	47.0	57.2	7.6	11.4	
7.0	14.3	17.1	50.8	65.4	7.0	9.5	Nice particle crescent
8.0	16.2	18.7	50.8	72.4	10.8	10.8	
9.0	15.9	20.0	52.7	78.7	12.7	11.4	
10.0	15.9	19.4	56.5	87.0	13.3	10.8	
11.0	17.8	21.0	60.3	94.0	12.7	10.8	

Table A.17 Experimental Run #17 - 23 g of 0.0548 cm Diameter Glass Particles
Date: April 16/94
Time: 12:14 PM

Measurement Scale = 1.57480 pixels/cm

Time (s	a (cm)	a_p (cm)	z (cm)	z_p (cm)	b (cm)	b_p (cm)	Observations
0.0	2.0	2.0	0.0	0.0	2.0	2.0	
1.0	6.7	6.7	13.3	13.3	8.9	8.9	
2.0	7.3	7.3	31.8	31.8	7.0	7.0	
3.0	8.6	8.6	40.6	40.6	7.6	7.6	Two phase behaviour
4.0	10.5	10.5	48.9	48.9	6.4	8.3	
5.0	11.8	11.8	55.3	55.3	6.4	11.4	Verge of separation
6.0	13.0	14.9	63.5	63.5	6.4	12.7	Separation
7.0	12.4	16.2	66.7	68.0	7.0	15.2	
8.0	14.0	17.1	70.5	75.6	6.4	15.9	
9.0	14.6	18.4	73.7	83.8	7.6	15.9	
10.0	15.9	19.1	75.6	90.2	9.5	16.51	

Table A.18 Experimental Run #18 - 23 g of 0.0548 cm Diameter Glass Particles
Date: April 16/94
Time: 1:57 PM

Measurement Scale = 1.57480 pixels/cm

Time (s	a (cm)	a_p (cm)	z (cm)	z_p (cm)	b (cm)	b_p (cm)	Observations
0.0	2.0	2.0	0.0	0.0	2.0	2.0	
1.0	7.6	15.24/2	14.6	14.6	8.9	8.9	
2.0	7.9	7.9	28.6	28.6	7.0	7.0	
3.0	11.2	11.2	36.2	36.2	6.4	8.9	Two phase behaviour
4.0	12.4	12.4	43.2	43.2	3.2	8.9	Partial separation
5.0	10.5	14.9	50.2	54.0	8.3	12.7	Total separation
6.0	12.4	16.5	53.3	57.8	8.3	14.0	
7.0	14.9	17.5	55.9	68.0	10.2	13.3	
8.0	16.5	17.8	57.8	73.7	13.3	13.3	
9.0	17.1	19.1	57.8	81.3	17.2	14.0	
10.0	17.1	19.1	59.7	87.0	17.8	13.97	
11.0	17.1	20.3	72.4	93.4	8.9	14.6	

Table A.19 Experimental Run #19 - 23 g of 0.0548 cm Diameter Glass Particles
Date: April 18/94
Time: 10:51 AM

Measurement Scale = 1.57480 pixels/cm

Time (s	a (cm)	a_p (cm)	z (cm)	z_p (cm)	b (cm)	b_p (cm)	Observations
0.0	2.0	2.0	0.0	0.0	2.0	2.0	
1.0	6.4	6.4	14.6	14.6	5.1	5.1	
2.0	8.9	8.9	23.5	23.5	6.4	6.4	
3.0	11.8	11.8	32.4	32.4	5.7	9.5	Two phase behaviour
4.0	12.1	12.7	34.9	38.1	5.1	10.8	Close to total separation
5.0	13.0	14.3	41.3	43.2	3.8	13.3	Total separation
6.0	14.6	15.9	41.9	51.4	8.3	13.3	
7.0	15.6	16.8	44.5	59.1	9.5	14.6	
8.0	16.5	17.8	45.1	66.7	13.3	14.6	
9.0	16.8	18.1	45.7	77.5	16.5	11.4	
10.0	15.9	19.4	56.5	83.8	10.2	11.43	

Table A.20 Experimental Run #20 - 23 g of 0.0548 cm Diameter Glass Particles
Date: April 18/94
Time:

Measurement Scale = 1.57480 pixels/cm

Time (s	a (cm)	a_p (cm)	z (cm)	z_p (cm)	b (cm)	b_p (cm)	Observations
0.0	2.0	2.0	0.0	0.0	2.0	2.0	
1.0	6.0	6.0	15.9	15.9	7.6	7.6	
2.0	7.6	7.6	31.2	31.2	7.0	7.0	
3.0	8.9	8.9	42.6	42.6	7.0	7.0	Start of two phase behaviour
4.0	11.4	11.8	47.6	50.8	6.4	8.3	Close to separation
5.0	12.4	13.3	47.6	57.2	11.4	9.5	Separation
6.0	14.6	14.9	57.8	65.4	6.4	9.5	
7.0	15.9	16.2	58.4	73.7	10.8	10.2	
8.0	15.9	17.1	61.0	80.7	12.7	9.5	
9.0	15.9	17.5	71.1	87.0	6.4	12.1	
10.0	17.5	16.5	71.8	97.8	9.5	10.16	

Appendix B - Theoretical Derivations for Chapter 2

2.1.2 Internal Flow - Expanding Hill's Spherical Vortex

Starting with the stream function for a Hill's spherical vortex, in cylindrical coordinates, the axisymmetric velocity components can be determined. The stream function for a coordinate system fixed at the center of the vortex is:

$$\Psi = \frac{3Ur^2}{4a^2}\left(a^2 - r^2 - z_T^2\right) \qquad (2.1)$$

In the equation, r and z_T are the radial and vertical coordinates, U is the translational thermal velocity and a is the radius of the vortex or thermal. U and z_T are positive in the downwards direction. By partially differentiating equation (2.1) with respect to r and z_T the internal velocity flow field is:

$$\frac{d\Psi}{dr} = \frac{3Ur}{2} - \frac{3Ur^3}{a^2} - \frac{3Urz_T^2}{2a^2}$$

and

$$\frac{d\Psi}{dz_T} = \frac{-3Ur^2 z_T}{2a^2}$$

$$u_z = -\frac{1}{r}\frac{d\Psi}{dr} = -\frac{3U}{2} + \frac{3Ur^2}{a^2} + \frac{3Uz_T^2}{2a^2} \Rightarrow u_z = \frac{3U}{2a^2}(2r^2 + z_T^2 - a^2) \qquad (2.2)$$

and

$$u_r = \frac{1}{r}\frac{d\Psi}{dz_T} = \frac{-3Urz_T}{2a^2} \qquad (2.3)$$

2.1.3 Potential Flow Theory

Starting with the stream function for potential flow theory, in cylindrical coordinates, the axisymmetric velocity components can also be determined. The stream function for flow approaching a stationary spherical object is:

$$\Psi = \frac{-Ur^2}{2} + \frac{Ua^3 r^2}{2}\left(z_T^2 + r^2\right)^{-3/2} \qquad (2.5)$$

The coordinate system is one fixed at the center of the spherical object and z_T and U are positive in the downwards direction. By partially differentiating equation (2.5) with respect to r and z_T the fluid flow field around the sphere is found.

$$\frac{d\Psi}{dr} = -Ur + \frac{Ua^3 r}{\left(z_T^2 + r^2\right)^{3/2}} - \frac{3Ua^3 r^3}{2\left(z_T^2 + r^2\right)^{5/2}}$$

and

$$\frac{d\Psi}{dz_T} = \frac{-3Ua^3 r^2 z_T}{2\left(z_T^2 + r^2\right)^{5/2}}$$

Now, the two velocity components are:

$$u_z = \frac{-1}{r}\frac{d\Psi}{dr} = U - \frac{Ua^3}{\left(z_T^2 + r^2\right)^{3/2}} + \frac{3Ua^3 r^2}{2\left(z_T^2 + r^2\right)^{5/2}}$$

$$\Rightarrow \quad u_z = U\left[1 + \frac{a^3\left(r^2 - 2z_T^2\right)}{2\left(z_T^2 + r^2\right)^{5/2}}\right] \tag{2.6}$$

and

$$u_r = \frac{1}{r}\frac{d\Psi}{dz_T} = \frac{-3Ua^3 r z_T}{2\left(z_T^2 + r^2\right)^{5/2}} \tag{2.7}$$

Equations (2.6) and (2.7) represent the fluid flow field outside the boundary of a thermal.

2.1.4 Nonuniform Thermal Velocity

Morton, Taylor, and Turner (1955) investigated the behaviour of plumes and instantaneous point sources (thermals). By manipulating their conservation equations for volume, momentum, and density deficiency relationships can be found for a nonuniform translational thermal velocity and the thermal radius. The three conservation equations for volume, momentum and density deficiency are:

$$\frac{d}{dt}\left(\frac{4}{3}\pi a^3\right) = 4\pi a^2 \alpha U \tag{2.8}$$

$$\frac{d}{dt}\left(\frac{4}{3}\pi a^3 \rho U\right) = \frac{4}{3}\pi a^3 g(\rho_0 - \rho) \tag{2.9}$$

$$\frac{d}{dt}\left(\int(\rho_1 - \rho)\cdot d(\text{volume})\right) = 4\pi a^2 \alpha U(\rho_1 - \rho_0) \tag{2.10}$$

where:

a = mean radius of a thermal cloud
U(t) = the mean thermal velocity
αU = the rate of entrainment at the cloud surface
ρ = fluid density inside of a thermal
ρ_0 = fluid density outside of a thermal
ρ_1 = reference density of the system = $\rho_0(0)$ = density outside of a thermal at point of release

From the above equations the following two relationships for the thermal radius a and velocity U are derived. Equation (2.10) can be rearranged using equation (2.8) as follows:

$$\frac{d}{dt}\left(\int(\rho_l-\rho)\cdot d(\text{volume})\right)=(\rho_l-\rho_0)\frac{d}{dt}\left(\frac{4}{3}\pi a^3\right) \tag{B.1}$$

Now, equation (B.1) is rearranged as follows to get equation (B.2).

$$(\rho_l-\rho_0)\frac{d}{dt}\left(\frac{4}{3}\pi a^3\right)=\frac{d}{dt}\left[\left(\frac{4}{3}\pi a^3\right)(\rho_l-\rho_0)\right]-\left(\frac{4}{3}\pi a^3\right)\frac{d}{dt}(\rho_l-\rho_0)$$

$$\frac{d}{dt}\left(\int(\rho_l-\rho)\cdot d(\text{volume})\right)=\frac{d}{dt}\left[\left(\frac{4}{3}\pi a^3\right)(\rho_l-\rho_0)\right]-\left(\frac{4}{3}\pi a^3\right)\frac{d}{dt}(\rho_l-\rho_0)$$

$$\frac{d}{dt}\left[\int(\rho_l-\rho)\cdot d(\text{volume})-\left(\frac{4}{3}\pi a^3\right)(\rho_l-\rho_0)\right]=\left(\frac{4}{3}\pi a^3\right)\frac{d\rho_0}{dt}$$

$$\frac{d}{dt}\left[a^3(\rho_0-\rho)\right]=a^3\frac{d\rho_0}{dt} \tag{B.2}$$

Using Boussinesq's approximation, density variations are small, i.e. $\rho = \rho_l$, equations (2.8), (2.9), and (B.2) can be written as:

$$\frac{d}{dt}\left(a^3\right)=3a^2\alpha U \tag{B.3}$$

$$\frac{d}{dt}\left(a^3U\right)=a^3g\frac{(\rho_0-\rho)}{\rho_l} \tag{B.4}$$

$$\frac{d}{dt}\left[a^3 g\frac{(\rho_0-\rho)}{\rho_l}\right]=\frac{a^3 g}{\rho_l}\frac{d\rho_0}{dt} \qquad \text{(B.5)}$$

where: $\frac{g}{\rho_l}$ is multiplied to both sides of equation (B.5)

The boundary conditions for the thermal are:

1. $\rho_0 \approx \rho_l$
2. $a = 0$ at $t = 0$
3. $\rho_l = \rho_0$ at $t = 0$

From the boundary conditions, the right side of equation (B.5) disappears making the left side equal to a constant value, Q.

$$a^3 g\frac{(\rho_l-\rho)}{\rho_l}=Q \qquad \text{(B.6)}$$

To solve equations (B.3), (B.4), and (B.5) solutions of the following forms are assumed.

$$a^3 = jQ^m t^n \qquad \text{(B.7)}$$

and

$$a^2U = cQ^e t^s \qquad \text{(B.8)}$$

These solutions assume the left and right sides of equation (B.3) are a function of constant Q and time t. It is necessary to determine the coefficients j and c and the exponents m, n, e and s. First, equation (B.7) is differentiated with respect to time.

$$\frac{d}{dt}\left(a^3\right) = jnQ^m t^{n-1}$$

Therefore,

$$\mathbf{n-1 = s}$$

$$\mathbf{m = e}$$

$$\mathbf{jn = 3\alpha c}$$

Equation (B.4) is rearranged into the correct form.

$$\frac{d}{dt}\left(a \cdot a^2U\right) = a^2U\frac{d(a)}{dt} + a \cdot \frac{d\left(a^2U\right)}{dt} = Q$$

Substitution of expressions (B.7) and (B.8), as well as their respective derivatives, gives:

$$cQ^{e}t^{s}\left(\frac{j^{\frac{1}{3}}nQ^{\frac{m}{3}}t^{\frac{n-3}{3}}}{3}\right)+\left(j^{\frac{1}{3}}Q^{\frac{m}{3}}t^{\frac{n}{3}}\right)\left(scQ^{e}t^{s-1}\right)=Q$$

which reduces to:

$$j^{\frac{1}{3}}cQ^{\frac{m}{3}+e}t^{s}\left(\frac{nt^{\frac{n-3}{3}+s}}{3}+st^{\frac{n}{3}+s-1}\right)=Q$$

From this last equation and the previous relationships for n, s, m, e, j and c the following relationships are found.

$$e+\frac{m}{3}=1 \;\Rightarrow\; e+\frac{e}{3}=1 \;\Rightarrow\; \mathbf{e=m=\frac{3}{4}}$$

$$\frac{n-3}{3}+s+\frac{n}{3}+s-1=0 \;\Rightarrow\; \frac{2(s+1)-3+6s-3}{3}=0$$

$$\Rightarrow\; \mathbf{s=\frac{1}{2}} \text{ and } \mathbf{n=\frac{3}{2}}$$

$$j^{\frac{1}{3}}c\left(\frac{n}{3}+s\right)=1 \;\Rightarrow\; j^{\frac{1}{3}}\left(\frac{3j}{6\alpha}\right)\left[\frac{1}{2}+\frac{1}{2}\right]=1$$

$$\Rightarrow\; \mathbf{j=(2\alpha)^{\frac{3}{4}}} \text{ and } \mathbf{c=\frac{(2)^{\frac{3}{4}}}{2\alpha^{\frac{1}{4}}}}$$

Substitution of these solutions into equations (B.7) and (B.8) leads to the following relationships for the thermal radius and velocity.

$$a = (2\alpha Q)^{\frac{1}{4}} t^{\frac{1}{2}} \tag{2.11}$$

$$U = \frac{Q^{\frac{1}{4}}}{(2\alpha)^{\frac{3}{4}} t^{\frac{1}{2}}} \tag{2.12}$$

Thus, from expression (2.12) the thermal velocity varies inversely with the square root of time, which is the behaviour Figure 2.3 suggests. Equation (2.11) shows a relationship for the radial growth of the vortex for a nonuniform thermal velocity. Introducing $K = \frac{Q^{\frac{1}{4}}}{(2\alpha)^{\frac{3}{4}}}$ as a constant reduces equation (2.11) and (2.12) to:

$$a = 2\alpha K t^{\frac{1}{2}} \tag{2.13}$$

$$U = \frac{K}{t^{\frac{1}{2}}} \tag{2.14}$$

Appendix C - Theoretical Results for 0.0274 cm Diameter Glass Particles

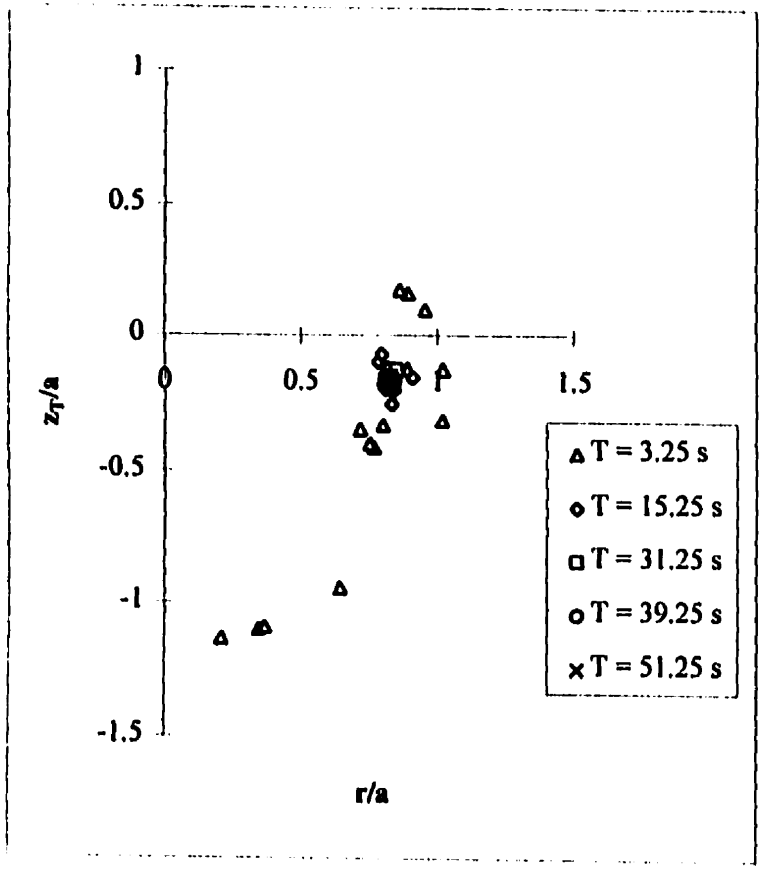

Figure C.1

Dimensionless plot for 0.0274 cm diameter particles. Uniform speed thermal above the terminal velocity with Stokes drag (U = -6.38 cm/s).

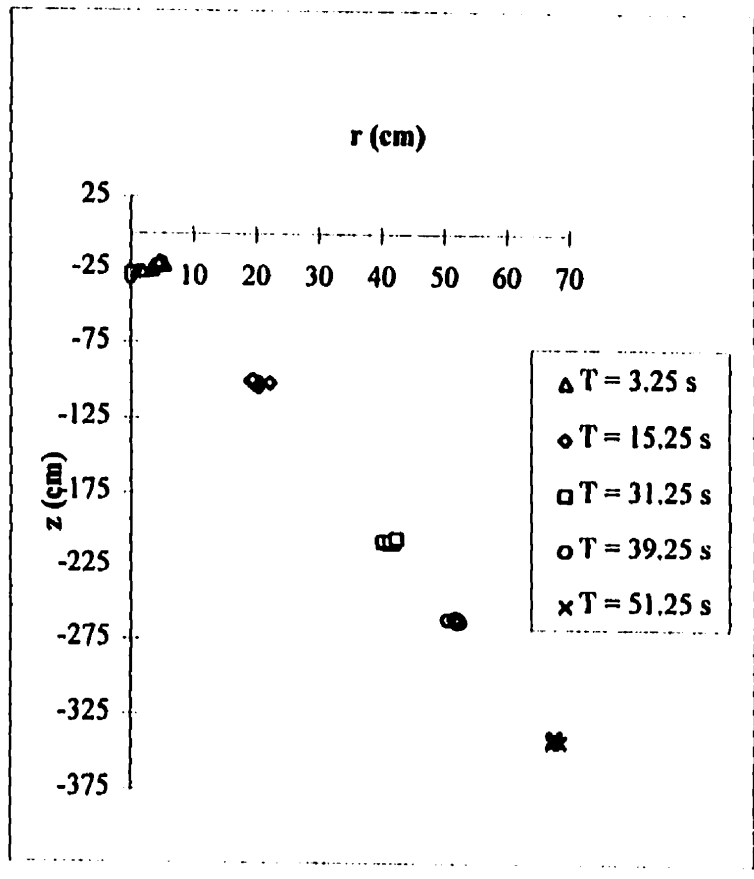

Figure C.2

Vertical and radial particle positions for 0.0274 cm diameter particles. Uniform speed thermal above the terminal velocity with Stokes drag (U = -6.38 cm/s).

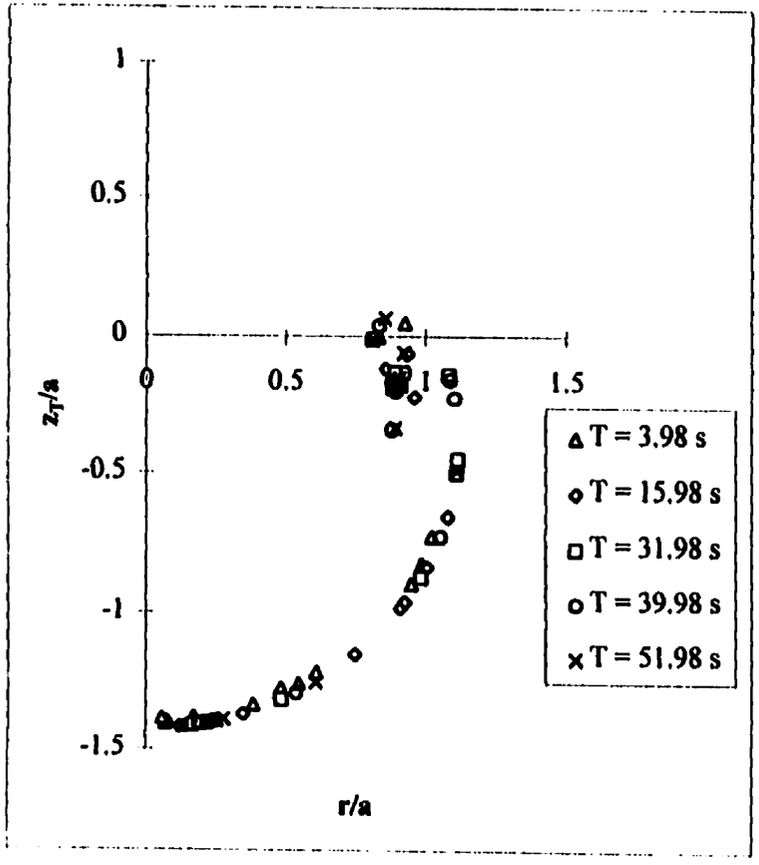

Figure C.3

Dimensionless plot for 0.0274 cm diameter particles. Uniform speed thermal at the terminal velocity with Stokes drag (U = -4.05 cm/s).

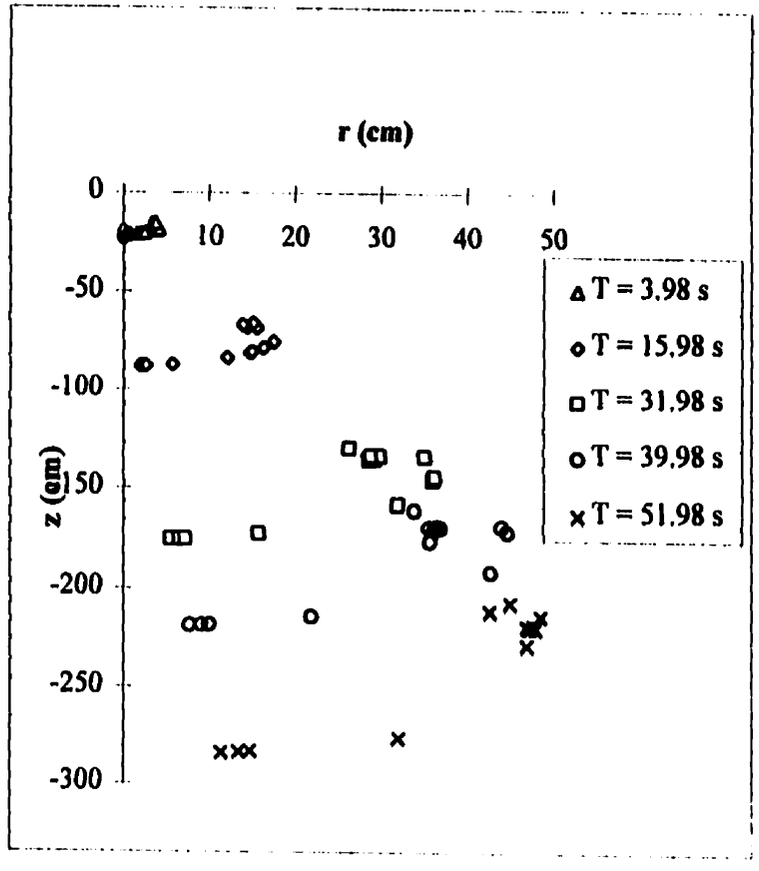

Figure C.4

Vertical and radial particle positions for 0.0274 cm diameter particles. Uniform speed thermal at the terminal velocity with Stokes drag (U = -4.05 cm/s).

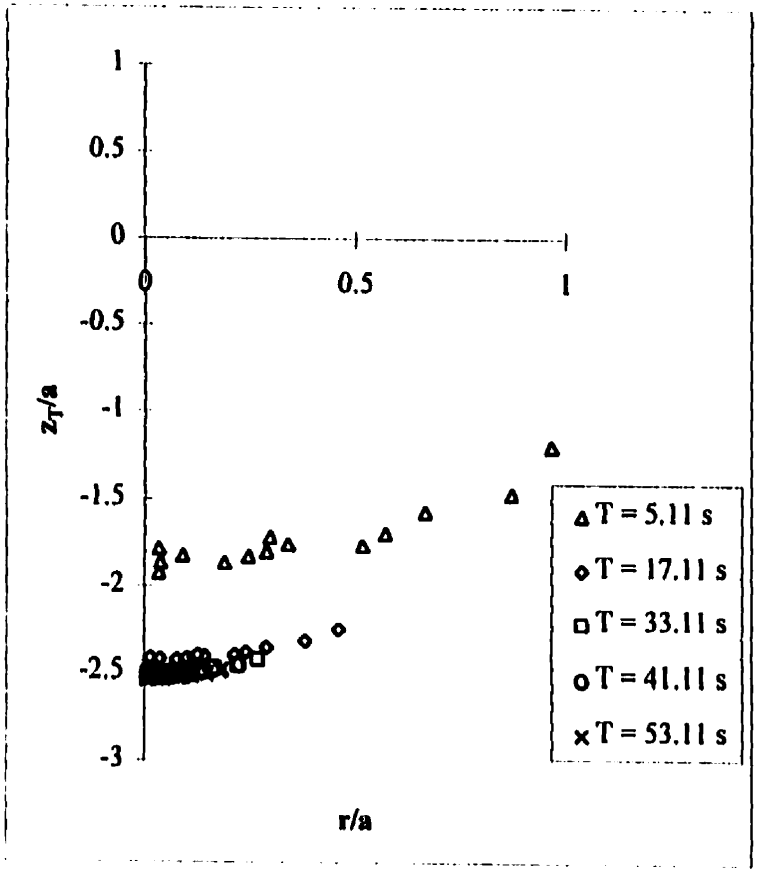

Figure C.5

Dimensionless plot for 0.0274 cm diameter particles. Uniform speed thermal below the terminal velocity with Stokes drag (U = -2.57 cm/s).

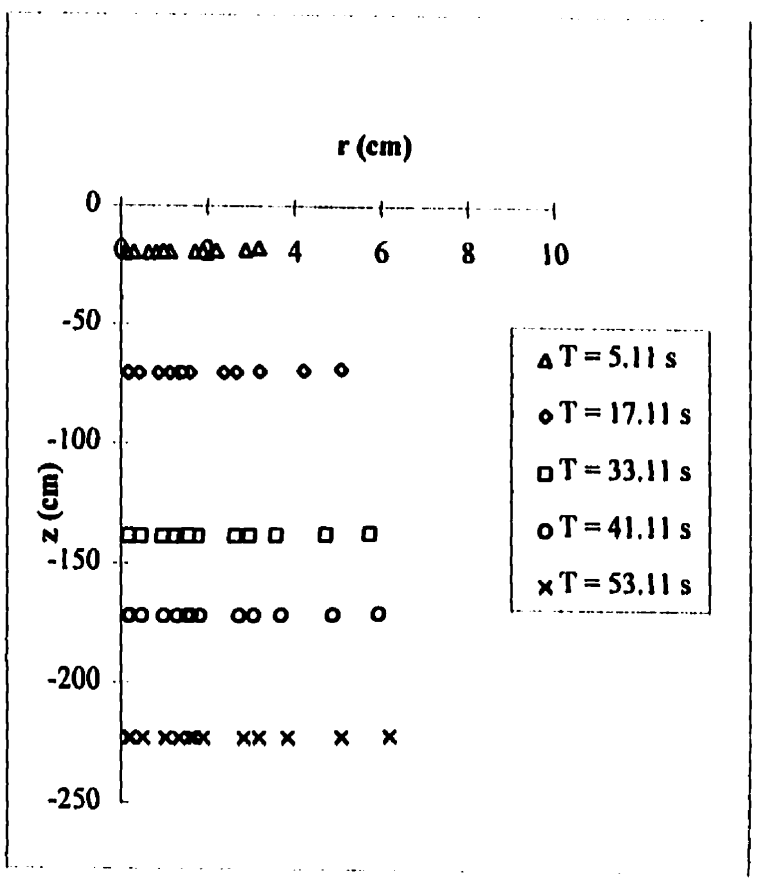

Figure C.6

Vertical and radial particle positions for 0.0274 cm diameter particles. Uniform speed thermal below the terminal velocity with Stokes drag (U = -2.57 cm/s).

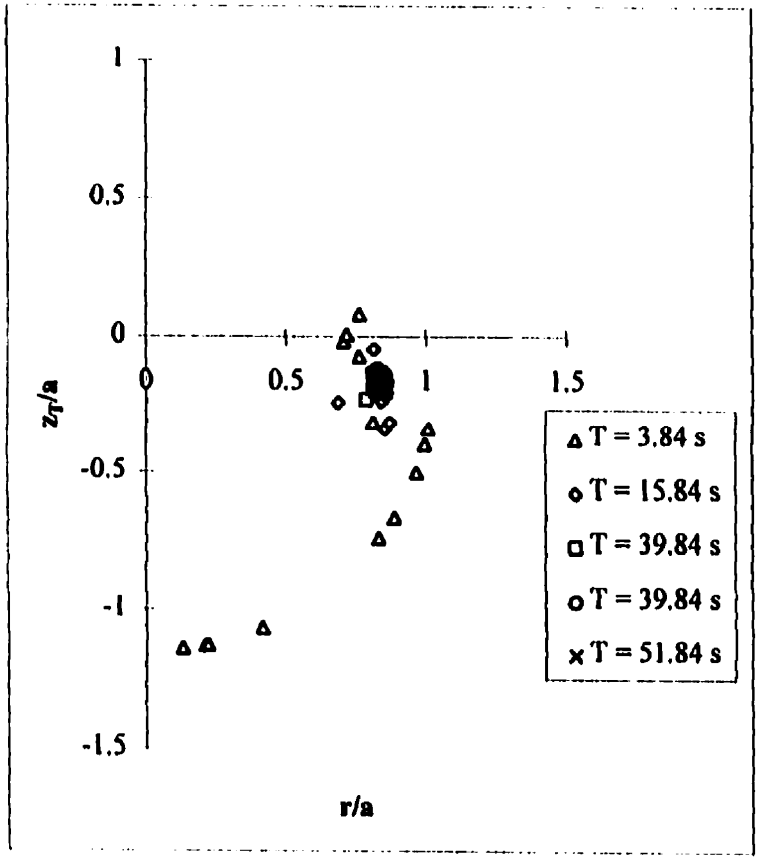

Figure C.7

Dimensionless plot for 0.0274 cm diameter particles. Uniform speed thermal above the terminal velocity with non-Stokes drag (U = -4.35 cm/s).

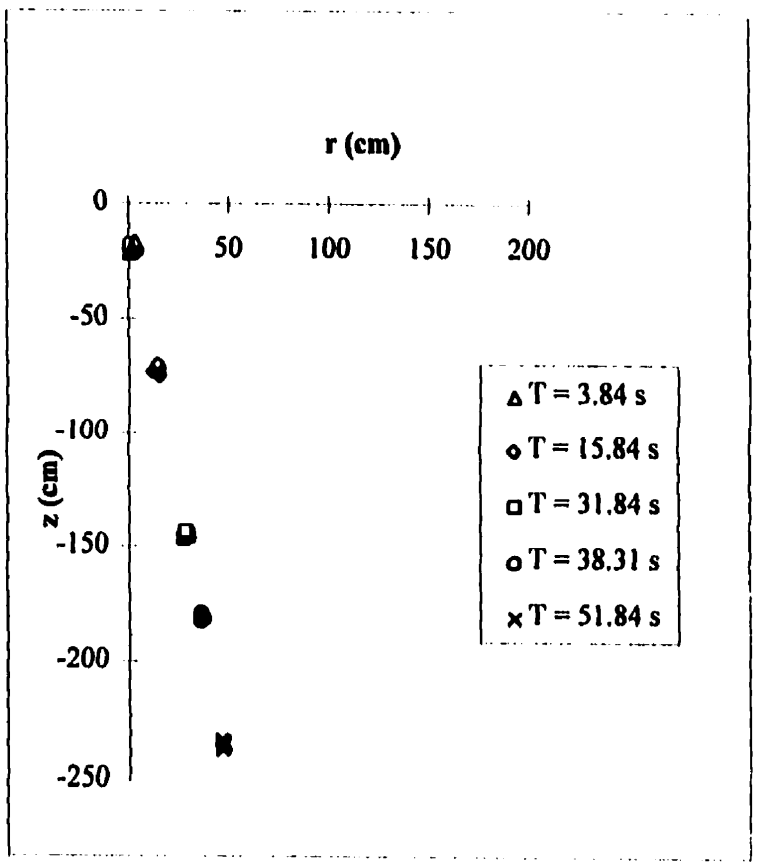

Figure C.8

Vertical and radial particle positions for 0.0274 cm diameter particles. Uniform speed thermal above the terminal velocity with non-Stokes drag (U = -4.35 cm/s).

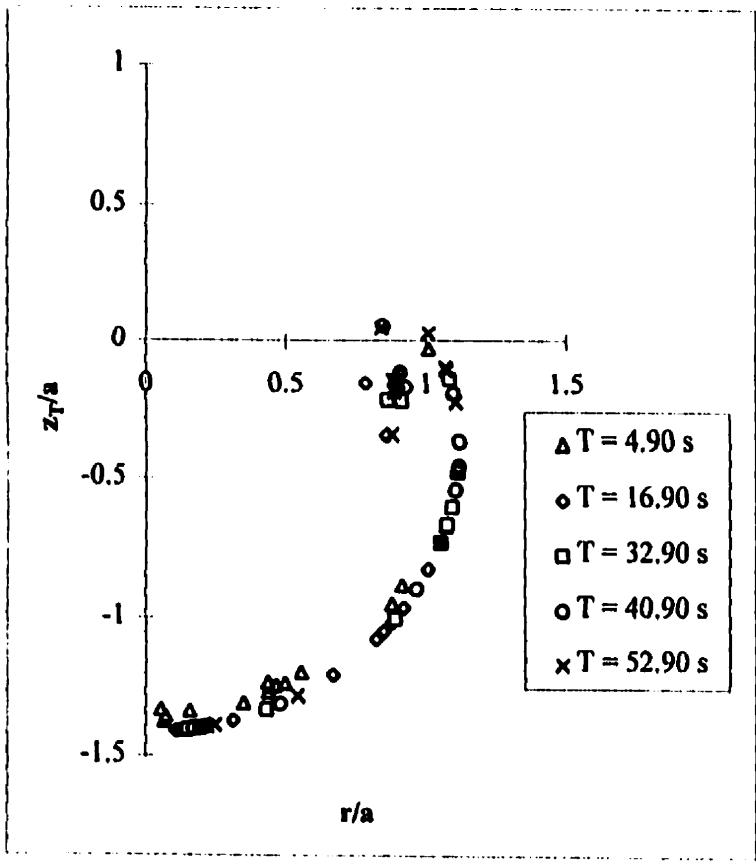

Figure C.9

Dimensionless plot for 0.0274 cm diameter particles. Uniform speed thermal at the terminal velocity with non-Stokes drag (U = -2.76 cm/s).

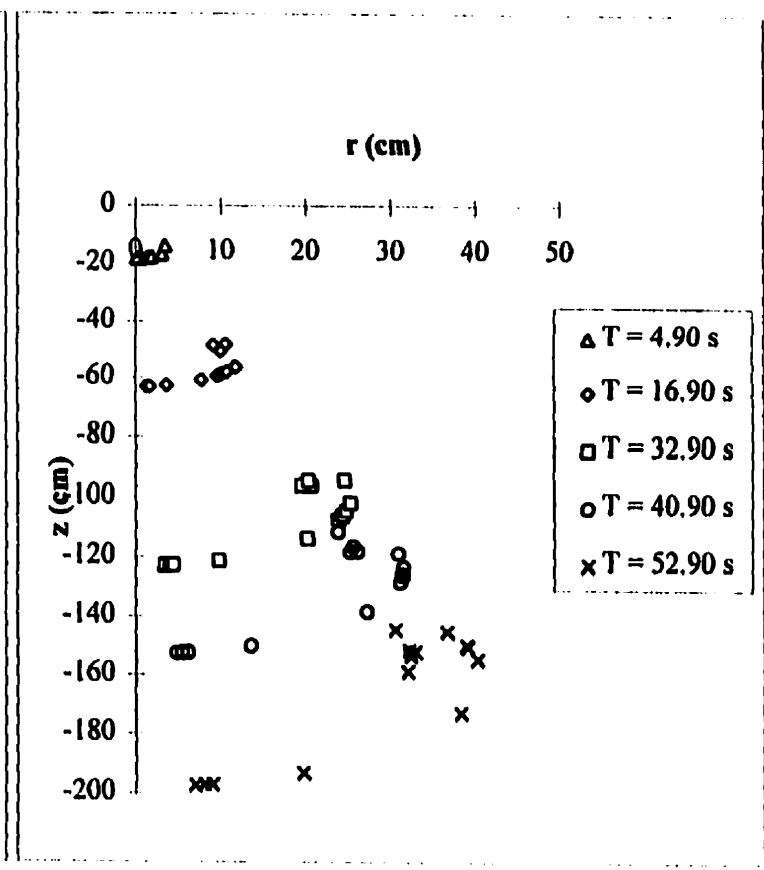

Figure C.10

Vertical and radial particle positions for 0.0274 cm diameter particles. Uniform speed thermal at the terminal velocity with non-Stokes drag (U = -2.76 cm/s).

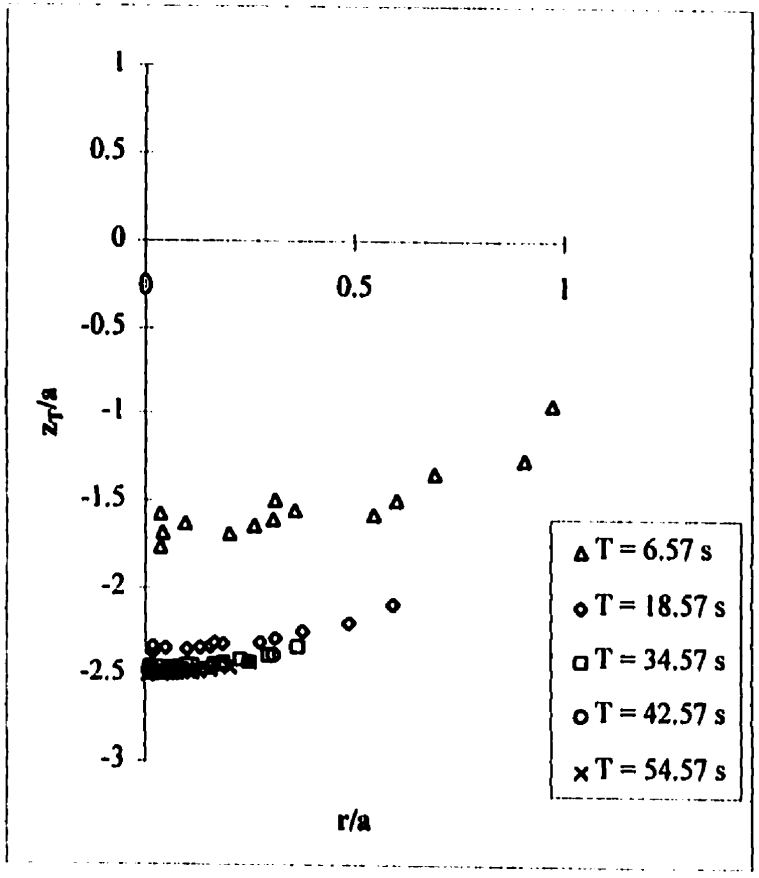

Figure C.11

Dimensionless plot for 0.0274 cm diameter particles. Uniform speed thermal below the terminal velocity with non-Stokes drag (U = -1.75 cm/s).

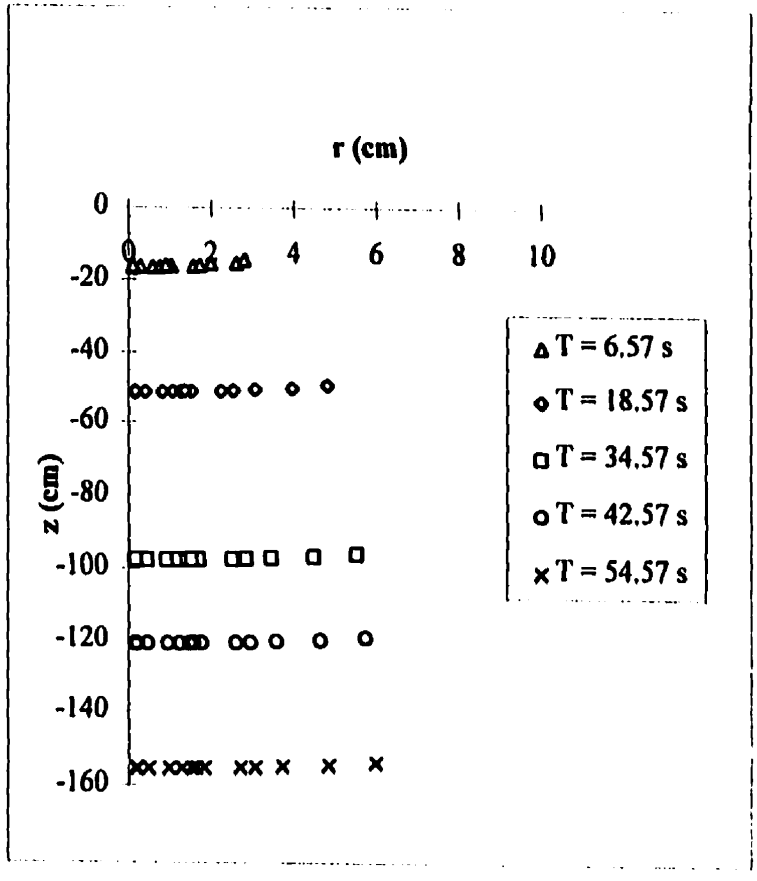

Figure C.12

Vertical and radial particle positions for 0.0274 cm diameter particles. Uniform speed thermal below the terminal velocity with non-Stokes drag (U = -1.75 cm/s).

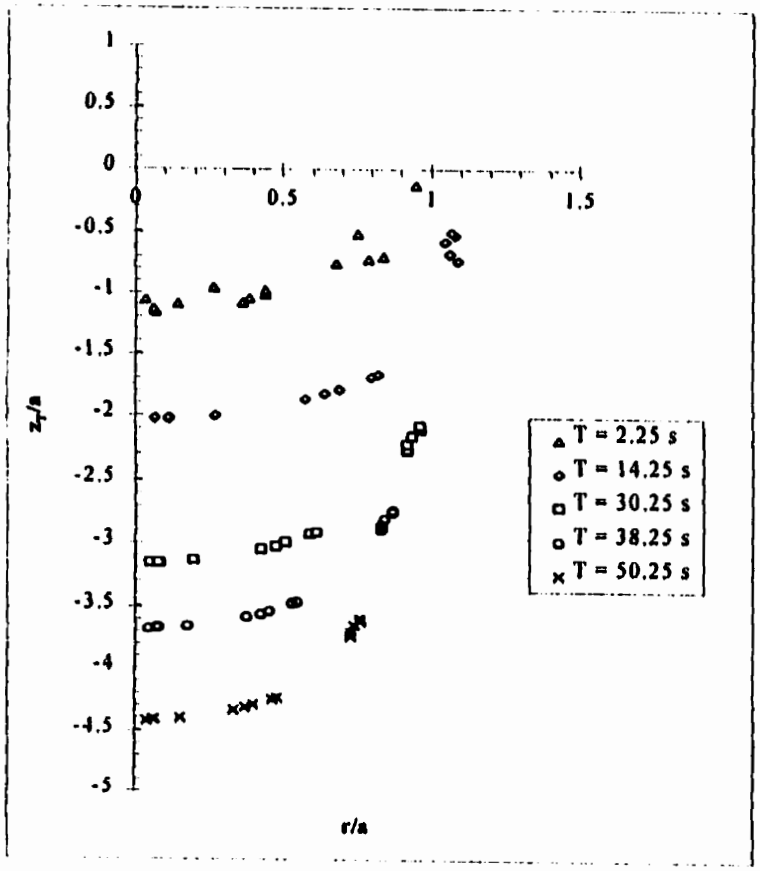

Figure C.13

Dimensionless plot for 0.0274 cm diameter particles. Nonuniform speed thermal starting at U = -7.22 cm/s with Stokes drag.

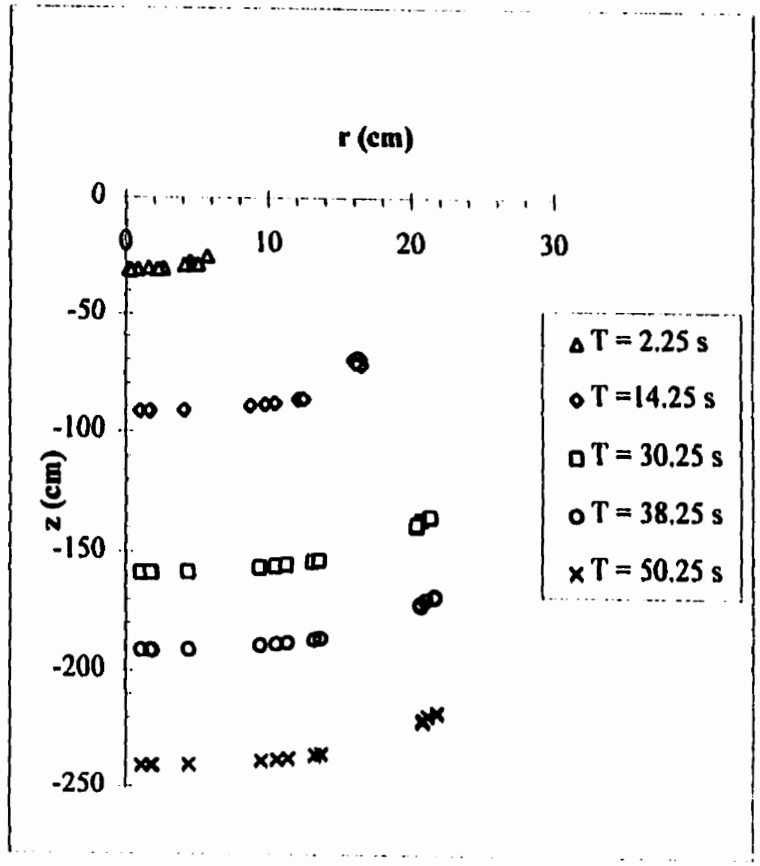

Figure C.14

Vertical and radial particle positions for 0.0274 cm diameter particles. Nonuniform speed thermal starting at U = -7.22 cm/s with Stokes drag.

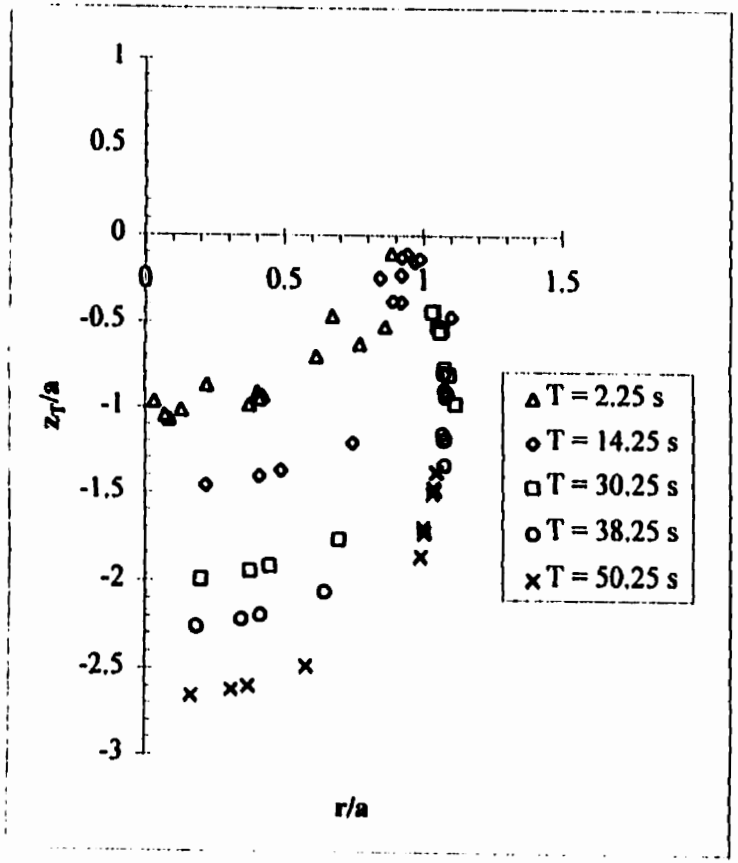

Figure C.15

Dimensionless plot for 0.0274 cm diameter particles. Nonuniform speed thermal starting at U = -7.22 cm/s with non-Stokes drag.

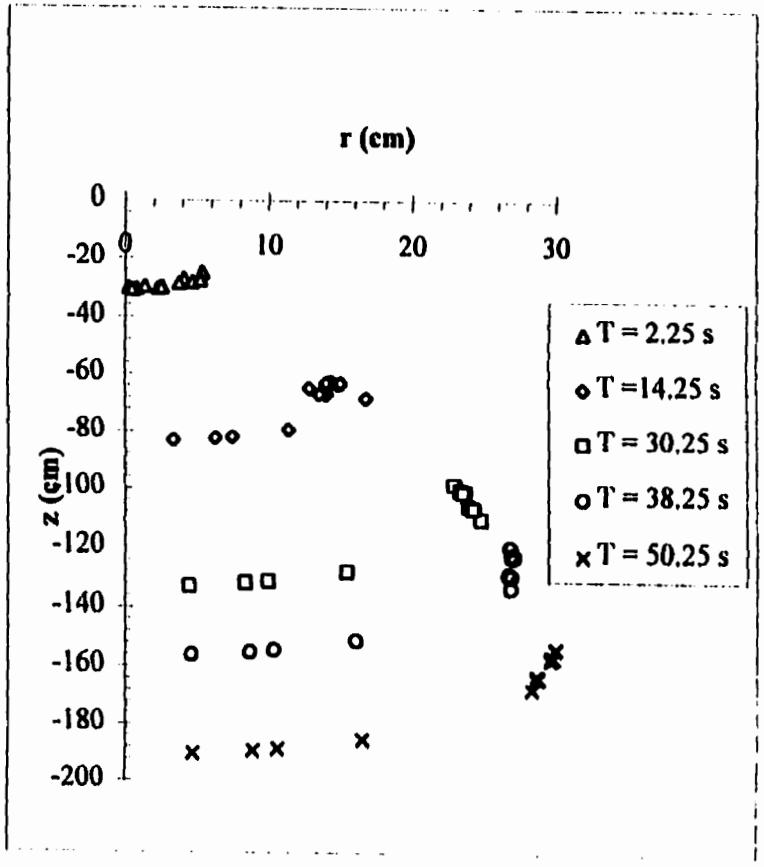

Figure C.16

Vertical and radial particle positions for 0.0274 cm diameter particles. Nonuniform speed thermal starting at U = -7.22 cm/s with non-Stokes drag.

Appendix D - Computer Code of Theoretical Model

Uniform Speed Model with Stokes Drag using 0.0548 cm Particles

```
// PARTICLE MODEL
IndVars: T
DepVars: A, R, Z, RHO, GAM, ZT, GAMO, VPR, VPZ, U, VFR, VFZ
Params: ALPHA, KP, VIS, RP, G, SG
// SIMPLIFYING EQUATIONS
A=ABS(ALPHA*U*T)
EPS1=SQRT(R^2+ZT^2)
ZT=Z-U*T
MF=(4/3)*PI*RP^3
MP=SG*MF
C1=1/(MP+KP*MF)
C2=6*PI*RP*VIS
C3=(1+KP)*MF
C4=(MP-MF)*G
FLAG=UNIT(A-EPS1)
//
// FLUID EQUATIONS
// RADIAL EQUATIONS
// VFR2 IS FOR EXTERNAL RADIAL FLOW; VFR1 IS FOR INTERNAL RADIAL
//FLOW
VFR1=(3*R*(Z-U*T)*U)/(2*A^2)
VFR2=(3*A^3*U*R*(Z-U*T))/(2*((Z-U*T)^2+R^2)^(5/2))
VFR=VFR2*(1-FLAG)+VFR1*FLAG
// Z DIRECTION EQUATIONS
// VFZ2 IS FOR EXTERNAL FLOW; VFZ1 IS FOR INTERNAL FLOW
VFZ1=((-3*U)/(2*A^2))*(2*R^2+(Z-U*T)^2-A^2)+U
VFZ2=(-U*(1+(A^3*(R^2-2*(Z-U*T)^2))/(2*((Z-U*T)^2+R^2)^(5/2))))+U
VFZ=VFZ2*(1-FLAG)+VFZ1*FLAG
//
// PARTICLE EQUATIONS
// RADIAL DIRECTION
VPR'=C1*(C2*(VFR-VPR)+C3*(DERIV(VFR,T)+VFR*DERIV(VFR,R)))
R'=VPR
//Z DIRECTION
VPZ'=C1*(C4+C2*(VFZ-VPZ)+C3*(DERIV(VFZ,T)+VFZ*DERIV(VFZ,Z)))
Z'=VPZ
```

continued

```
//
RHO=R/A
GAM=Z/A
GAMO=ZT/A
// Parameter values and Constraints:
U=-16.23
ALPHA=0.25
G=-981
SG=2.5
VIS=0.0151
KP=0.5
RP=0.0274
// Initial conditions:
R=0.38
Z=-7.88
VPR=-0.278
VPZ=-22.500
0.493<T<50.493
***
```

Uniform Speed Model with non-Stokes Drag using 0.0548 cm Particles

```
// PARTICLE MODEL
IndVars: T
DepVars: A, R, Z, RHO, GAM, ZT, GAMO, VPR, VPZ, U, VFR, VFZ
Params: ALPHA, KP, VIS, RP, G, SG, VT
// SIMPLIFYING EQUATIONS
A=ABS(ALPHA*U*T)
EPS1=SQRT(R^2+ZT^2)
ZT=Z-U*T
MF=(4/3)*PI*RP^3
MP=SG*MF
C1=1/(MP+KP*MF)
C2=(G*(MP-MF)/VT
C3=(1+KP)*MF
C4=(MP-MF)*G
FLAG=UNIT(A-EPS1)
```

continued

```
//
// FLUID EQUATIONS
// RADIAL EQUATIONS
// VFR2 IS FOR EXTERNAL RADIAL FLOW; VFR1 IS FOR INTERNAL RADIAL
//FLOW
VFR1=(3*R*(Z-U*T)*U)/(2*A^2)
VFR2=(3*A^3*U*R*(Z-U*T))/(2*((Z-U*T)^2+R^2)^(5/2))
VFR=VFR2*(1-FLAG)+VFR1*FLAG
// Z DIRECTION EQUATIONS
// VFZ2 IS FOR EXTERNAL FLOW; VFZ1 IS FOR INTERNAL FLOW
VFZ1=((-3*U)/(2*A^2))*(2*R^2+(Z-U*T)^2-A^2)+U
VFZ2=(-U*(1+(A^3*(R^2-2*(Z-U*T)^2))/(2*((Z-U*T)^2+R^2)^(5/2))))+U
VFZ=VFZ2*(1-FLAG)+VFZ1*FLAG
//
// PARTICLE EQUATIONS
// RADIAL DIRECTION
VPR'=C1*(C2*(VFR-VPR)+C3*(DERIV(VFR,T)+VFR*DERIV(VFR,R)))
R'=VPR
//Z DIRECTION
VPZ'=C1*(C4+C2*(VFZ-VPZ)+C3*(DERIV(VFZ,T)+VFZ*DERIV(VFZ,Z)))
Z'=VPZ
//
RHO=R/A
GAM=Z/A
GAMO=ZT/A
// Parameter values and Constraints:
VT=-6.10
U=-6.10
ALPHA=0.25
G=-981
SG=2.5
VIS=0.0151
KP=0.5
RP=0.0274
// Initial conditions:
R=0.38
Z=-7.88
VPR=-0.104
VPZ=-8.456
1.311<T<51.311
```

Nonuniform Speed Model with Stokes Drag using 0.0548 cm Particles

```
// PARTICLE MODEL
IndVars: T
DepVars: A, R, Z, RHO, GAM, ZT, GAMO, VPR, VPZ, U, VFR, VFZ
Params: ALPHA, KP, VIS, RP, G, SG, K
// SIMPLIFYING EQUATIONS
U=K/SQRT(T)
A=ABS(2*ALPHA*K*SQRT(T))
ZT=Z-(2*K*SQRT(T))
EPS=(R^2+ZT^2)
EPS1=SQRT(EPS)
MF=(4/3)*PI*RP^3
MP=SG*MF
C1=1/(MP+KP*MF
C2=6*PI*RP*VIS
C3=(1+KP)*MF
C4=(MP-MF)*G
FLAG=UNIT(A-EPS1)
//
// FLUID EQUATIONS
// RADIAL EQUATIONS
// VFR2 IS FOR EXTERNAL RADIAL FLOW; VFR1 IS FOR INTERNAL RADIAL
//FLOW
VFR1=(3*R*(Z-(2*K*SQRT(T)))*U)/(2*A^2)
VFR2=(3*A^3*U*R*(Z-(2*K*SQRT(T))))/(2*((Z-(2*K*SQRT(T)))^2+R^2)^(5/2))
VFR=VFR2*(1-FLAG)+VFR1*FLAG
// Z DIRECTION EQUATIONS
// VFZ2 IS FOR EXTERNAL FLOW; VFZ1 IS FOR INTERNAL FLOW
VFZ1=((-3*U)/(2*A^2))*(2*R^2+(Z-(2*K*SQRT(T)))^2-A^2)+U
VFZ2=(-U*(1+(A^3*(R^2-2*(Z-(2*K*SQRT(T)))^2))/(2*((Z-
(2*K*SQRT(T)))^2+R^2)^(5/2))))+U
VFZ=VFZ2*(1-FLAG)+VFZ1*FLAG
//
// PARTICLE EQUATIONS
// RADIAL DIRECTION
VPR'=C1*(C2*(VFR-VPR)+C3*(DERIV(VFR,T)+VFR*DERIV(VFR,R)))
R'=VPR
//Z DIRECTION
VPZ'=C1*(C4+C2*(VFZ-VPZ)+C3*(DERIV(VFZ,T)+VFZ*DERIV(VFZ,Z)))
Z'=VPZ
//
```

continued

```
RHO=R/A
GAM=Z/A
GAMO=ZT/A
// Parameter values and Constraints:
K=-10.0
ALPHA=0.25
G=-981
SG=2.5
VIS=0.0151
KP=0.5
RP=0.0274
// Initial conditions:
R=0.38
Z=-7.90
VPR=-0.428
VPZ=-59.658
0.16<T<50.16
***
```

Nonuniform Speed Model with non-Stokes Drag using 0.0548 cm Particles

```
// PARTICLE MODEL
IndVars: T
DepVars: A, R, Z, RHO, GAM, ZT, GAMO, VPR, VPZ, U, VFR, VFZ
Params: ALPHA, KP, VIS, RP, G, SG, K, VT
// SIMPLIFYING EQUATIONS
U=K/SQRT(T)
A=ABS(2*ALPHA*K*SQRT(T))
ZT=Z-(2*K*SQRT(T))
EPS=(R^2+ZT^2)
EPS1=SQRT(EPS)
MF=(4/3)*PI*RP^3
MP=SG*MF
C1=1/(MP+KP*MF)
C2=(G*(MP-MF)/VT
C3=(1+KP)*MF
```

continued

```
C4=(MP-MF)*G
FLAG=UNIT(A-EPS1)
//
// FLUID EQUATIONS
// RADIAL EQUATIONS
// VFR2 IS FOR EXTERNAL RADIAL FLOW; VFR1 IS FOR INTERNAL RADIAL
//FLOW
VFR1=(3*R*(Z-(2*K*SQRT(T)))*U)/(2*A^2)
VFR2=(3*A^3*U*R*(Z-(2*K*SQRT(T))))/(2*((Z-(2*K*SQRT(T)))^2+R^2)^(5/2))
VFR=VFR2*(1-FLAG)+VFR1*FLAG
// Z DIRECTION EQUATIONS
// VFZ2 IS FOR EXTERNAL FLOW; VFZ1 IS FOR INTERNAL FLOW
VFZ1=((-3*U)/(2*A^2))*(2*R^2+(Z-(2*K*SQRT(T)))^2-A^2)+U
VFZ2=(-U*(1+(A^3*(R^2-2*(Z-(2*K*SQRT(T)))^2))/(2*((Z-
(2*K*SQRT(T)))^2+R^2)^(5/2))))+U
VFZ=VFZ2*(1-FLAG)+VFZ1*FLAG
//
// PARTICLE EQUATIONS
// RADIAL DIRECTION
VPR'=C1*(C2*(VFR-VPR)+C3*(DERIV(VFR,T)+VFR*DERIV(VFR,R)))
R'=VPR
//Z DIRECTION
VPZ'=C1*(C4+C2*(VFZ-VPZ)+C3*(DERIV(VFZ,T)+VFZ*DERIV(VFZ,Z)))
Z'=VPZ
//
RHO=R/A
GAM=Z/A
GAMO=ZT/A
// Parameter values and Constraints:
VT=-6.10
K=-10.0
ALPHA=0.25
G=-981
SG=2.5
VIS=0.0151
KP=0.5
RP=0.0274
// Initial conditions:
R=0.38
Z=-7.90
```

continued

VPR=-0.428
VPZ=-59.658
0.16<T<50.16
****

Appendix E

The Dynamics of Solid Particle and Bubble Groups

D.R. Topham
Institute of Ocean Sciences, Victoria, Canada

C.J. Laureschen, Y.G. Lee and R.D. Rowe
Department of Mechanical Engineering
The University of Calgary, Calgary, Canada

14-TP-24

THE DYNAMICS OF SOLID PARTICLE AND BUBBLE GROUPS

D.R. Topham
Institute of Ocean Sciences, Victoria, Canada

C.J. Laureshen, Y.G. Lee and R.D. Rowe
Department of Mechanical Engineering
The University of Calgary, Calgary, Canada

ABSTRACT

Two-phase flows consisting of liquid/bubble and liquid/solid particle mixtures occur in many industrial processes, which often involve both chemical reactions and heat transfer. This paper discusses the dynamics of discrete groups of either solid particles or bubbles released under gravity into quiescent fluid, and compares the experimental results with a simple theoretical model. The experimental work showed that the initial flow generated on the release of either solid particles or bubbles closely resembles that of a single-phase thermal (*e.g.* Turner, 1973). As the two-phase system evolves, the discrete particles or bubbles migrate through the circulation pattern and finally enter a state of free-fall. The model, which uses an expanding Hill's spherical vortex for the background fluid flow, can be used to predict individual particle or bubble motions. The particle/bubble paths generated by the model are shown to lie within the limits given by the experimental results.

1. INTRODUCTION

Previous studies concerning the behaviour of solid material dumped into water have concentrated on the motion of the solid phase only and neglected the details of the associated fluid motion. Modelling efforts have been confined to a description in terms of an equivalent single-phase dense fluid. Krishnappan (1975), for example, fits the results of an extensive series of experiments to a single-phase thermal model in which the parameters are taken to be functions of a Grashof number based on the properties of the individual particles in the cloud. Fannelop (1982) performed a similar theoretical analysis for bubble groups, but the experimental data of Laureshen (1992) conclusively show significant discrepancies between pseudo-single-phase thermal theory and nature.

A closer examination of the problem suggests that it is necessary to consider both the fluid and particle motion in order to arrive at a consistent momentum balance. Although the bulk formulation of the single-phase thermal can be extended to the two-phase case, it introduces an unknown "slip velocity" between the fluid and the particles or bubbles, thus requiring a further assumption to close the problem.

Experimental work by Lee (1992) on neutrally-buoyant dye/solid particle mixtures and by Laureshen (1992) on air bubble groups released into quiescent water with strong dye solutions was carried out to separately trace the motion of the two phases. The following stages of development were identified in both sets of experiments, although the residence time within each of the stages was much less in the bubble experiments:

(a) Initial acceleration: on release, a dye/particle mixture forms a near-spherical vortex structure with the fluid phase. The diameter and velocity of this initial vortex varies in a random manner for repeated releases. Similar results were obtained for bubble/dye mixtures, except that differences were observed only with regards to the vortex velocity.

(b) Single-phase behaviour: particles or bubbles closely follow the fluid circulation.

(c) Two-phase behaviour: particles or bubbles drift towards the front of the fluid vortex, taking up a stable position slightly ahead of the vortex.

(d) Phase separation: particles or bubbles move far ahead of the fluid vortex, finally attaining a free-fall condition with each generating an individual wake.

For high enough Reynolds numbers with a solid/liquid mixture, the initial fluid motion maintains its thermal-like circulation pattern throughout this series of events, and continues as such even after the particles have fully separated. With a bubble/liquid mixture, the large density difference between the liquid and the gas causes the fluid structure to appear more as a closed vortex ring than as a thermal. Once the particles or bubbles have migrated through the vortex structure, the momentum of their wakes continues to be entrained so that the vortex continues to maintain its buoyant character. Further evidence of thermal-like behaviour is given in Figures 1 and 2, which are derived from the release of 1000 mm³ of 0.2 mm diameter glass beads mixed with neutrally buoyant dye. Figure 1 shows the variation of the maximum horizontal dimension of the dye structure as a function of its

frontal position. The dependence is linear up to the start of phase separation and returns to this state after separation is complete, implying a degree of self-similar development during these periods. During phase separation, the rear of the structure elongates and the cross-section ceases to grow, which suggests that a change in the internal circulation pattern is taking place. This is consistent with the small change in slope between the linear portions of Figure 1. In contrast, the front of the dye structure is well-modelled as a single-phase thermal throughout its entire progression. Figure 2, which plots the square of the frontal displacement of the fluid vortex with respect to a virtual origin as a function of time, shows a close linear fit over the entire range of data, thus indicating thermal-like behaviour both before and after phase separation.

2. THEORETICAL MODEL

The consistent thermal-like behaviour of the fluid suggests that the expanding vortex model of Turner (1964) can be used as a background fluid flow for the examination of individual particle or bubble motions. The equations presented by Turner are for a Hill's spherical vortex whose radius a expands linearly with time t, which corresponds to a change in radius proportional to distance travelled, as is commonly observed for entraining thermals. In a cylindrical coordinate system moving with the vortex centre at a velocity U, the fluid velocity components of the external flow are:

$$V_r = \frac{3a^3 Urz}{2(z^2 + r^2)^{5/2}}$$
$$V_z = -U\left[1 + \frac{a^3(r^2 - 2z^2)}{2(z^2 + r^2)^{5/2}}\right] \qquad (1)$$

and, for the internal flow:

$$V_r = \frac{3U}{2a^2} rz$$
$$V_z = -\frac{3U}{2a^2}(2r^2 + z^2 - a^2) \qquad (2)$$

where the vortex radius:

$$a = \alpha Ut$$

and α is the entrainment constant, or half angle of spread of the vortex.

The motion of a small rigid sphere in a non-uniform flow has been examined in some detail by Maxey and Riley (1983) and, for Stokes flow, the equations of motion in cylindrical coordinates in a reference frame moving uniformly and centred on the vortex reduce to:

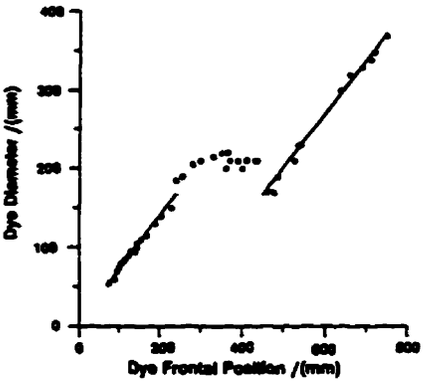

Fig. 1 Variation of the diameter of the dyed patch of fluid with its axial translation distance for 1000 mm³ of 0.2 mm diameter glass beads.

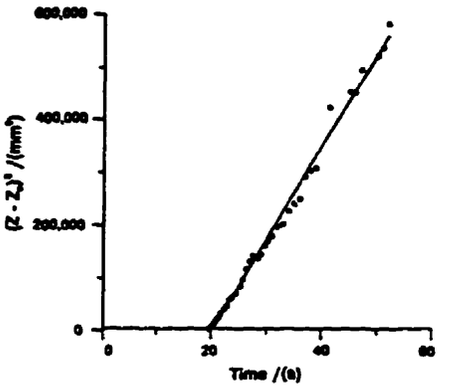

Fig. 2 Trajectory of the dyed fluid in single-phase thermal scaled coordinates for 1000 mm³ of 0.2 mm diameter glass beads.

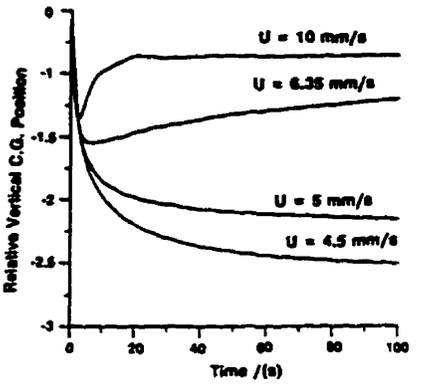

Fig. 3 Vertical motion of the centre of mass of an assembly of 80 0.27 mm diameter polystyrene particles in a 20 mm radius vortex for translational speeds of 4.5, 5.0, 6.35 and 10.0 mm/s with an entrainment constant of 0.25.

$$(m+k_v m_f)\frac{dv_z}{dt} = (m-m_f)g + 6\pi\mu r_p(V_z-v_z) + (1+k_v)\,m_f\left(\frac{\partial V_z}{\partial t} + V_z\frac{\partial V_z}{\partial z}\right) \quad (3)$$

$$(m+k_v m_f)\frac{dv_r}{dt} = 6\pi r_p\mu(V_r-v_r) + (1+k_v)\,m_f\left(\frac{\partial V_r}{\partial t} + V_r\frac{\partial V_r}{\partial r}\right) \quad (4)$$

where V_r and V_z are the components of fluid velocity at the 0° and 90° directions, and v_r and v_z are the corresponding components of solid particle velocity. The lift forces arising from the background vorticity (Auton *et al*, 1988) and the Basset history terms have been dropped for the present analysis. The particle is assumed to have a radius r_p and mass m, the fluid viscosity is μ, m_f is the mass of fluid displaced by the particle and k_v is the virtual mass coefficient, which would be 0.5 for a sphere. Similar numerical simulations have recently been reported for buoyant and heavy particles in different vortical flows (*e.g.* Ruetsch and Meiberg (1993) and Tio *et al* (1993)).

The equations of motion (3) and (4), subject to the velocity fields (1) and (2) have been integrated forward in time for an assembly of non-interacting solid particles released symmetrically about the centre, with velocities equal to that of the local fluid. The vertical progression of the centre of mass of the assembly has been calculated as a function of time for a range of vortex speeds, together with the particle positions, at selected times. The results shown are for an assembly of 80 polystyrene particles of 0.27 mm diameter (specific gravity of 1.04) released in a 20 mm radius vortex with an entrainment constant of 0.25. These have a free-fall speed of 6.35 mm/s, and are representative of some of the solid particle experimental conditions. Figure 3 illustrates the vertical motion of the centre of gravity (in units of vortex radius, with the negative values denoting a downward movement) of the assembly relative to the vortex centre for vortex speeds of 10, 6.35, 5 and 4.5 mm/s. For speeds above the free-fall speed of 6.35 cm/s, the majority of the particles are permanently trapped within the vortex. As the free-fall speed is approached, the particles migrate through the vortex to take up a stable position just outside the front of the bounding streamline. Further reductions in the vortex speed result in a slow separation of the particles from the vortex boundary.

Figure 4 shows the corresponding particle configurations at four instants in time for each of the selected vortex speeds. For the 10 mm/s vortex speed, the particles collect in a tight ring formation towards the outer boundary; at still higher speeds, the ring of particles compacts and moves closer to the boundary. At the free-fall speed, the particles form a shell just outside the formation, and this configuration appears to be stable over long times. At velocities of 5 mm/s and below, all of the particles migrate ahead of the vortex.

4. COMPARISON WITH EXPERIMENTAL WORK

The images in Figure 5 illustrate the solid particle configurations observed in the laboratory which correspond to the case study of the previous section. The images are illuminated with a thin sheet of light to provide a cross-section of the structure. A rapid transition can be observed between the widely-distributed formation in the early images to the crescent formation of the later images, as the solid particles fall through the vortex structure.

The changes in circulation and the accompanying departure from self-similarity which is observed during the final phase separation are more clearly delineated in the case of bubble groups, where an upwardly rising vortex ring is clearly visible in the liquid as the bubbles separate. A dramatic decrease in the value of the entrainment coefficient, α, for the vortex was observed in the bubble/dye experiments after phase separation (Laureshen, 1994). Figure 6 shows experimental data for seven bubble groups with volumes of 8000 mm^3(ST) which has been non-dimensionalized using the average vortex velocity of 120 mm/s and α values of 0.36 prior to and 0.073 following separation. The data points were generated by measuring the outer limits of the bubble group at fixed time intervals, and the vortex velocity and growth rate were calculated from similar measurements made on the dyed fluid. The upper limit of the graph was chosen as the height where the momentum transfer from the bubbles no longer appeared to affect the trailing vortex ring. The solid line shown in the figure is the particle path for a single bubble generated by integrating a set of equations derived in a similar manner to Equations (1) to (4), but which utilize a correlation for bubble terminal velocity from Clift *et al* (1978) instead of the assumption of Stokes flow which was used for the solid particles, and the same values of α used to non-dimensionalize the raw data. It should be noted, however, that a value of 8.0 cm/s was used rather than the experimentally-determined value of the vortex velocity, as it was found to give a closer approximation to the data points. This indicates that momentum transfer is taking place from the bubble wakes to the trailing vortex, and must be accounted for in order to correctly model the problem.

As was seen in the previous section, the location of the particle path given by the model is dependent on the initial coordinates chosen for the integration. In all of the cases examined, however, the generated bubble motion did not cross the boundary of the maximum bubble group radius given by the experimental data.

5. CONCLUSIONS

The theoretical model discussed in this paper assumes that the vortex is in steady translational motion which is not coupled to the particle momentum transfer. The strong resemblance to the experiments suggests that, up to the point where the bubble or

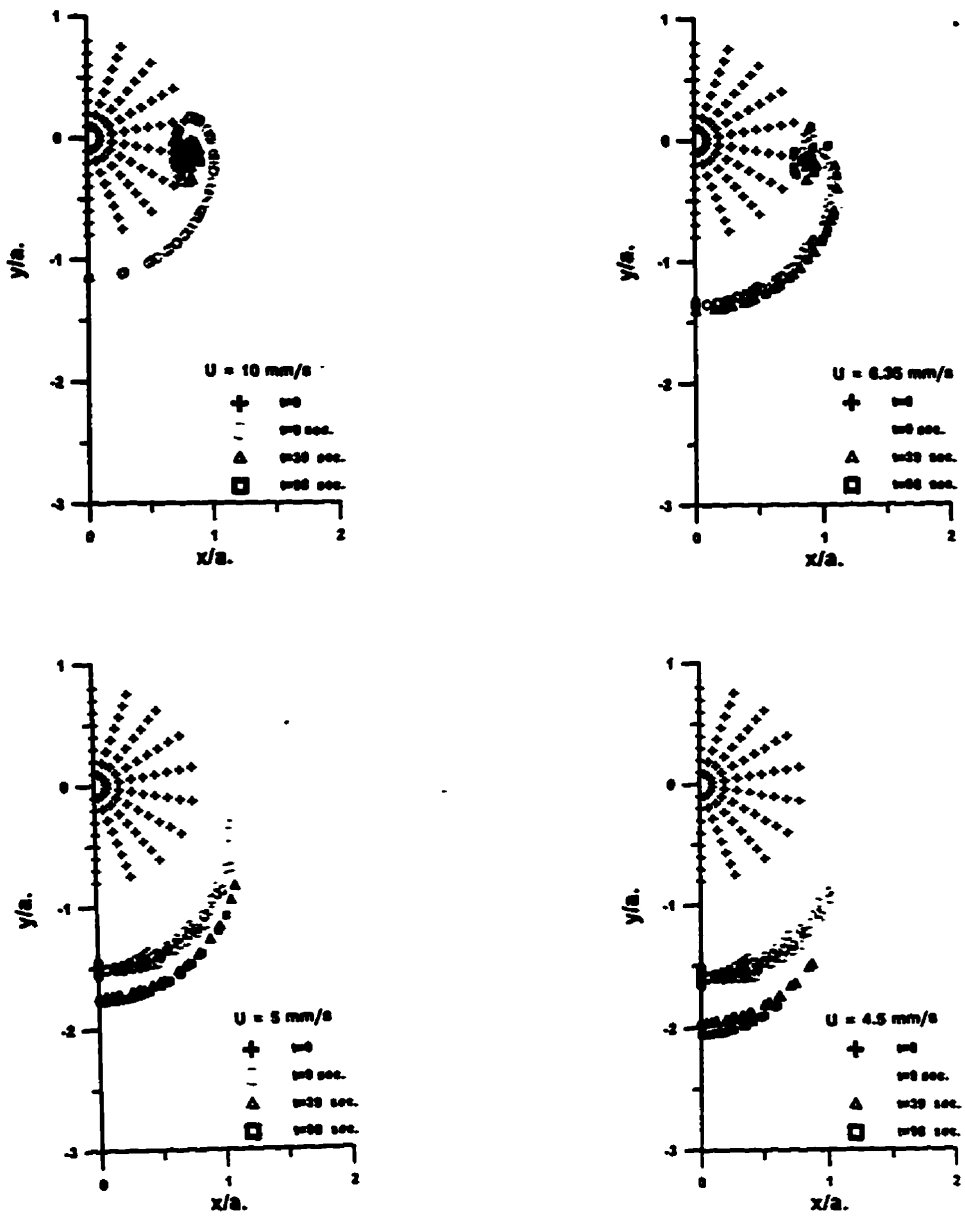

Fig. 4 Particle configurations at 0, 9, 39 and 98 second intervals for the vortex conditions of Figure 3.

particle motion no longer affects the trailing vortex, the vortex model could be extended to a description of the overall dynamics of the problem.

The continuing entrainment of momentum by the initial vortex structure is important in cases where a range of particle or bubble sizes is present. The smaller particles continue to be transported with the full momentum of the original mass released, in contrast to conventional models of dumped granular material which reduce the driving buoyancy in proportion to the residual. At long times after separation, the trailing vortex loses its distinctive character and becomes an integral part of the overall wake structure of the free-falling group of particles.

Although the two-phase problem under discussion is usually associated with discrete clouds of material, it could also serve as a generic eddy structure for the more complex two-phase turbulent flows which occur in many natural and industrial situations.

NOMENCLATURE

a	Vortex Radius	[m]
g	Gravitational Acceleration	[m/s^2]
k_p	Virtual Mass Coefficient of Particle	
m	Particle Mass	[kg]
m_f	Mass of Fluid Displaced by Particle	[kg]
r	Radial Coordinate	[m]
r_p	Particle Radius	[m]
t	Time	[s]
U	Vortex Velocity	[m/s]
v_r	Component of Particle Velocity in 0° Direction	[m/s]
v_z	Component of Particle Velocity in 90° Direction	[m/s]
V_r	Component of Fluid Velocity in 0° Direction	[m/s]
V_z	Component of Fluid Velocity in 90° Direction	[m/s]
z	Vertical Coordinate	[m]
α	Entrainment Constant of Vortex	
μ	Fluid Viscosity	[Pa s]

REFERENCES

Auton, T.R., Hunt, J.C.R. & Prud'homme, M. 1988, The Force Exerted on a Body in Inviscid Unsteady Non-uniform Rotational Flow, J. Fluid Mech., Vol. 197, pp. 241-257.

Clift, R., Grace, J.R. & Weber, M.E. 1978, Bubbles, Drops and Particles, Academic Press, New York.

Pasnelop, T.K. 1982, Laboratory Experiments With Bubble Plumes, Proc. 2nd Sub-sea Containment Workshop, Oslo, Norway, pp. 77-108.

Krishnappan, B.G. 1975, Dispersion of Granular Material Dumped in Deep Water, Scientific Series No. 55, Information Canada, Ottawa, Canada.

Laureshen, C.J. 1992, Dynamics of Bubble Groups: Raw Data, Department of Mechanical Engineering Report No. 468, The University of Calgary, Calgary, Canada.

Laureshen, C.J. 1994, Dynamics of Bubble Groups, Ph.D. Dissertation, Department of Mechanical Engineering, The University of Calgary, Calgary, Canada.

Lee, Y.G., 1992, An Investigation of the Dynamics of Solid Particle Thermals, M.Sc. Thesis, Department of Mechanical Engineering, The University of Calgary, Calgary, Canada.

Maxey, M.R. and Riley, J.J. 1983, Equations of Motion for a Small Rigid Sphere in a Non-uniform Flow, Phys. Fluids, Vol. 26, No. 4, pp. 883-889.

Ruetsch, G.R. and Meiberg, E. 1993, On the Motion of Small Spherical Bubbles in Two-Dimensional Vortical Flow, Phys. Fluids A, Vol. 5, pp. 2326-2341.

Tio, K-K., Linan, A., Lasheras, J.C. and Ganan-Calvo, A.M. 1993, On the Dynamics of Buoyant and Heavy Particles in a Periodic Stuart Vortex Flow, J. Fluid Mech., Vol. 254, pp. 671-208.

Turner, J.S. 1964, The Flow into an Expanding Spherical Vortex, J. Fluid Mech., Vol. 18, pp. 195-208.

Turner, J.S. 1973, Buoyancy Effects in Fluids, Cambridge University Press, Cambridge, UK.

Fig. 5 Images of polystyrene particle experiments at stages of development corresponding to the calculations of Figure 4. The dye cloud appears darker in successive pictures, due to a color change in the fluorescien from yellow to green as it dilutes. The bright image in the upper right-hand corner of each picture is a reflection from the lighting system.

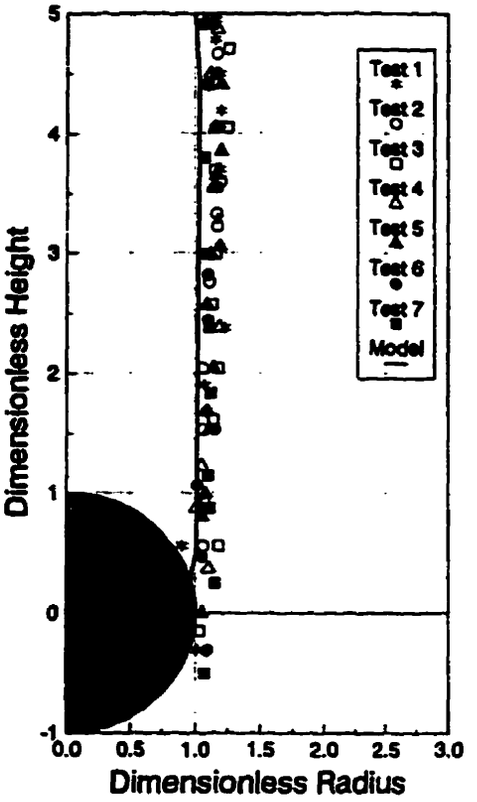

Fig. 6 Comparison of a bubble path as calculated by the model for a vortex velocity of 80 mm/s and α values of 0.36 while the bubble is within the fluid vortex and 0.073 following separation, with dimensionless experimental data from seven corresponding tests. The shaded portion of the figure denotes the vortex, and the coordinate system moves with the vortex centre at velocity U. Both height and radius for the experimental data have been normalized by dividing by $a = \alpha Ut$, in a similar manner to Figure 4.